

LIBRARY
Michigan State
University



RETURNING MATERIALS:

Place in book drop to
remove this checkout from
your record. FINES will
be charged if book is
returned after the date
stamped below.

--	--	--

This is to certify that the

dissertation entitled

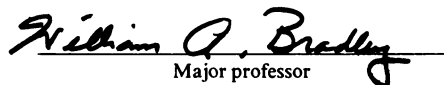
FINITE DISPLACEMENT BEHAVIOR OF PRESTRESSED
AND UNPRESTRESSED ARCH-FRAMES

presented by

Mostafa Tavakoli

has been accepted towards fulfillment
of the requirements for

Ph.D. degree in Civil Engineering


Major professor

William A. Bradley

Date August 27, 1984

FINITE DISPLACEMENT BEHAVIOR OF PRESTRESSED
AND UNPRESTRESSED ARCH-FRAMES

By

Mostafa Tavakoli

A DISSERTATION

Submitted to

Michigan State University

in partial fulfillment of the requirements
for the degree of

DOCTOR OF PHILOSOPHY

Department of Civil and Sanitary Engineering

1984

3233248

© 1985

MOSTAFA TAVAKOLI

All Rights Reserved

ABSTRACT

FINITE DISPLACEMENT BEHAVIOR OF PRESTRESSED
AND UNPRESTRESSED ARCH-FRAMES

By
Mostafa Tavakoli

The behavior of prestressed and unprestressed arches is studied. The possible means of achieving better design through cables or end couples is also examined.

The arch being studied is approximated by a series of bars connected by rotational springs. The axial deformations occur in the bars which are incapable of bending. The bending is taken by the springs at the nodes.

The reactions and the rotation or the moment at the left support are guessed as initial values. The equilibrium equations are written at each node and the forces and moments at each element and node are found. The method proceeds to the right end where errors in horizontal and vertical displacements and either moment or rotation may occur. Having the errors and the initial values, the latter are improved by Newtonian iteration and the calculations are iterated until convergence is achieved.

The method is capable of taking into account both symmetrical and unsymmetrical force application, physical properties, geometry, and deformations.

The method is applied to several problems with known solutions and the results are compared in Chapter 3; these include the buckling of a half circle arch with a concentrated load at the crown, a straight beam with a distributed load over half of the span, a quarter circle arch with the distributed vertical and radial load over the entire span, and the non-prismatic arch under uniform load over the entire span. The results obtained compare favorably with the known solutions presented in the literature.

In Chapter 4 the two principal problems of this thesis are investigated: the effect of wind load and the combination of arch and cables at different positions; and prestressed arches with concentrated load at the crown and uniform load over the entire and half of the span. It is concluded that the cables do not reduce the crown displacement except under the wind load. Prestressing the arch is also not effective in achieving a better design.

The method of extrapolation to reduce the need for a large number of elements was used and proved to be effective.

To the members of my immediate
family whom I love very much,

ACKNOWLEDGEMENT

I would like to express my most sincere gratitude to my major professor, Dr. W. A. Bradley, professor of civil engineering for his encouragement, constant help, and guidance throughout the study which made this thesis possible.

Thanks are also expressed to the other members of my guidance committee; Dr. R. K. Wen, Dr. L. Segerlind, and Dr. N. Hills. Additional mention is also due Dr. J. Lubkin whose knowledge in computers has been a great help to me.

I also owe my appreciation to all my friends for their moral support throughout my college years, including;

Ms. Luz E. Quinones and her sister Simply,

Dr. A. Emami, his wife Cherie, and Mr. Reza Emami,

Mr. M. Kh. Amoli and his wife Patricia,

Mr. A. Kh. Amoli and his wife Angie,

Mr. A. Ghods, Mr. M. Ghobadi, Mr. A. Golian, and Mr. A. Sadeghi.

And finally, the patience and understanding of my parents and other members of my family must be included in any acknowledgment of assistance. Their steady confidence and support have certainly contributed to the successful completion of this project.

I
TABLE OF CONTENTS

<u>CHAPTER</u>	<u>PAGE</u>
I. INTRODUCTION	1
1.1 General	1
1.2 Related Past Work	3
1.3 Notations	5
II. THEORY AND FORMULATION	8
2.1 Physical Model and Assumptions Made	8
2.2 Procedure	12
III. CASES WITH KNOWN SOLUTIONS	16
3.1 Arch with Concentrated Load at the Crown	16
3.2 Half Span Loaded Beam	25
3.3 Distributed Load	26
3.4 Nonprismatic Parabolic Arch	34
IV. EFFECTS OF CABLES AND PRESTRESSING	39
4.1 Cable-Supported Arches	39
4.2 Prestressed Arch	57
4.3 Prestressing by Axial Force	65
V. CONCLUSIONS AND FUTURE STUDY	85
5.1 The Problem Summary and Conclusions	85
5.2 Future Study	86
APPENDICES	88
A. Newton's Algorithm	88
B. Computer Program Listing to Find the Peak Value of Load-Displacement Curve	90
C. Listing of the Main Computer Program	93
D. Alternative Method for 2-D Problems	100
E. Space Arch	101
BIBLIOGRAPHY	109

II
LIST OF TABLES

<u>TABLE</u>	<u>PAGE</u>
1. Comparison of Results for Cantilever Loaded at the End	12
2. Comparison of Results for Case 3.1 (Circular Arch with Concentrated Load at the Crown)	18
3. Results for Case 3.2 (Half Span Loaded Beam)	26
4. Comparison of the Results for Quarter Circle with Vertical Distributed Load	28
5. Comparison of the Results for Quarter Circle with The Radial Distributed Load	34
6. Comparison of the results for Non-prismatic Arch	36
7. Maximum Moment for Straight Bar Bent into an Arch	64
8. Optimum for the Prestressed Arch of Table 7	64
9. Optimum Span and Maximum Moment for the Prestressed Arch of Fig. 40	65
10. Buckling Loads (for the Arch Prestressed by Axial Force)	67
11. Maximum Moments and Axial Forces (for the Arch Prestressed by Axial Force)	68



III

LIST OF FIGURES

<u>FIGURE</u>	<u>PAGE</u>
1. Modeling the Arch	10
2. A Typical Bar and a Typical Node	10
3. Sign Convention for Axial Deformation and Rotation	10
4. Cantilever with End Couple	11
5. Arch Under General Load	12
6. Flow Chart of the Computer Program	15
7. The Arch of Case 3.1	16
8. Load-Deflection Curve for Case 3.1	20
9. Arch Deflected Shapes, Case 3.1, 4 Elements	21
10. Arch Deflected Shapes, Case 3.1, 6 Elements	22
11. Arch Deflected Shapes, Case 3.1, 8 Elements	23
12. Arch Deflected Shapes, Case 3.1, 20 Elements	24
13. Quarter Circle with Vertical Distributed Load	27
14. Quarter Circle with Radial Distributed Load	28
15. Load-Displacement Curve for Vertical Distributed Load	29
16. Deflected Shapes of Arch with Vertical Distributed Load	30
17. Load-Deflection Curve for Radial Distributed Load	31
18. Deflected Shapes of Arch with Radial Distributed Load	32
19. Load-Deflection Curve	33
20. Parabolic Arch Under Uniform Load	34
21. Deflected Shapes of Non-Prismatic Arch	37
22. Load Displacement Curves for Non-Prismatic Arch	38
23. Projection of Cables	39
24. Load-Deflection Curves for an Arch with Cables having Different Cross-Sections	45
25. Deflected Half Circle Arch with Cables	46
26. Load-Deflection Curve for Half Circle Arch with Cables, 8 and 12 Elements	47



(CONT.)
LIST OF FIGURES

<u>FIGURE</u>	<u>PAGE</u>
27. Deflected Shapes of Arch with Cables, 8 and 12 Elements	48
28. Different Cable Base Position	49
29. (a) Arch Deflected Shape; (b) Effect of Base Position	50
30. Half Circle Arch with 4 Pairs of Cables	51
31. Deflected Shapes of Arch with 4 Pairs of Cables	52
32. Arch Deflected Shapes - Horizontal Loads at Different Nodes	53
33. LF - Displacement Curves	54
34. LF - Deflection Curve, Wind Loads, with and without Cables	55
35. Deflected Arch Under Wind, with and without Cables	56
36. Prestressing the Straight Bar into an Arch	57
37. Prestressing the Arch, Load-Displacement Curve	59
38. Prestressed Deflected Arch	60
39. Moment Diagrams for Prestressed Arches	61
40. Maximum Moment - Span Curve for a Half Circle Prestressed Arch	63
41. Prestressed Arch, Axial Force	66
42. Load-Displacement Curve for Concentrated Load, $H/L = 0.5$, Prestressing by Axial Force	69
43. Load-Displacement Curve for Uniform Load over Entire Span, $H/L = 0.5$, Prestressed by Axial Force	70
44. Load Displacement Curve for Uniform Load Over Half of the Span, $H/L = 0.5$, Prestressing by Axial Force	71
45. Load-Displacement Curve for Concentrated Load, $H/L = 0.375$, Prestressing by Axial Force	72
46. Load-Displacement Curve for Uniform Load over Entire Span, $H/L = 0.375$, Prestressed by Axial Force	73
47. Load-Displacement Curve for Uniform Load over Half of the Span, $H/L = 0.375$, Prestressed by Axial Force	74



(CONT.)

LIST OF FIGURES

<u>FIGURE</u>	<u>PAGE</u>
48. Load-Displacement Curve for Concentrated Load, $H/L = 0.125$, Prestressing by Axial Force	75
49. Load-Displacement Curve for Uniform Load, over Entire Span, $H/L = 0.125$, Prestressed by Axial Force	76
50. Load-Displacement Curve for Uniform Load over Half of the Span, $H/L = 0.125$, Prestressing by Axial Force	77
51. Moment Diagrams, Prestressing by Axial Force	78
52. Axial Force Diagrams, Prestressing by Axial Force	80
53. Arch Shapes, Prestressing by Axial Force	82
54. Arch Deflected Shapes, Prestressing by Axial Force, $H/L = 0.5$	83
55. Typical Mass Point, Forces and Moments	101
56. Local and Global Axes (Space Arch)	102



CHAPTER I

INTRODUCTION

1.1 General

Arches are among the oldest forms of structures and devices that have been used for many centuries. Bows as a hunting device and a weapon have been used since the ancient times. The sport of modern archery started even before the 13th century (12).

Arches have had other important applications. In many cases such as bridges, buildings, decorative structures, mechanical bodies, and the approximation of shells by a series of arches, they have formed a major structural component. In lightweight structures, arches are being used, sometimes in connection with cable nets or fabric covering. For ease in erection, these arches are sometimes made from initially straight bars, bent into an arch shape, secured at the ends by clamping or pinning, and then loaded.

It is this extensive application of the arch-frames that motivated this investigation.

This thesis is concerned with the behavior of an arch under large enough loads to produce large deflections. The study is done using a finite number of discrete elements to approximate the arch. This method makes it possible to consider problems such as arches with variable section where the application of exact methods would be

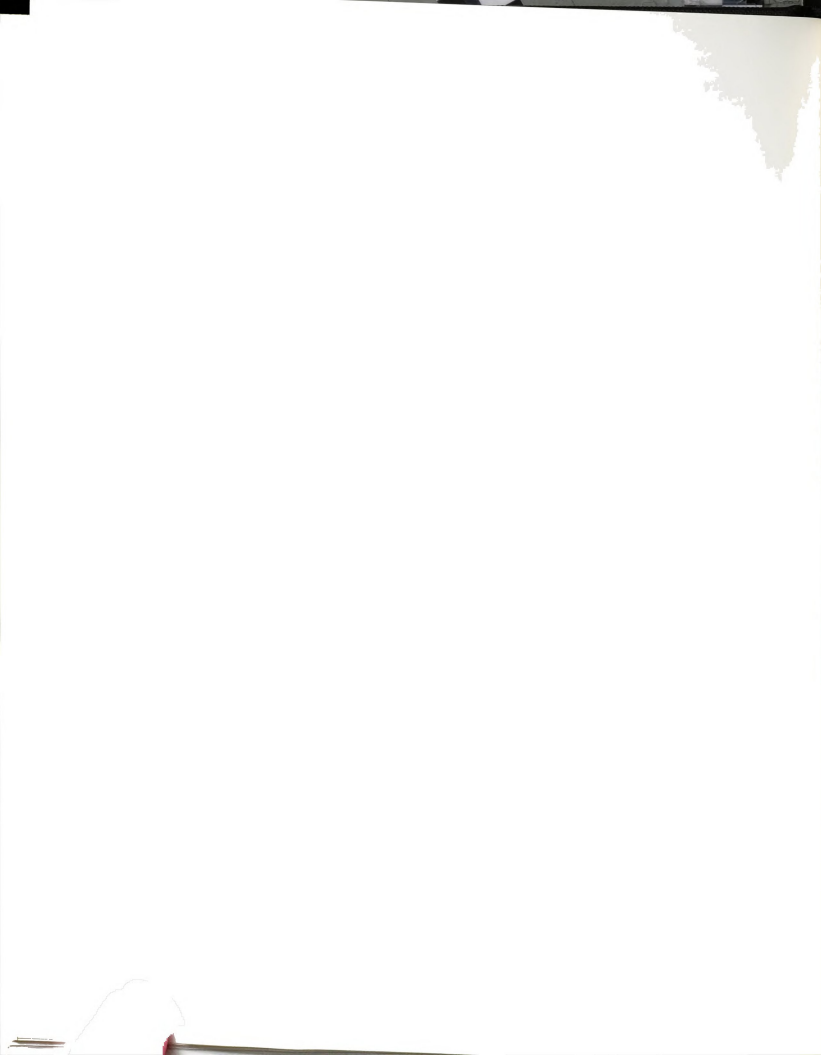
difficult, if possible. Even if it was possible, to solve the problem using the methods available in statics and mathematics would be often not easy.

In this investigation, a rigid bar spring node model is used. Both axial deformations, taken by the bars, and rotations, taken by the springs at the nodes, are allowed. Using the equilibrium equations and Newton's algorithm, an iteration procedure is developed to find the forces and moments in all elements and nodes. The final configuration is also found. The model has been used to solve the following problems for which known solutions are available:

1. The symmetric and unsymmetric behavior of a half circle arch, pinned at the ends and loaded at the crown with a concentrated load applied vertically.
2. A straight beam, pinned at the supports and subjected to a uniform load over half of the span.
3. A parabolic arch with variable moment of inertia under uniform load over the entire span.
4. A quarter circle arch pinned at the ends and loaded radially or vertically over the entire span.

The problems investigated in Chapter 4 are as follows:

1. A circular arch pinned at the ends, supported by cables at different positions and loaded horizontally or vertically.
2. Circular arcs with various initial spans prestressed into an arch with a fixed span, s , then pinned at the ends and loaded. A straight bar was also prestressed into arches with different spans, fixed at the ends and loaded.



3. A straight bar prestressed into an arch by an axial force, fixed at the ends, and then loaded with 3 different loadings; concentrated at the crown, uniform over the entire span, and uniform over half of the span. The results are compared with the unprestressed parabolic fixed arch with the same span and the same loadings.

The program written is in BASIC and was run with the TRS-80 micro-computer.

Included as the appendices of the thesis are; the main computer program, the method used to improve the initial values, a computer program used to find the peak values of the load-displacement curves, and an alternative method for 2-dimensional problems and methods to solve 3-dimensional problems which did not lead to satisfactory results.

1.2 Related Past Works

The buckling of curved structures has been investigated by many researchers. Austin (1) has summarized the state of the knowledge of the in-plane bending and buckling of arches. Austin and Ross (3) have compared numerical procedures for elastic analysis of arches by large deflection, 2nd order and classical theories using repeated numerical integrations similar to the Newmark procedure for beams and beam-columns. Following Watwood and Harts (40), Gallert and Laursen (14) have used equilibrium models to study an elastic arch of arbitrary geometry and loading by a finite element method based on a mixed variational principle. They removed the restriction of prior satisfaction of equilibrium on the trial set of unknowns, i.e., the



stress field was directly obtained by analysis. Using the variational approach, Schreyer and Masur (33) wrote the equilibrium equations in radial and tangential directions to find the equations of buckling load and load-displacement curves for a clamped arch loaded by a concentrated force at the apex. They concluded that the symmetric snap-through buckling always governs. Kerr and Soifer (20) gave an analysis of the effect of linearizing the prebuckling state for clamped shallow arches, overestimating the snap-through load. Using Koiter's initial post buckling theory, Dym (11) considered a symmetric buckling from a linear prebuckling stage and its postbuckling aftermath.

Oran and Bayazid (29) analysed the stability of uniformly loaded circular arches without the assumption of shallow and inextensional arch and showed that the critical load (both limit and bifurcation) can be expressed in terms of a combined problem parameter in the form of asymptotic formulas. Sheinman (35) has developed a numerical procedure modifying Newton's method and by finite difference based on large deflection, small strain, and moderately small rotations. The equilibrium equations admit shear deformation and geometric imperfection.

Using the Newton-Raphson method to solve non-linear equilibrium equations, Wood and Zienkiewicz (45) have worked on geometrically non-linear analysis of elastic in-plane oriented bodies in a total Lagrangian coordinate system, developing a parilinear isoparametric element. A non-linear elastic finite element for a beam initially curved in one plane but deformable in the three dimensional space has been presented by Wen and Lange (42). In this work the quadratic and

linear eigenproblems were formulated to calculate the in-plane and out of plane buckling loads of arches. Wen and Rahimzadeh (43) investigated non-linear elastic frames including arches, approximated by a series of finite elements and using different coordinate systems such as Euler and Lagrange (small rotations and updated).

Other studies of interest include, Ojalvo and Newman (28), Ojalvo and Demuts (27), Bathe and Bolourchi (4), Chajes (5), DaDeppo and Schmidt (9), Dawe (8), Wempner and Patrick (41), Yamada and Ezawa (47), Harrison (16), and Sabir and Lock (32).

The survey article by Schmidt and DaDeppo (34) provides additional historical comments and a more complete bibliography than that undertaken here.

1.3 Notations

The following symbols have been used in this investigation:

A = Cross Sectional Area of Each Element;

A_c = Cross Sectional Area of Cables;

AD = Axial Deformation of Each Element;

AF = Axial Force in Each Element;

CB = Combined Components of the Axial Forces of the Pair of Cables in
the Plane of the Arch;

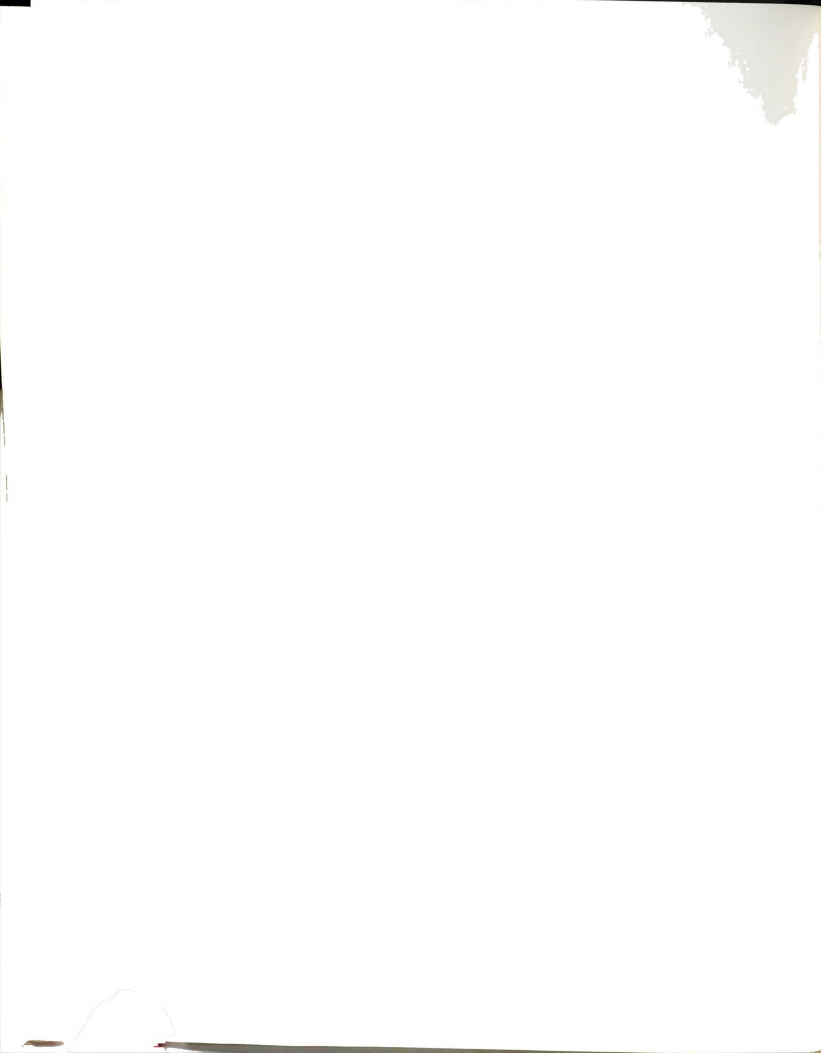
CD = Cable Axial Deformation (Positive if Compression);

CF = Cable Axial Force;

CH = Horizontal Component of CB;

CL = Cable Original Length;

CN = Cable Final Length = CL - CD;



CV= Vertical Component of CB;

E = Modulus of Elasticity of Each Member;

E_c = Modulus of Elasticity of Cables;

GR= Guessed Value for Rotation of the First Element;

HL= Applied Horizontal Load at Each Node;

I = Moment of Inertia of Each Member;

L = Element Length;

LF= Load Factors of the Distributed Horizontal Load;

M_i = Moment of Each Node;

M_{max} = Maximum moment;

M_0 = Prestressing Moment at Each Node (When Bar is Prestressed By
Couples Applied at the Ends);

N = Number of Elements;

P = Concentrated Applied Load;

P_b = Bifurcation Load (Where Unsymmetric Buckling May Occur);

P_c = Critical Load (Maximum P on the Symmetric Part of Load-Vertical
Displacement of the Crown Curve);

P_L = Limit Applied Load After Which the Deflection of Crown Gets Larger
By Adding Cables;

R=Radius of the Arch;

SC= The Angle Between the Two Neighboring Elements, Unless Otherwise
Specified;

SF= The Shear Force in Each Element;

V_b = Vertical Displacement of the Crown Corresponding to Bifurcation
Load;

V_c = Vertical Displacement of the Crown Corresponding to the Critical



Load;

V_L = Applied Vertical Load at Each Node;

V_m = Vertical Displacement of the Crown Corresponding to the Critical
Distorted Load;

W = Distributed Load Per Unit Length;

W_b = Bifurcation W (Where Unsymmetric Buckling May Occur);

W_c = Critical W (Max. w on The Sym. Part of Load-Displ. Curve);

W_N = Radial Distributed Load Per Unit Length That Changes Direction to
Stay Normal to the Arch During and After Deformation;

W_{NN} = Radial Distributed Load Per Unit Length That Does Not Change
Direction and Stays Radial;

X = x - Coordinate of Each Node;

Y = y -Coordinate of Each Node;

$\Delta\theta$ = Rotation of Each Element;

θ = Angle between the Element and a Vertical Line, Measured
Clockwise From The Vertical;

$\theta_n = \theta + \Delta\theta.$

CHAPTER II

THEORY AND FORMULATION

2.1 Physical Model and Assumptions Made

The arch is modeled as a combination of rigid bars and rotational springs. The bars are considered to have axial elastic properties, but are incapable of bending. The rotations are taken by the springs at the nodes (Fig. 1).

It is also assumed that the material is isotropic and linearly elastic. No shear deformations are allowed.

Fig. 2 illustrates the forces and moments on a typical bar and a typical node. On the first node and element there are also the horizontal and vertical reactions in the positive x and y directions, respectively. The applied horizontal load is considered to be positive if in the positive x direction. The positive applied vertical load is in the negative y direction. For a fixed support a moment also exists at the support.

If the forces and moments on the element (or node) $i-1$ are known, the forces and moments on element (or node) i can be found using the following equilibrium equations at node i .

$$\begin{aligned} SF(i) &= -AF(i-1)S \sin(SC) + SF(i-1)\cos(SC) + HL(i)\cos(\theta) + VL(i)S \sin(\theta) & (a) \\ AF(i) &= AF(i-1)\cos(SC) + SF(i-1)S \sin(SC) + HL(i)S \sin(\theta) - VL(i)\cos(\theta) & (b) \\ AD(i) &= AF(i)L(i)/E(i)I(i) & (c) \end{aligned} \quad (2.1)$$

$$M(i)=M(i-1)+SF(i-1)L(i-1) \quad (d)$$

$$\Delta \theta(i)=M(i) \left\{ L(i)/2E(i)I(i)+L(i-1)/2 E(i-1)I(i-1) \right\} \quad (e)$$

Axial deformation and rotation of a node are shown in Fig. 3 in the positive sense.

As with most finite element solutions, taking more elements leads to a better accuracy.

The results obtained using this model agree well with the ones previously obtained by others. Table 1 shows the results for a cantilever beam loaded at the free end with a vertical downward load. As can be seen, with extrapolation between 6, 8 and 10 elements exact results (23) are obtained. The 4, 6 extrapolation differs from the exact value by only .06%. The 4, 6, 8 and 10, 20 extrapolations are more accurate than the solution with 100 elements.

Fig. 4 shows the results for a cantilever beam with end couple. The results are very good again compared with the exact ones.

The effectiveness of this model and the procedure used will be compared with some other previously worked out models and procedures later in the next chapter.



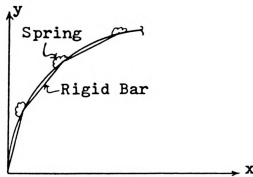


Fig.1. Modeling The Arch

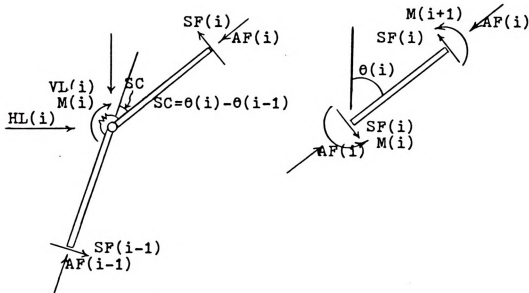


Fig.2. Typical Bar And Node

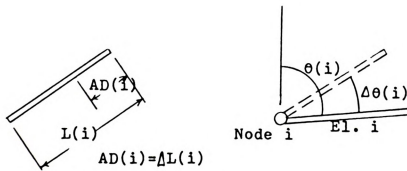


Fig.3. Sign Convention For Axial Deformation And Rotation



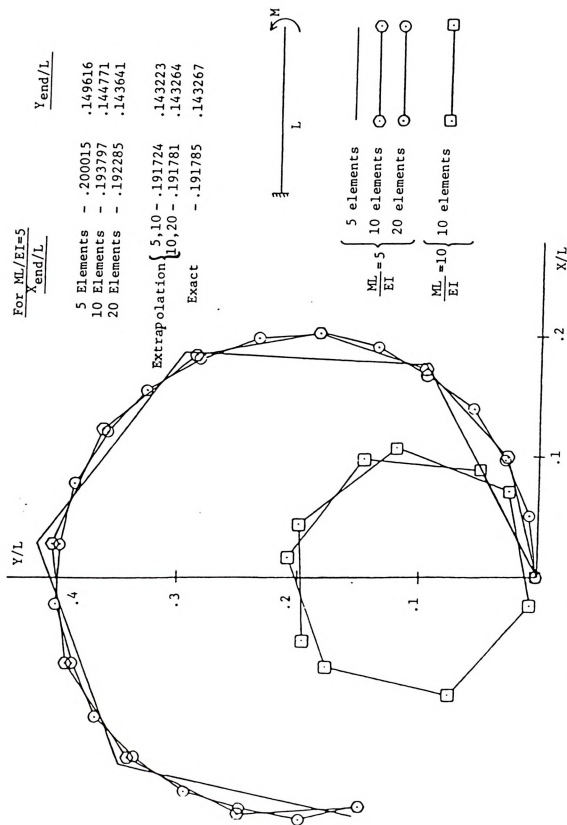
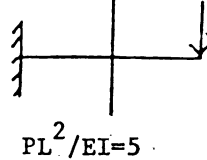


Table 1 - Comparison of Results For Cantilever Loaded At The End

# of elements	x free end	y free end	slope (free end)
4	60.3019	73.3951	1.20618
6	60.8407	72.2761	1.21116
8	61.018	71.8834	1.21298
10	61.098	71.7018	1.21383
20	61.2028	71.4597	1.21498
100	61.2358	71.3823	1.21535
4,6	61.27174	71.3809	1.21514
4,8	61.2567	71.3795	1.21525
6,8	61.24596	71.3785	1.21532
8,10	61.24022	71.37896	1.21534
10,20	61.23773	71.37900	1.21536
4,6,8	61.23736	71.3777	1.21538
6,8,10	61.23700	71.37921	1.21535
exact (23)	61.237	71.379	1.21537
ref. (13) 4el.	61.29	71.91	1.223
ref. (13) 10el.	61.25	71.46	1.221



2.2 Procedure

The procedure used in satisfying the boundary conditions for a frame is the so-called "shooting method". It starts out with assuming values for the unknowns at the left support of the arch under any loading condition (Fig. 5). The final configuration of the arch after

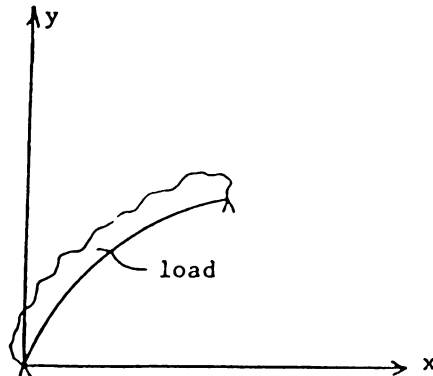


Fig. 5. Arch Under General Load



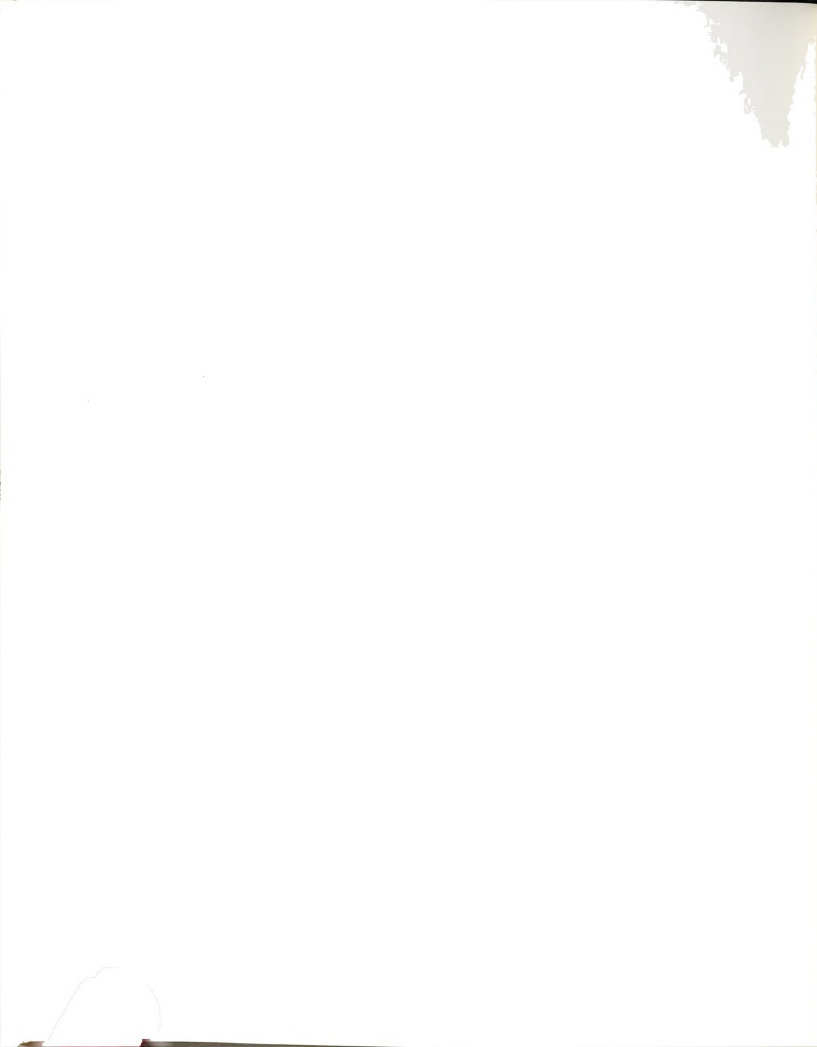
loading is to be determined. The assumed unknowns would include reactions and rotation (for pinned end) or moment (for fixed end). Having this information and using formulas 2.1, we can find the forces and deformation of the next element and moment and rotation of the next node and proceed to the right support. We will end up with certain values for the x and y displacements and moment (for pinned end) or rotation (for fixed end) which are the errors (if not equal to zero).

Having the initial guessed values and the final errors and using Newton's algorithm (appendix A), we improve the initial values and iterate until convergence is achieved, i.e., the errors are within acceptable range. In Newton's algorithm, to find the derivative of $f(x,y,z)$ representing each one of the 3 errors at the right support with respect to say, x representing one of the 3 initial values, we find $f(x,y,z)$ and then $f(x+\Delta x,y,z)$, Δx being a small increment in x. Then
$$\frac{\partial f(x,y,z)}{\partial x} = \frac{f(x+\Delta x,y,z)-f(x,y,z)}{\Delta x} \quad (2.2)$$
$$\Delta x = .01$$
 has given the best results in all cases.

A listing of the computer program is given in appendix C. Fig. 6 shows the flow chart of the program.

In the process of inputting data, variable thickness, properties, shape, element length, and loading can be allowed for. The uniform loading is assumed to be lumped at the nodes. Components of the loads at the nodes in x and y directions are input.

A double precision program has also been used and the results have not changed significantly from the ones using single precision.



It should also be noted that the choice of the initial values may change the speed of convergence significantly. Another point to consider is that a set of initial values intended for one case of equilibrium, such as symmetric, may lead to another equilibrium configuration, such as unsymmetric. With a little experience, one will have a feeling of what the initial values for a better and a faster convergence in the right direction should be.



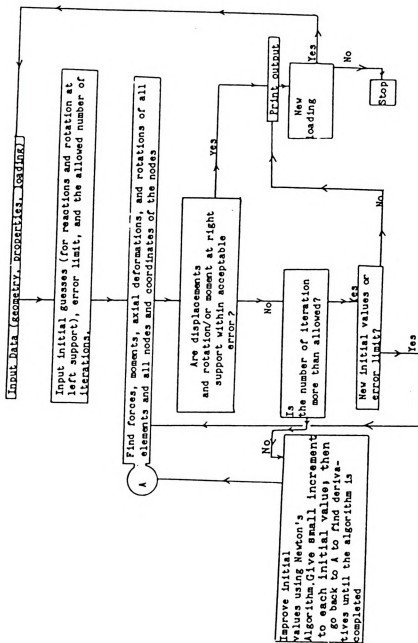


Figure 6. Flow Chart of the Computer Program



CHAPTER III

CASES WITH KNOWN SOLUTIONS

The following cases have been studied.

3.1 Arch With Concentrated Load at the Crown

A simply supported half circle arch with a concentrated vertical downward load at the crown was considered (Fig. 7).

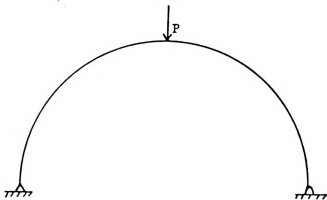


Fig. 7. The Arch of Case 3.1

The program was run for different initial guesses, all leading to the same results. Convergence was fast, except at the loads very close to the critical load. To overcome this problem a third degree curve fitting was taken passing through 4 neighboring points on both sides of the peak value. The 4 points had already been found using the program. So the equation of the curve was written. If the coordinates of the 4 points are (x_1, y_1) , (x_2, y_2) , (x_3, y_3) , and (x_4, y_4) then the coefficients of the third degree polynomials can be found as follows:

$$\begin{Bmatrix} y_1 \\ y_2 \\ y_3 \\ y_4 \end{Bmatrix} = \begin{bmatrix} x_1^3 & x_1^2 & x_1 & 1 \\ x_2^3 & x_2^2 & x_2 & 1 \\ x_3^3 & x_3^2 & x_3 & 1 \\ x_4^3 & x_4^2 & x_4 & 1 \end{bmatrix} \begin{Bmatrix} a \\ b \\ c \\ d \end{Bmatrix} \quad (3.1)$$

$$\begin{Bmatrix} a \\ b \\ c \\ d \end{Bmatrix} = \begin{bmatrix} x_1^3 & x_1^2 & x_1 & 1 \\ x_2^3 & x_2^2 & x_2 & 1 \\ x_3^3 & x_3^2 & x_3 & 1 \\ x_4^3 & x_4^2 & x_4 & 1 \end{bmatrix}^{-1} \begin{Bmatrix} y_1 \\ y_2 \\ y_3 \\ y_4 \end{Bmatrix} \quad (3.2)$$

Knowing the coefficients, the peak value can be determined by solving the following equation for x and finding the corresponding y . The program to do so is listed in appendix B.

$$dy/dx = 3ax^2 + 2bx + c$$

The bifurcation load was determined by approximating the symmetric and the unsymmetric branches of the load-displacement curve by two polynomials passed through determined points on the branches and then solving for the intersection of these two curves.

Fig. 8 shows the load vs. crown vertical displacement curve. The reference curve (15) is also plotted.

Figs. 9-11 show the deflected shapes of the arch under different loads for 4, 6, and 8 elements, respectively. Fig. 12 shows the deflected shapes of a 20 element arch with different properties.

Table 2 compares the results obtained using this method and other references. The % differences in results are also shown. In this table:

P_c = critical load (peak value on the symmetric part of load-displacement curve)

P_b = bifurcation load (load at which unsymmetric buckling may occur)

V_p = displacement of the crown corresponding to P_c

Table 2 - Comparison of Results For Case 3.1

No. of Elements	$\frac{P_b R^2}{EI}$	$\frac{P_c R^2}{EI}$	$\frac{V_p}{R}$	Z Difference					
				$\frac{In P_b R^2}{EI}$		$\frac{In P_c R^2}{EI}$		$\frac{In v}{R}$	
				4, 6, 8	6, 8	4, 6, 8	6, 8	4, 6, 8	6, 8
4	4.66	6.960	.82						
6	5.335	8.075	.78						
8	5.600	8.915	.765						
6, 8	5.940	10.00	.75						
4, 6, 8	5.960	10.32	.75						
(15)50El.	5.875	10.15	.75	1.45%	1.11%	1.67%	1.48%	0%	0%
(42)16El.	6.766			11.92%	12.21%				
(21)	6.540			8.87%	9.17%				
(43)	5.700			4.56%	4.21%				

Fig. 8 is for the arch with $E=200$, $I=10^8$, $A=10^5$, and $R=5000$.

Table 2 corresponds to the same arch. For an arch with different properties ($E=1.04 \times 10^7$, $I=6.21 \times 10^{-6}$, $A=.0775$, $R=10$), the values for 4, 6, and 8 elements shown in Table 2 did not change significantly.

It should be noted that the results are for a much fewer number of elements than many others.

The larger difference with two of the references in Table 2 is mainly due to the difference in assumptions. In reference (42) the weakening effect of bending deformations on the axial stiffness is

neglected. The displacement of the structure is assumed to increase linearly with the applied load until buckling occurs. The assumptions in reference (21) were based on the cross sections being inextensional. Although the term involving the cross sectional area does not appear in the dimensionless term PR^2/EI , the effect of the area is significant in many cases (42). The present study is not based on any of the above assumptions.

The 3 point Richardson's extrapolation has been done using the following formula:

$$A = A_f \frac{n_f^4}{(n_f^2 - n_c^2)(n_f^2 - n_i^2)} - A_i \frac{n_i^4}{(n_f^2 - n_i^2)(n_i^2 - n_c^2)} + A_c \frac{n_c^4}{(n_f^2 - n_c^2)(n_i^2 - n_c^2)} \quad (3.3)$$

where A_f , A_i , and A_c are the values corresponding to n_f , n_i , and n_c number of elements, respectively. For a 2 point extrapolation the following formula has been used:

$$A = A_f \frac{n_f^2}{(n_f^2 - n_c^2)} - A_c \frac{n_c^2}{(n_f^2 - n_c^2)} \quad (3.4)$$

The energy can also be checked. For a body in equilibrium the energy due to the external forces should be equal to the internal energy. The external energy due to load p is equal to the area under the load-displacement curve from load=0 to the point corresponding to p . This area can easily be found by approximating the curve by some straight lines. The internal energy would be equal to:

$$\text{Internal Energy} = 1/2 \sum (i) \Delta \theta(i) + A F(i) \Delta D(i) \quad (3.5)$$

Using Fig. 8, the external energy for a load of 7000 (before the peak value on the curve) would be equal to 1.507376×10^7 and the



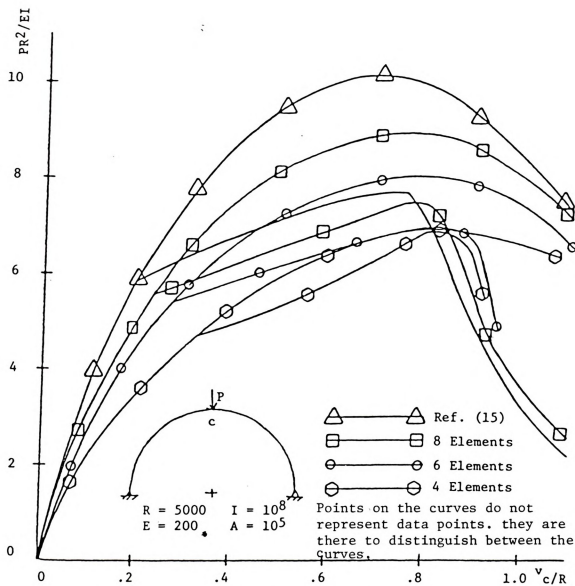


Fig. 8. Load - Deflection curve for case 3.1



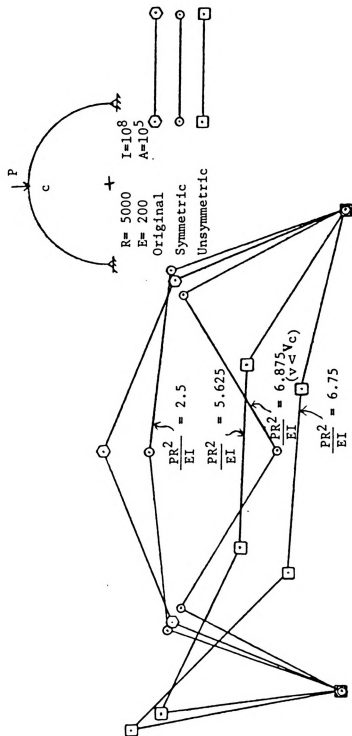


Fig. 9. Arch Deflected Shapes, Case 3.1, 4 Elements



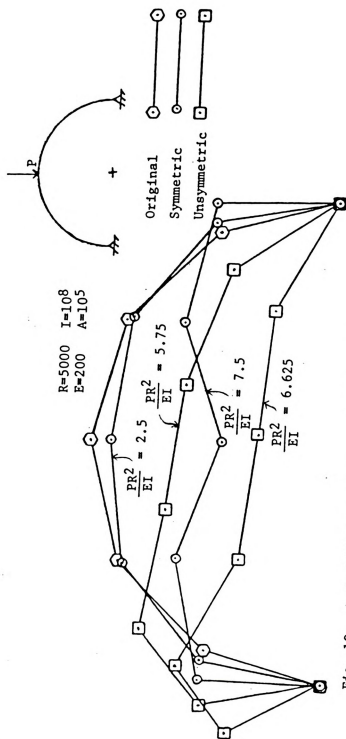


Fig. 10. Arch Deflected Shapes, Case 3.1, 6 Elements

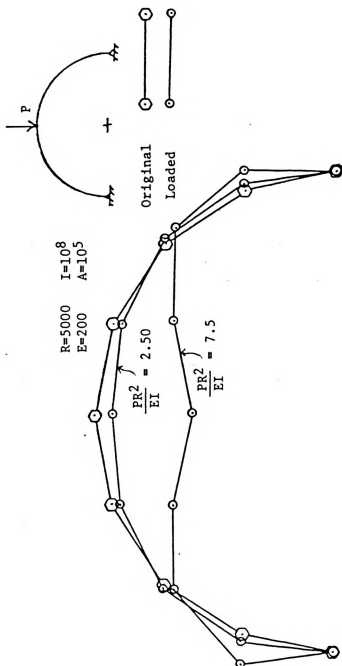


Fig. 11. Arch Deflected Shapes, Case 3.1, 8 Elements



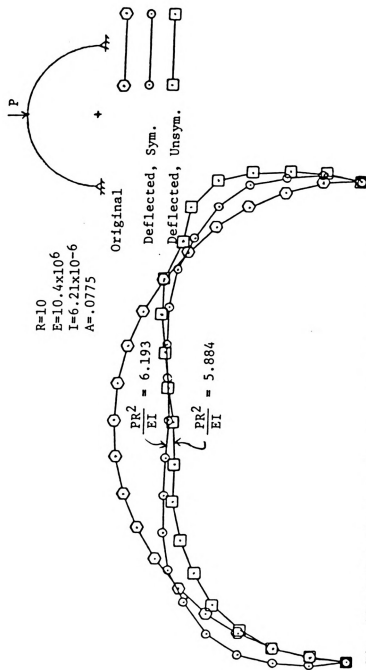
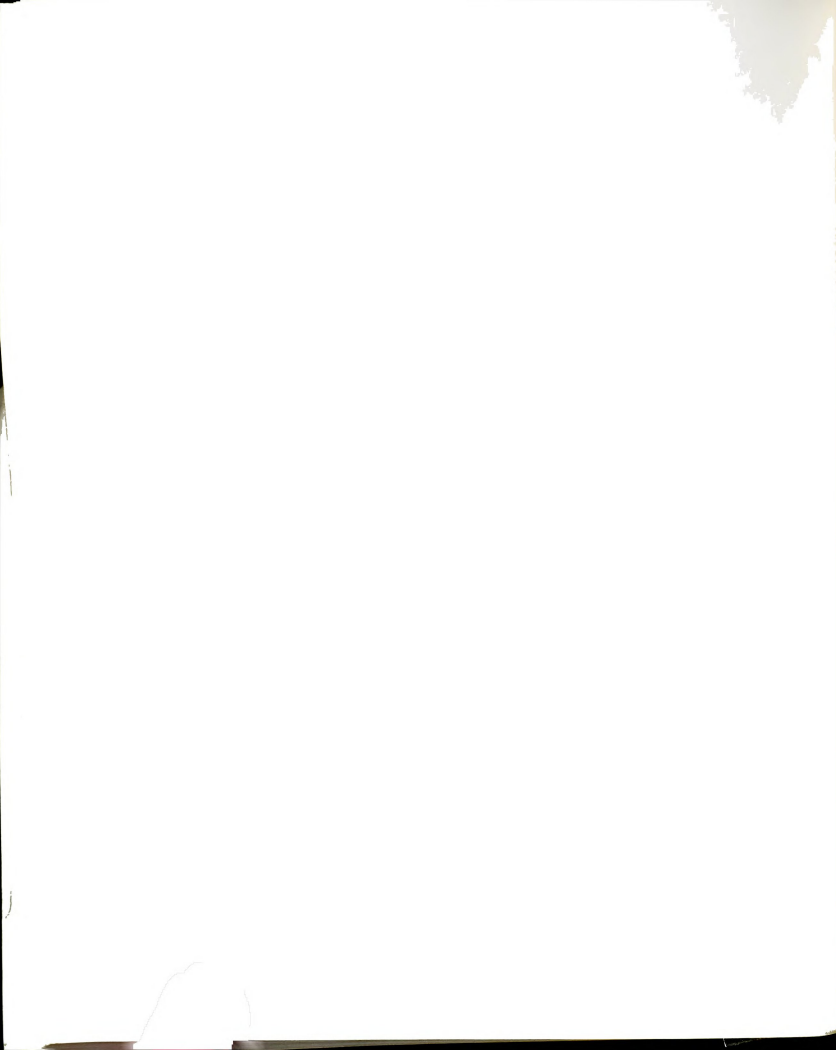


Fig. 12. Arch Deflected Shapes, Case 3.1, 20 Elements



internal energy is equal to 1.5152700×10^7 . There is a 0.52% difference. For a load of 6000, (on the curve passed the peak value) the external and internal energy and the percentage difference are equal to 2.9865619×10^7 , 2.9924650×10^7 and 0.2%, respectively. These were all for the 8 element case. Therefore the external energy and internal energy are equal, which confirms again that the configurations obtained are the equilibrium configurations.

We see that the model and procedure work very well for this case.

3.2 Half Span Loaded Beam

A simply supported beam with a horizontal restraint at the end was loaded uniformly over half of the span. Table 3 shows the results for different w using different numbers of elements. The values for 6 divisions seem to be away from the normal accuracy. This is possibly because of the length of elements not being exactly entered as $100/6$ in the data for computer program. In the data, instead of $100/6$ the length was taken as 16.6667 which caused the difference in the length of $16.6667 \times 6 = 100.0002 \Rightarrow$ difference = .0002.

The .0002 extension results in the axial force of $(.0002)(EA/L) = .2$ which may have caused the difference. As can be seen in Table 3, using double precision did not change the results significantly.

With no horizontal restraint at the end (referred to as the exact results in Table 3).

$$v_{\text{center}} = .651042 \times 10^{-2} w L^4 / EI \quad (a)$$

$$M_{\text{center}} = .0625 w L^2 \quad (b)$$

(3.6)



For a small load (W=1) the results from Table 3 are about 1%

Table 3 - Results for Case 3.2

# of elements	W=1			W=10			W=50		
	V _C	M _C	H	V _C	M _C	H	V _C	M _C	H
4	.675847	617.677	-10.788	4.50755	4052.46	-484.128	9.74334	8325.3	-2310.28
6	.658504	618.175	-10.3143	4.43921	4095.93	-481.573	9.63835	8416.02	-2322.75
8	.652249	618.178	-10.4073	4.4149	4111.76	-480.591	9.60418	8453.8	-2326.2
10	.649421	618.243	-10.353	4.40383	4119.42	-480.04	9.58889	8472.48	-2327.6
20	.645630	610.323	-10.2903	4.3890	4129.79	-479.271	9.56896	8498.47	-2329.29
4,6	.644630	618.573							
4,8	.644383	618.345	-10.2804	4.38402	4131.53	-479.412	9.55779	8496.63	-2331.51
6,8	.644206	618.182							
8,10	.644393	618.359	-10.2565						
10,20	.644366	618.350	-1026.94	4.38407	-479.015	-479.015	9.56232	8507.13	-2329.85
4,6,8	.644066								
6,8,10	.644498								
8,10,20	.644361	618.348	-10.2719						
4,8,10	.644395	618.361	-10.2519						
Double Precision									
4	.6758516810	617.677459	-10.7873779	4.5075603	4052.450	-484.1294	9.74332	8325.3049	-2310.279
8	.65224944	618.179029	-10.4063318	4.41490	4111.7507	-480.5910	9.6041376	8453.76837	-2326.211
				59488	5177	91654	220	950	68405
4,8	.64438207	618.34622	-10.279316	4.3840216	4131.51762	-479.41165	9.5577409	8496.5895	-2331.5224
Exact	.651042	625	one end on roller						
% dif	1.02%	1.06%							
4,8,10									

L=100
E=10
I=100
A=10

different from the exact ones obtained using formulas 3.6. Of course the non-linearity causes a small horizontal reaction which makes the two cases (Table 3 and formulas 3.6) slightly different.

3.3 Distributed Load

First a quarter circle with pinned ends and a vertical distributed load over the entire span was considered (Fig. 13).



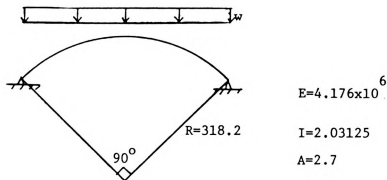


Fig. 13, Quarter Circle with Vertical Distributed Load

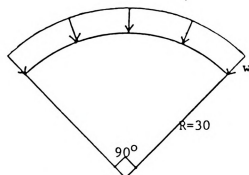
The loads on the two half lengths of the two elements adjacent to each node were taken as the concentrated load at that node.

Fig. 15 shows $W-V_c$ curve where V_c =vertical displacement of the crown. Fig. 16 shows some deflected shapes of the arch. Let W_b be the point where the symmetric and unsymmetric curves meet (buckling load), W_c be the critical load which is the max. value of w corresponding to the symmetric curve, and V_b and V_m be the corresponding vertical displacements of the crown. Table 4 compares the results obtained using this and other methods. As shown with extrapolation between 6 and 8 elements, the maximum difference between this and other procedures is about 2%.

Table 4- Comparison of The Results for Quarter Circle With
Vertical Distributed Load

No. of El.	$w_b R^3/EI$	% Difference With			$w_c R^3/EI$	V_b/R	V_m/R
		6El.	8El.	6,8			
6	15.27				25.55	.0125	.0845
8	15.5				26.98	.0127	.0875
6,8	15.78				28.83	.0130	.0914
(42)8El.	15.43	1%	1%	2%			
(2)	15.62	2%	1%	1%			

Next a quarter circle with pinned ends and radial distributed load was considered (Fig. 14).



$$E=10^7, I=.8789 \times 10^{-2}$$

$$A=.1875$$

Fig. 14. Quarter Circle With Radial Distributed Load

The load may or may not stay normal to the arch. It was again distributed among nodes as concentrated loads. Fig. 17 shows the load displacement curves for 8 and 10 element arch.

Table 5 compares the results for the case when the load stays normal to the arch. With extrapolation between 8 and 10 elements the difference is 6% from the one obtained by Wen and Lange(42) and .4% from that obtained by Timoshenko (37).



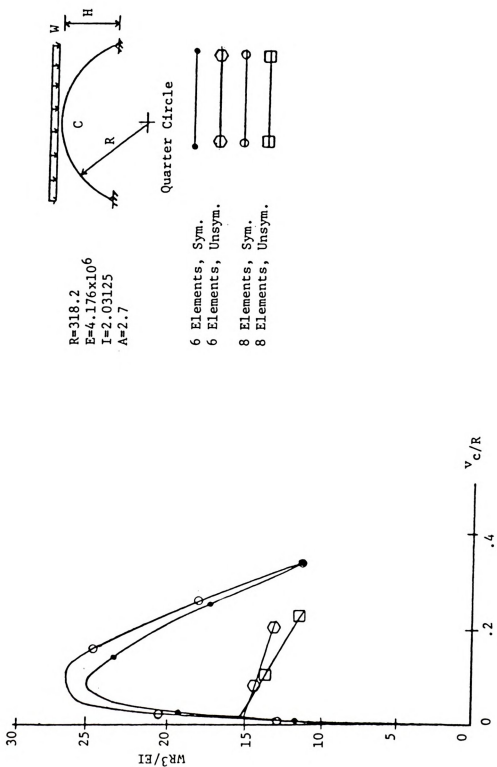


Fig. 15. Load-Displacement Curve for Vertical Distributed Load



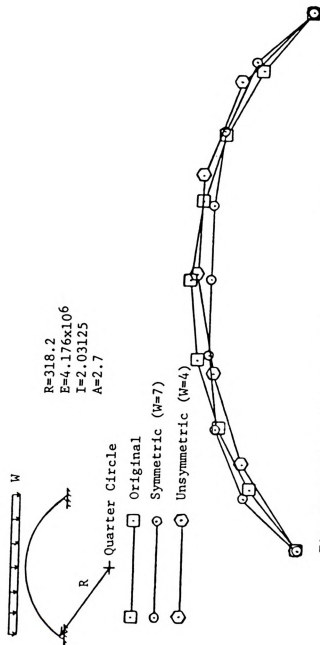
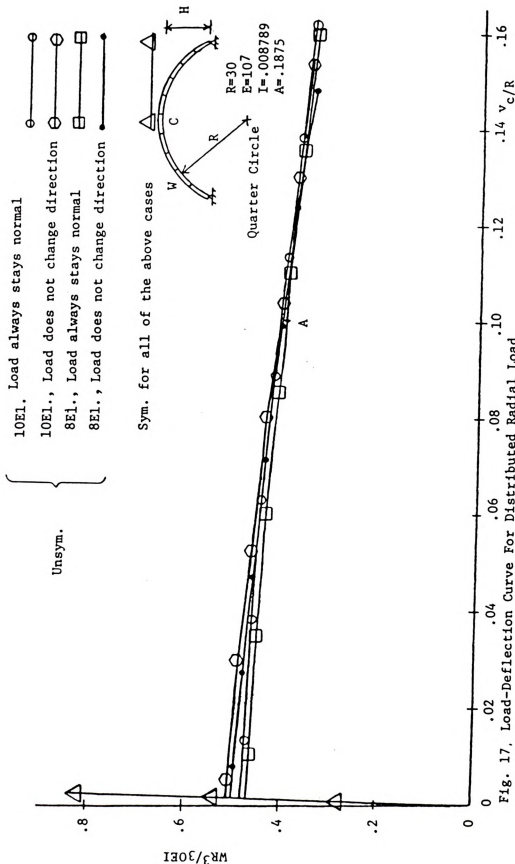
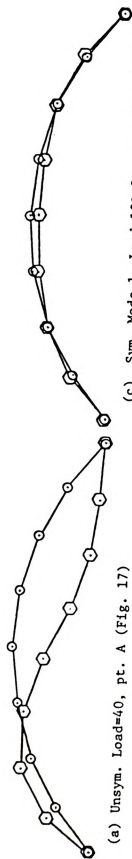


Fig. 16. Deflected Shapes of Arch With Vertical Distributed Load

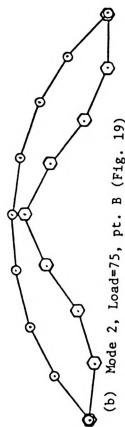








(c) Sym. Mode 1, Load=101.2, pt. A (Fig. 19)



(d) Mode 3, Load=104, pt. C (Fig. 19)

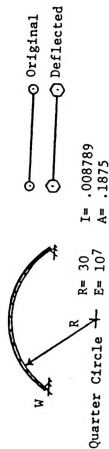
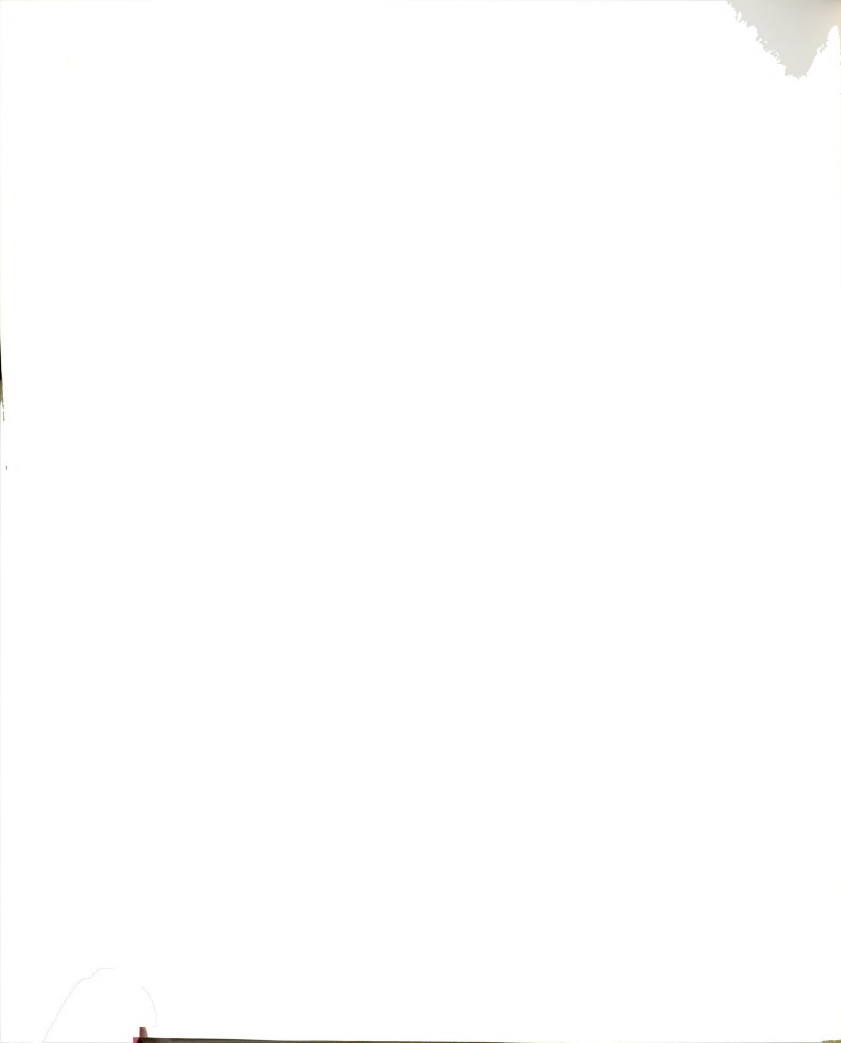


Fig. 18. Deflected Shapes of Arch with Radial Distributed Load



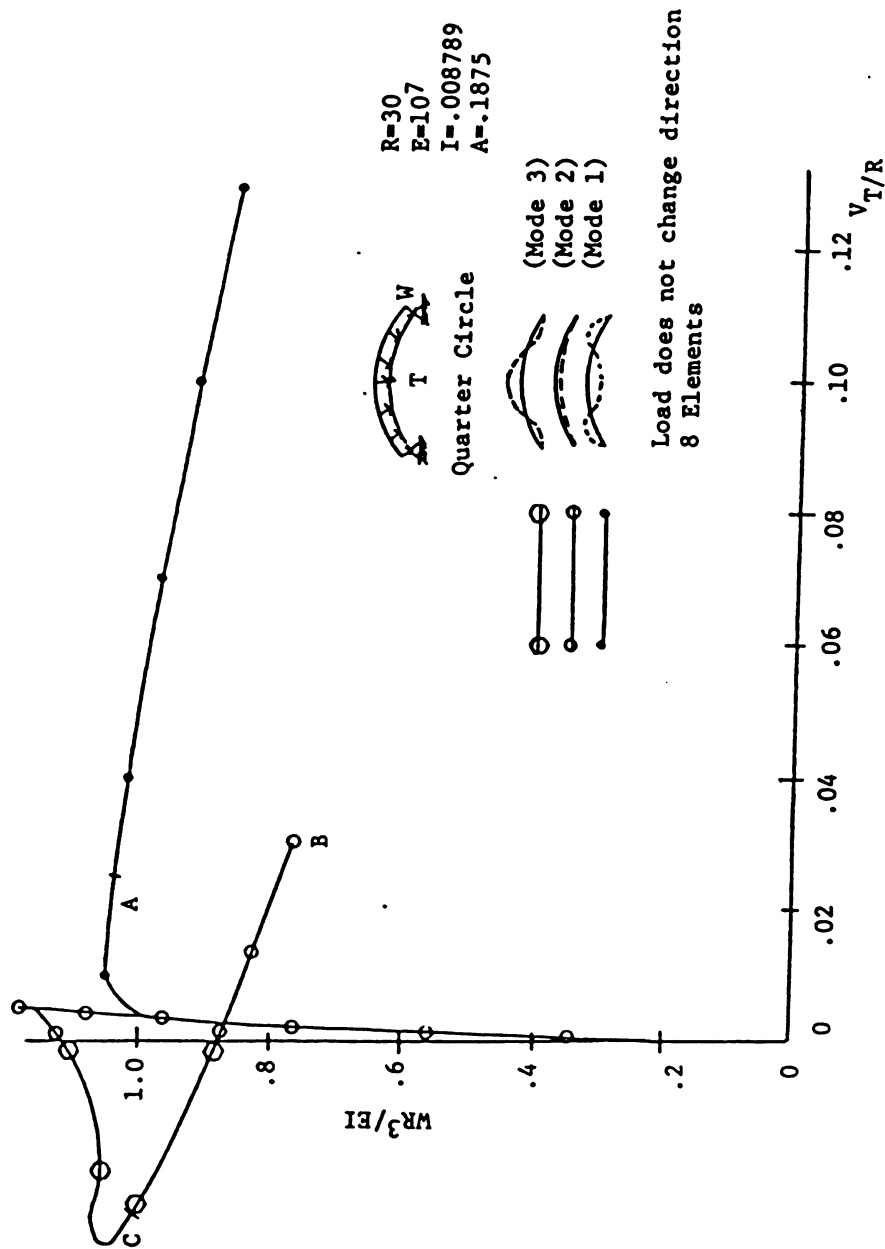


Fig. 19. Load - Deflection Curve

Table 5- Comparison of Results for Quarter Circle, Radial Dist. Load

No. of Elements	$\frac{w_N R}{30EI}$	% Difference With			$\frac{w_N R}{NN}$ 30EI	
		8 El.	10 El.	8,10		
8	.470	-	-	-	.503	N=Normal to Arch NN=Not Normal to Arch
10	.480	-	-	-	.51	
8,10	.498	-	-	-	.522	
(42)16El.	.5291	13%	10%	6%		
(37)	.50	6%	4%	.4%		

The deflected shapes are shown in Fig. 18 (a and b).

As can be seen, this case corresponds to one of the many modes of vibration. Fig. 18 (c and d) also shows the deflected shapes for 2 other modes of vibration. The corresponding load deflection curves are shown in Fig. 19.

3.4 Nonprismatic Parabolic Arch

The buckling of a nonprismatic parabolic arch, pinned at the ends and subjected to a uniform loading on a horizontal projection over the entire span was investigated for two different variations of the cross sectional area. In both cases the moment of inertia at a cross section is $I = I_c \sec \phi$ (3.7) where I_c = the moment of inertia at the crown; ϕ = the angle between the tangent to the arch axis and the horizontal (Fig. 20).

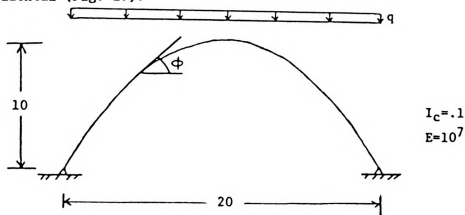


Fig. 20. Parabolic arch Under Uniform Load



The two variations of the cross sectional area are:

$$A = 10 I$$

$$A = 10,000 I$$

The rise-span ratio is taken as 0.5, that of a half circular arch.

The nodes were taken in such a way that they were on the arch axis and the lengths of the elements were equal.

Fig. 21 illustrates the deflected shapes of the arch. The load-crown vertical displacement curves are shown in Fig. 22. For the parabolic arch with uniform load, the axial forces are the main cause of displacement. As can be seen, the curves for the symmetric case do not have a decreasing segment. For the case of $A=10,000 I$, the symmetric curve is very close to a vertical line. The large cross sectional area causes small axial deformations and small displacement.

The critical values of the axial compressive force at the quarter points of the span can be expressed by the following equation, as is done by Austin (1).

$$P_e = \alpha \frac{EI}{S^2} \quad (3.8)$$

where

S = one half the length of the arch axis;

α = a coefficient.

The horizontal component of the thrust at buckling can be expressed as

$$H_e = P \frac{EI}{L^2} \quad (3.9)$$

where



L = span length; and

β = a coefficient.

The values of α and β obtained using this method are compared with the reference (1) values in Table 6. The 3 point extrapolation gives a very good set of results, specially for the case of $A=10I$. Part of the difference in the results can be due to the possible difference in the form of the variation of the cross-sectional area which is not specified in the reference literature.

Table 6 - Comparison of the Results for Non-Prismatic Arch

No. of Elements	$A=10 I$		$A=10^4 I$		$A=10 I$		$A=10^4 I$	
	α	%Diff. w/ Ref.	α	% Diff. w/ Ref.	β	% Diff. w/ Ref.	β	% Diff. w/ Ref.
6	11.423	1.70	11.078	4.66	14.522	3.19	14.3252	4.50
8	11.524	.83	11.277	2.95	14.788	1.41	14.5822	2.79
10	11.552	.59	11.3252	2.54	14.8665	.89	14.8301	1.07
6,8,10	11.5725	.41	11.3423	2.34	14.94	.40	15.4723	3.15
ref.(1)	11.62	-	11.62	-	15.0	-	15.0	-



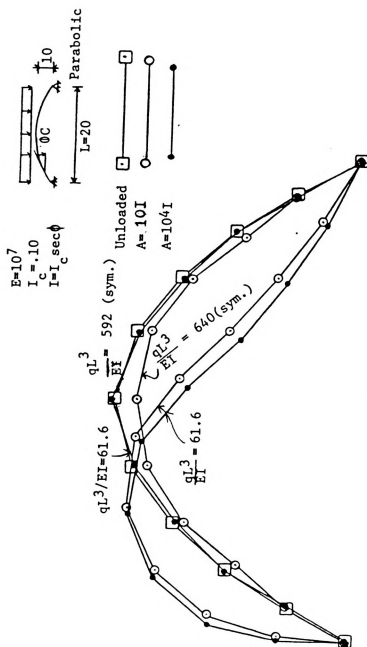


Fig. 21. Deflected Shapes of Non-Prismatic Arch

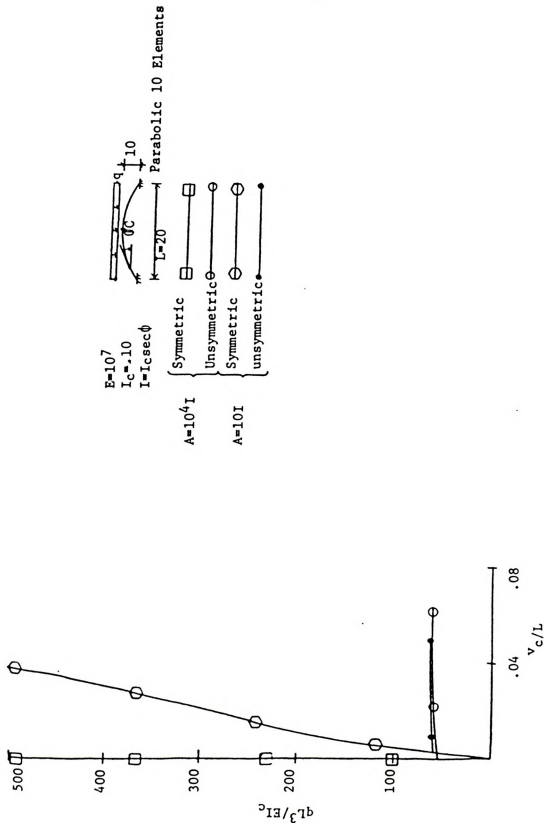


Fig. 22. Load - Displacement Curves for Non-Prismatic Arch

CHAPTER IV

EFFECTS OF CABLES AND PRESTRESSING

4.1 Cable Supported Arches

A slight modification in the program used for case 3.1 makes it possible to apply it to the cable supported arches. To keep it an in-plane problem, two cables, identical in property, length, and strength but on two opposite sides of the arch and symmetric with respect to the plane of the arch were attached to any desired node (Fig. 23).

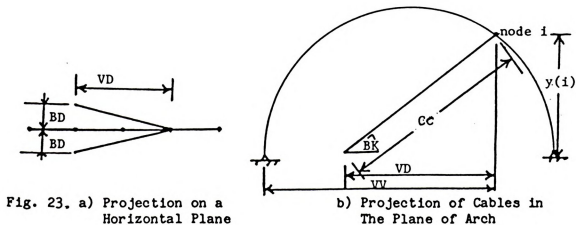


Fig. 23. a) Projection on a Horizontal Plane

b) Projection of Cables in The Plane of Arch



The symmetry would allow us to find the in-plane component of the axial force caused by extension in each cable and double it to find the total force due to the pair of cables on the node to which the cables are attached. The components of the cables axial forces in the direction perpendicular to the plane of the arch would be equal in magnitude but opposite in direction, therefore they cancel.

In the modified program, if there are any cables at a node, the coordinates of the node are found as if the cables did not exist. Having the new coordinates and VD (Fig. 23), new CC can be found.

$$CC = \left[VD^2 + y(i)^2 \right]^{1/2} \quad (4.1)$$

The new length of each cable is then equal to

$$CN = (CC^2 + BD^2)^{1/2} \quad (4.2)$$

So if CL = the original length of the cable, the change of length for each cable is (compression is positive)

$$CD = CL - CN \quad (4.3)$$

Now, if E_c and A_c are the cable modulus of elasticity and cross-sectional area, respectively, the axial force in each cable would be

$$CF = CD \cdot E_c \cdot A_c / CN \quad (4.4)$$

If θ_p = the angle between the cable and the arch plane, the components of CF of the two symmetric cables in the plane of the arch would be

$$CB = 2(CF) \cos(\theta_p) \quad (4.5)$$

Then CV and CH, the components of CB in vertical and horizontal directions are

$$CV = -(CB) \sin(\theta_k) \quad (4.6)$$

$$CH=(CB) \cos(BK)$$

(4.7)

These are added to the applied vertical and horizontal loads.

Having new forces, moment and axial deformation of the corresponding node and element can be found leading to the new coordinates of the node. Then, we proceed to the next node.

Note that cables are useless when compressed so they should be allowed to work in tension only.

To examine the effect of cables, a pinned-ends half circle arch with vertical and horizontal (wind) loads was studied.

With a vertical load at the crown and 16 elements, the program was tested for a set of weak cables. The critical load of 10.0 and the displacements agree well with the previously obtained results (in Table 2). Then the same arch with 4 elements and a set of strong cables at nodes 2 and 4 was studied. Fig. 24 shows the load-vertical deflection (of the crown) curves for cables with different cross sectional area or modulus of elasticity. As can be seen when the cables are strong, the pattern, in which after the critical load (right half of the curve) decreasing the load would increase the deflection, may not exist. Displacements are smaller and the critical load is bigger than without cables. When the cables are too strong, the corresponding node tends to stay where it was before loading. The neighboring nodes will be displaced large amounts, causing discontinuity, and therefore making convergence very hard or impossible. Fig. 25 shows the deflected arch.

The 4 element arch can not be a good representation of the problem because the arch together with the cables acts as a truss type



structure. For this reason an eight bar arch was considered.

The cables helped the structure by decreasing the deflection up to a limit load, P_L , smaller than, but close to the critical load, as can be seen from Fig. 26. At $P = P_L$, the cables cause an increase in the crown deflection up to a certain load after which the cables go into compression. Changing the position of the base of the cables did not improve it very much.

It was thought that this increased deflection was caused by the fact that for a large cross sectional area and after a certain deformation occurs, not much axial deformation is possible (compared with rotations) so the crown starts deflecting more as we add the cables. But with different cross sectional areas, the basic pattern still was unchanged (Figs. 26 and 27). However, it was noticed that the change in geometry due to the cables, for loads greater than P_L , increased the horizontal reaction causing larger moments therefore larger deflection as we add the cables.

As the number of elements increases, P_L gets closer to the critical load. As seen in Fig. 26, for 8 elements

$$P_L/P_c = 6.1/8.915 = .6842$$

and for 12 elements $P_L/P_c = 8.7/9.71 = .896$

Fig. 27 shows the deflected shapes of the arch with 8 and 12 elements. Figs. 28 and 29 show that changing the position of the bases of the cables or properties of the arch does not change the general behavior of the arch much. Figs. 30 and 31 show that with more cables the same pattern still exists (deflection of the crown increases with cables after a certain load P_L).

One of the main applications of cables is when wind forms an important part of the loads. Therefore, we now examine the behavior of the arch-cable combination under wind load.

The horizontal component of the wind on a circular arch is more important. For this reason, the horizontal load was considered even though it is just a matter of inputting the magnitudes of the vertical components as the vertical loads in the computer program to take into account the total effect of the wind loads.

A pair of concentrated loads were applied first. The two loads were equal in magnitude and opposite in direction, applied on two sides of the arch at the same position relative to the two supports to make it a symmetric problem. As expected, the lower part of the arch moves in and the upper part (including the crown) moves outward (Fig. 32).

The horizontal uniform load was distributed as concentrated loads among the nodes according to half of the total vertical length of the two elements adjacent to each node. These ratios are called wind load factor (LF). To increase the horizontal load, LF of each node is multiplied by a constant number. For 12 element arch the load factors for nodes 1-7 are 12.94, 25, 22.415, 18.7, 13.385, 6.825, and 1.785 (Radius of the half circle arch = 100).

Fig. 33 shows the LF - crown displacement (vertical and horizontal) curves without cables. The curve for LF - horizontal displacement of node 4 in a 12 element arch is also shown in Fig. 33. Node 4 follows the same pattern in terms of horizontal displacements except that they are bigger than the horizontal displacements of the crown for a certain load.

In Fig. 34 the LF - horizontal displacement curves with and without cables are shown. The load is scaled on the horizontal axis for a better illustration. The curves tend to approach a horizontal limit. Fig. 35 shows the deflected shapes of the arch for different loads, with and without cables.

As can be seen from Figs. 33 and 34, attaching cables would help the arch have less displacements and a greater horizontal limit of LF-displacement curve.

Therefore, when horizontal (or wind) loads are applied, cables are effective and useful.



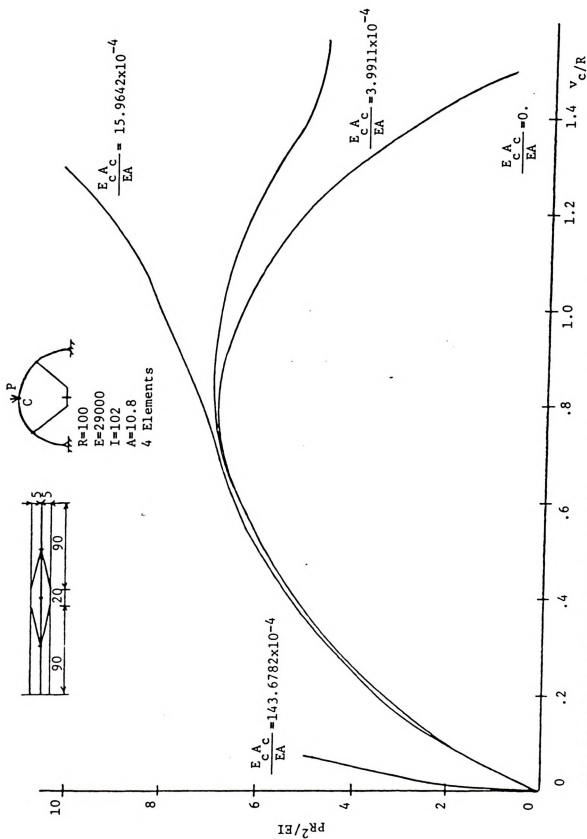


Fig. 24. Load - Deflection Curves for an Arch with Cables Having Variable Cross-Sections



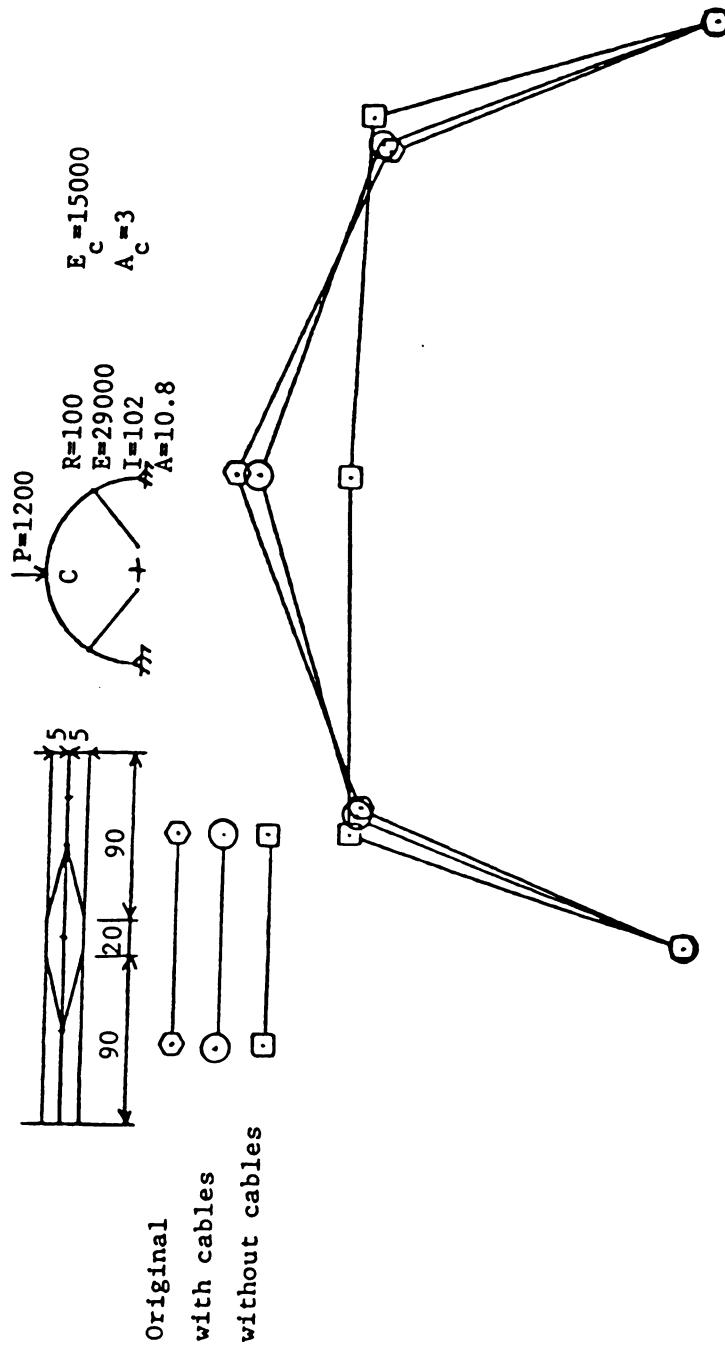


Fig. 25. Deflected 4 Element. Half Circle Arch



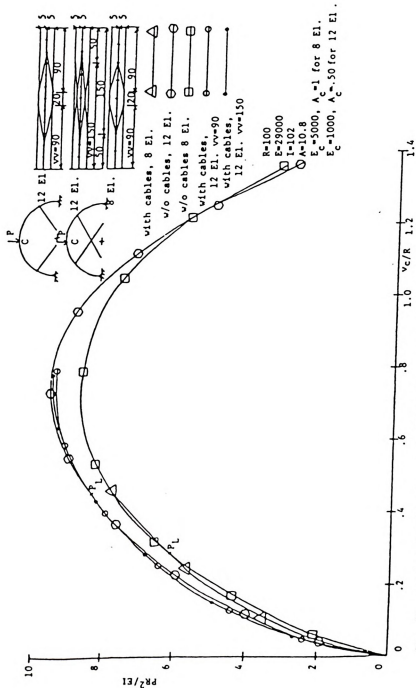


Fig. 26. Load-Deflection Curves for Half Circle Arch, 8 and 12 Elements



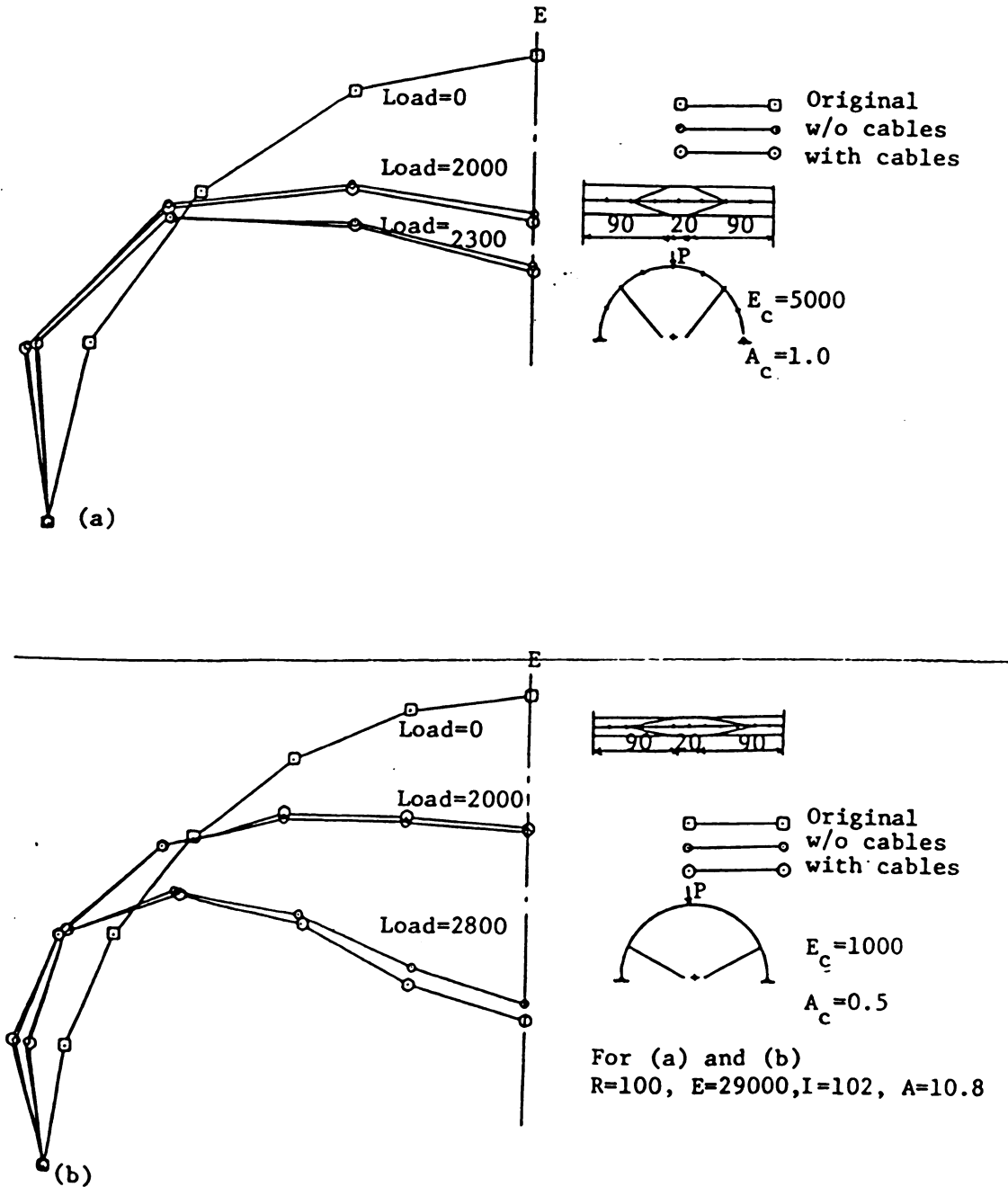


Fig. 27. Deflected Shapes of Arch, Different Number of Elements



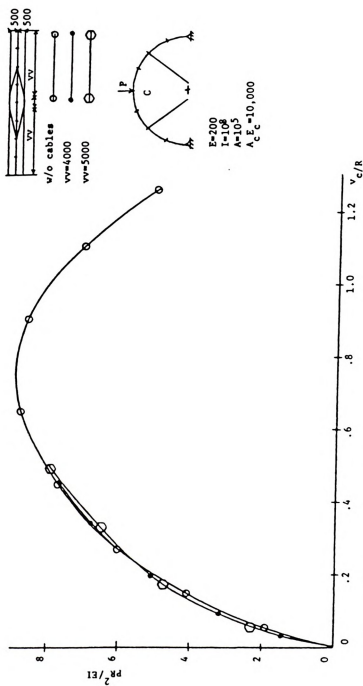


Fig. 28. Different Cable Base Position

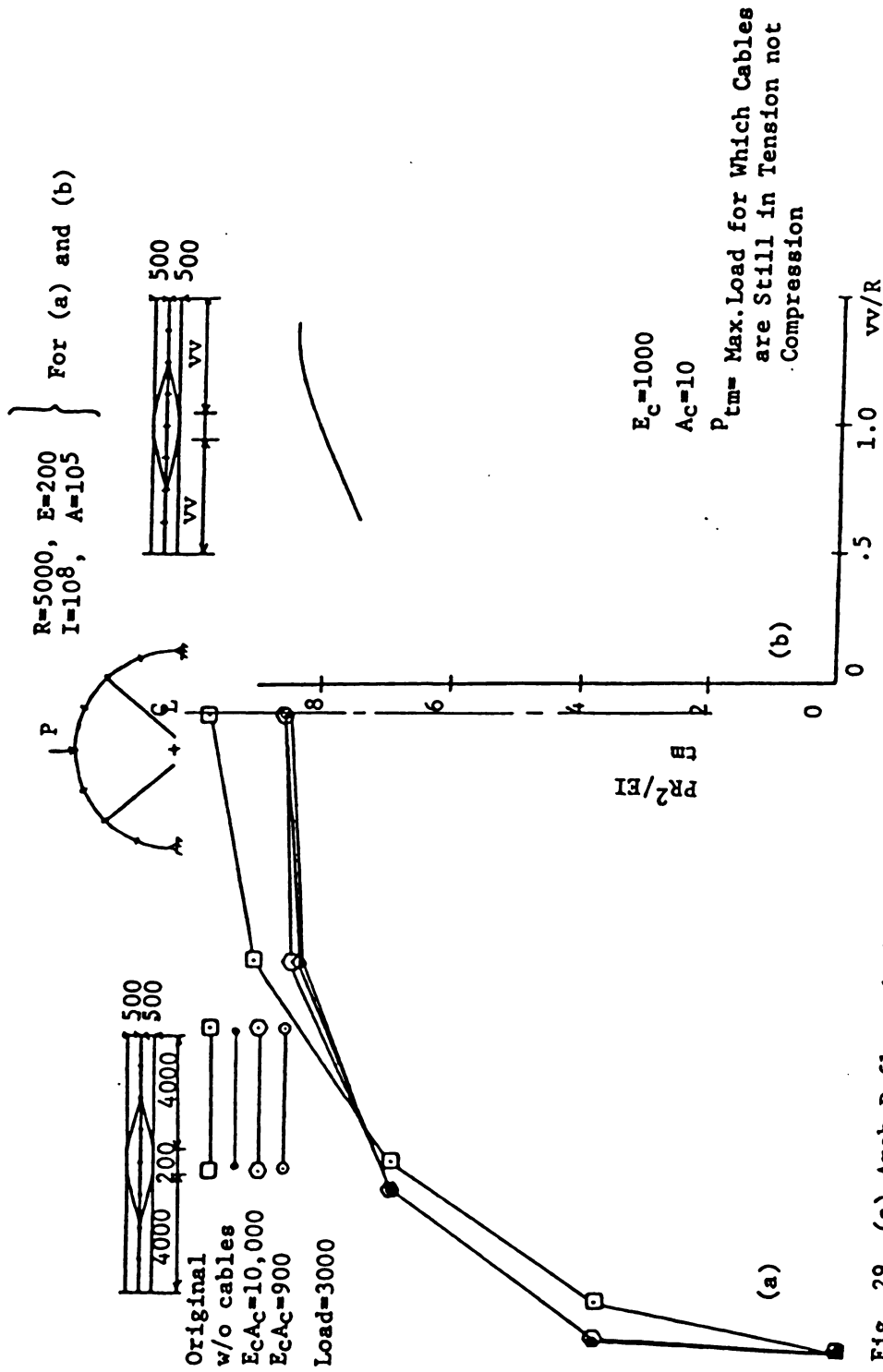
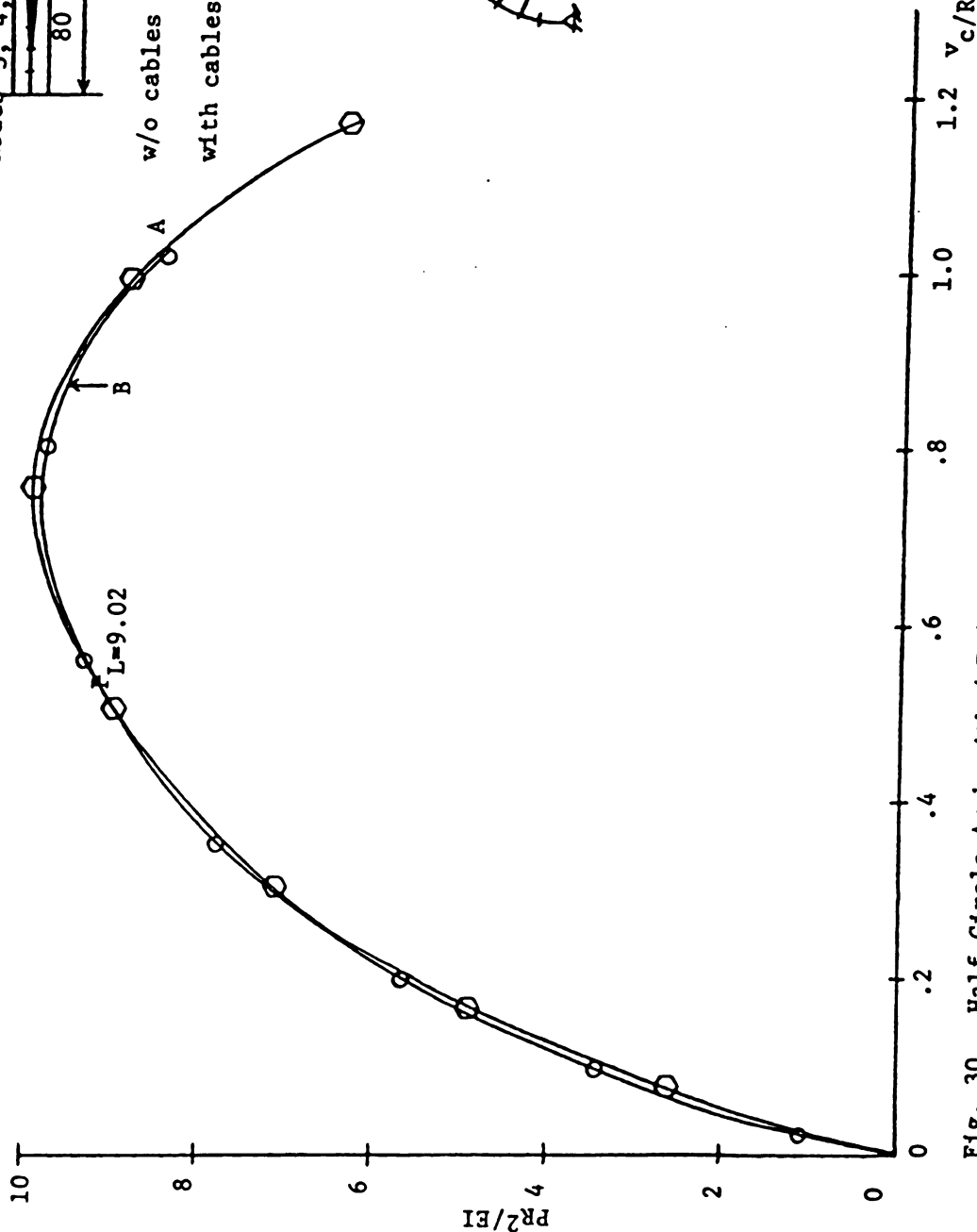
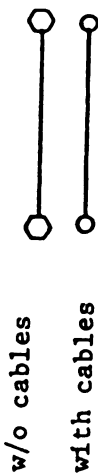
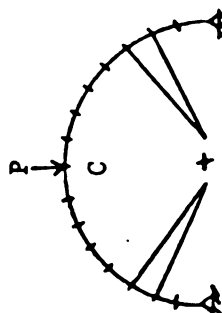


Fig. 29. (a) Arch Deflected Shape
 (b) Effect of Cable Base Position

16 Elements, 4 Pairs of Cables at
Nodes 3, 4, 14, 15



-51-



$R=100, E=29000$
 $I=102, A=10.8$
 $E_c=1000, A_c=0.5$

Fig. 30. Half Circle Arch with 4 Pairs of Cables

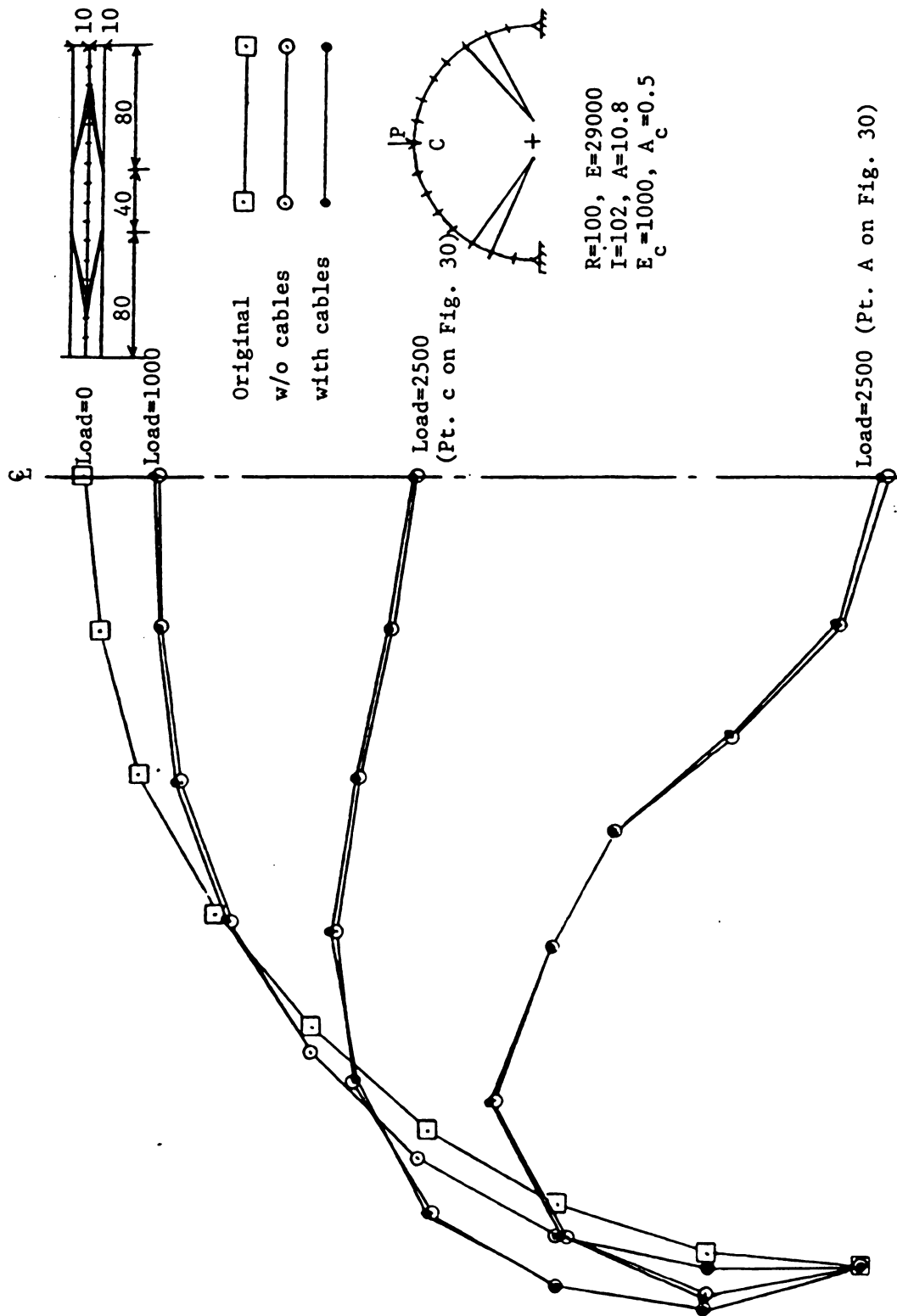


Fig. 31. Deflected Shapes of Arch with 4 Pairs of Cables



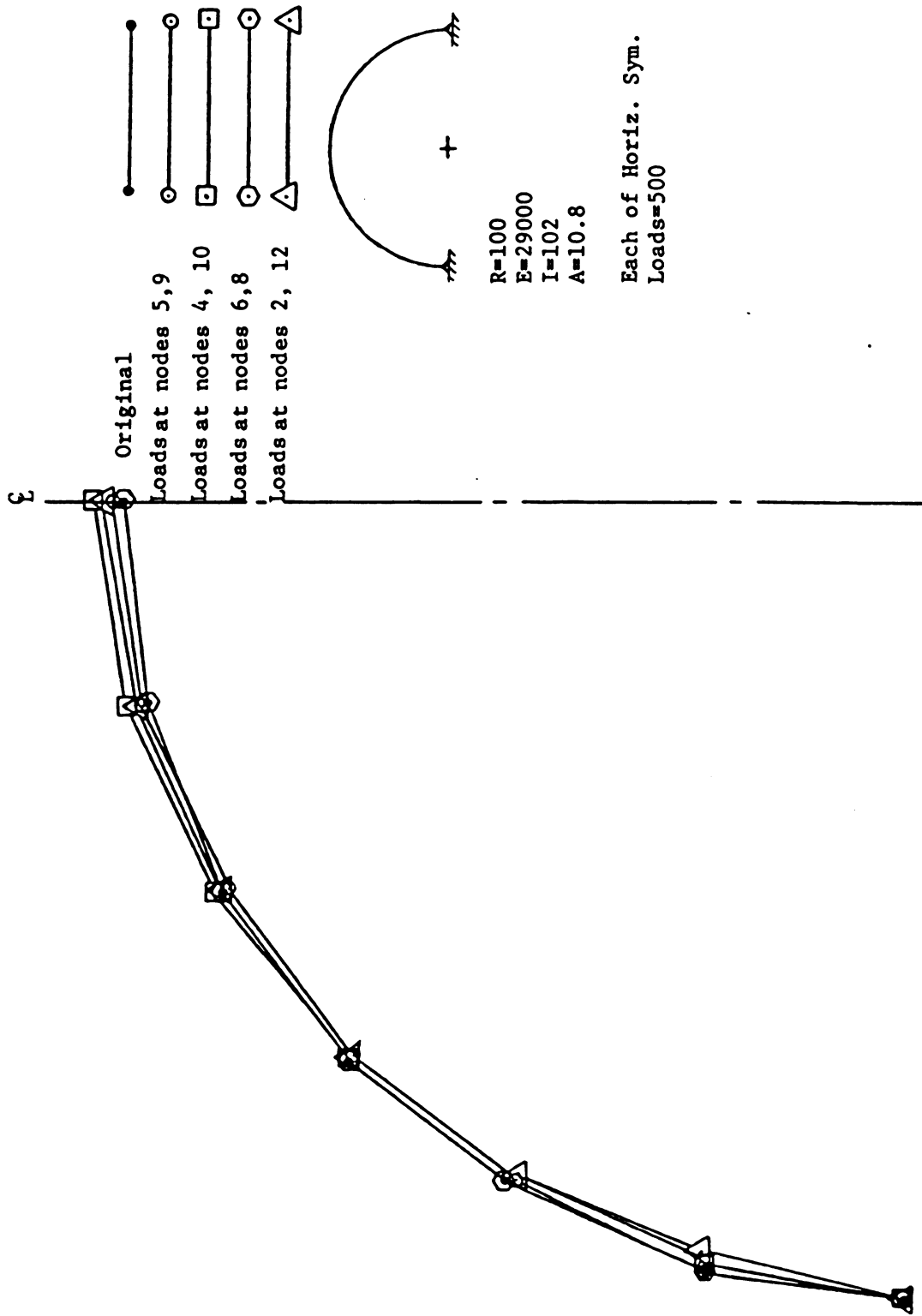


Fig. 32. Arch Deflected Shapes, Horizontal Loads at Different Nodes, No Cables



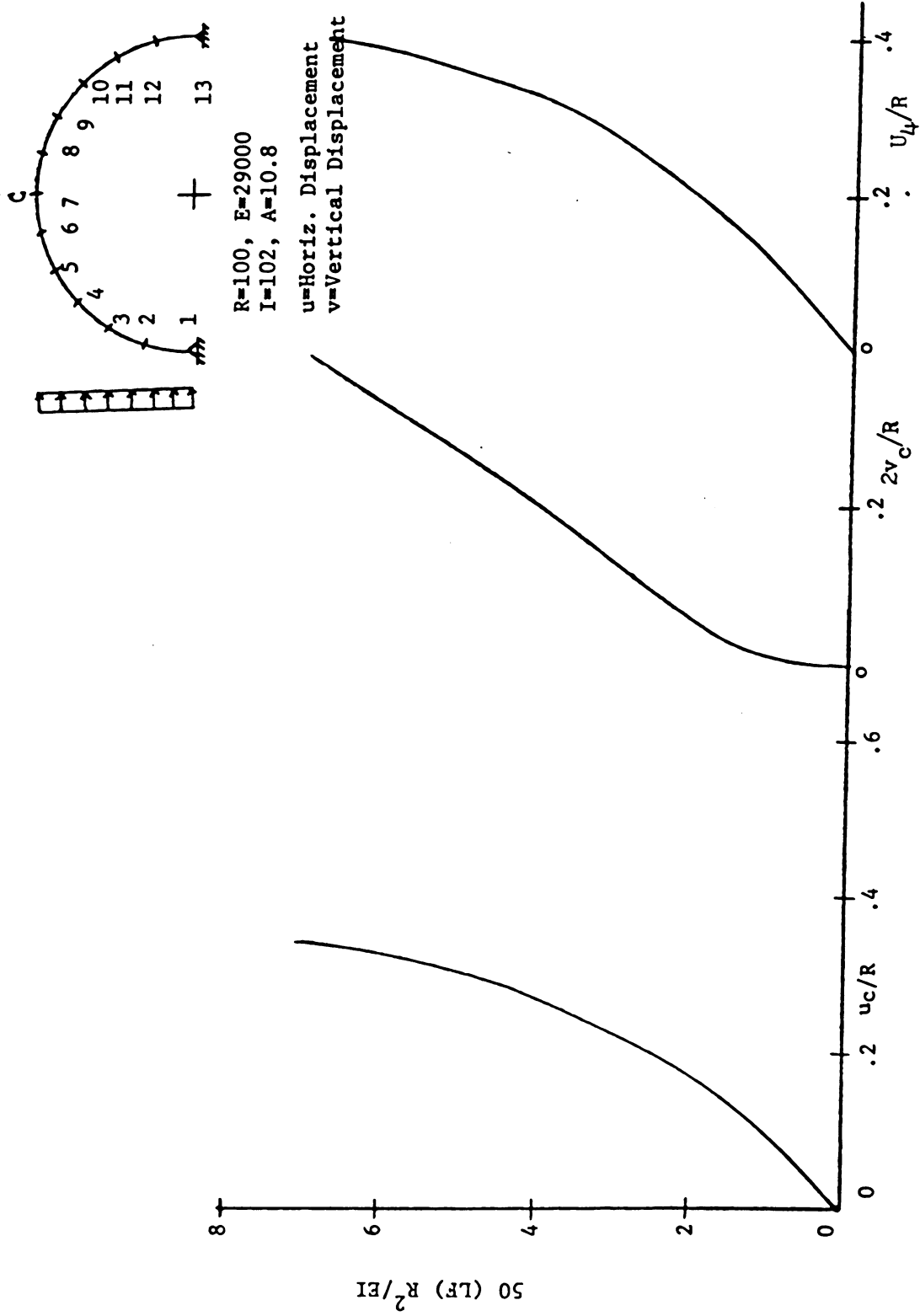


Fig. 33. LF - Displacement Curves



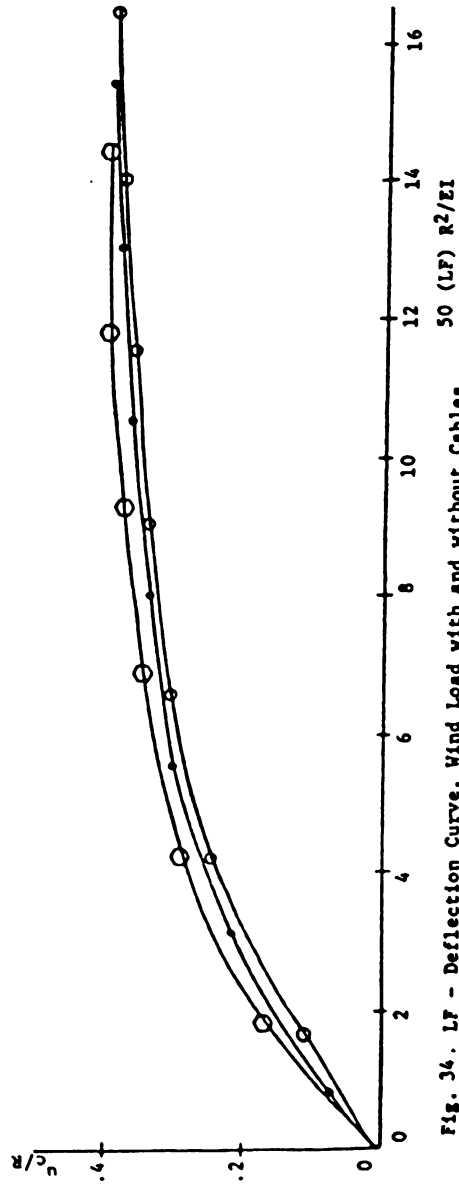
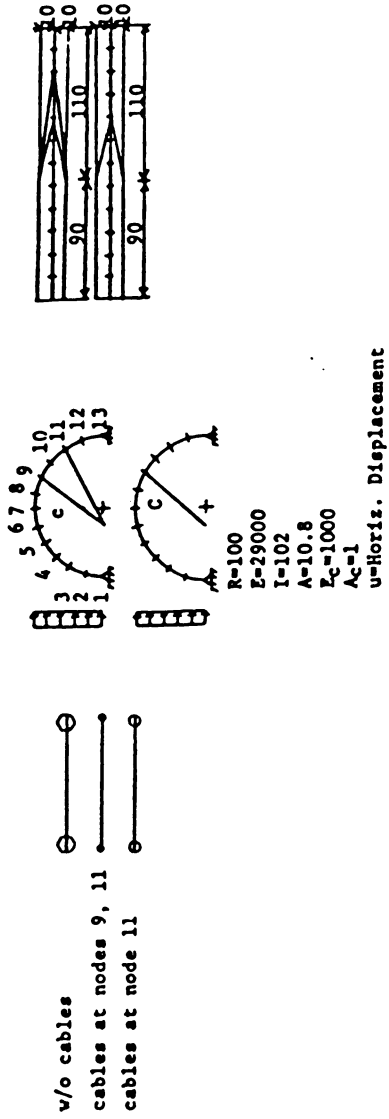


Fig. 36. LF - Deflection Curve, Wind Load with and without Cables

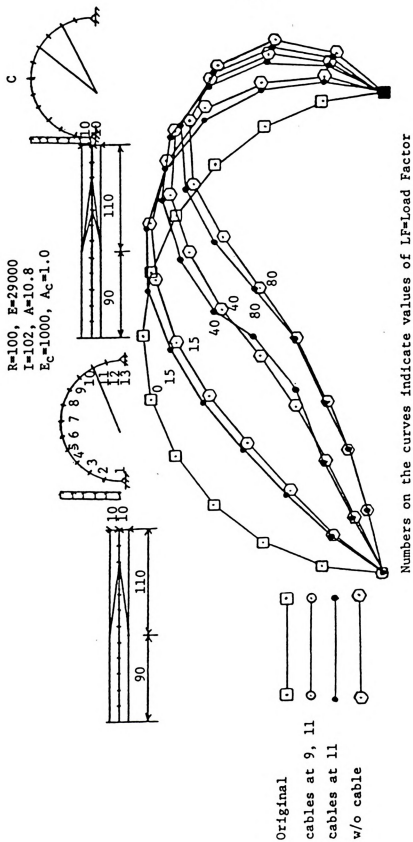


Fig. 35. Deflected Arch under wind Load, with and without cables

4.2 Prestressed Arch

A straight bar may be bent into an arch, then fixed and loaded. To take the effect of this prestressing into account, we have to find the prestressing moment, M_o , and add it to the moments at the nodes.

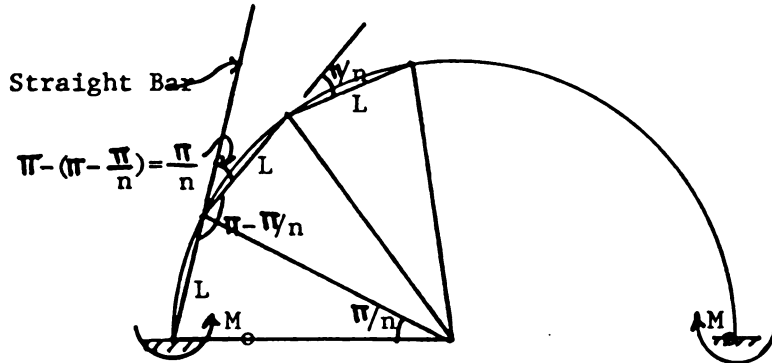


Fig. 36, Prestressing The Straight Bar Into An Arch

If n =number of elements, then the angle between element $i+1$ and i would be π/n (Fig. 36). To form this angle, the prestressing moment M_o is applied.

$$M_o = \frac{\pi}{n} \frac{EI}{L} \quad (4.8)$$

Then if GR =rotation of the first element due to the applied load, the moment at node 1 is

$$M(1) = M_o + (GR) \frac{EI}{L/2} \quad (4.9)$$

For a typical node i , if SF =shear force

$$M(i) = M(i-1) + SF(i-1) L(i-1) \quad (4.10)$$

Because M_o is included in $M(i)$, $\Delta\theta(i)$ in Fig. 3 would now include SC also.

Note that for an unprestressed arch with fixed ends, at node 1 we will still have a rotation, GR , in the first half of element one which is lumped at node one. But this GR is related to the moment at the first node through the following formula:



$$M(1) = (GR) \frac{EI}{L/2} \quad (4.11)$$

The rest of the program is the same as for the pinned end arch except the error term in the right support corresponding to rotation is

$$EM = M(n+1) - M_o - [\theta_N(n) - \theta(n)] \left[\frac{EI}{L/2} \right] \quad (4.12)$$

where

$$\theta_N(n) = \theta(n) + \Delta\theta(n) \quad (\text{Fig. 3})$$

An 8 element arch was studied. As shown in Figs. 37 and 38, fixing the supports will not help increasing the critical load compared with pinned supports but will reduce the displacements significantly.

Prestressing the arch will not change the forces and displacements but it will change the moments at the nodes. With different modulus of elasticity of the arch, the same behavior was observed.

Next, a fixed length bar was bent into arches with different central angles (α) and span s . It was then fixed at the two ends and loaded vertically at the crown with a load of 500. Table 7 shows the resulting maximum moment for 4, 6, and extrapolation between 4 and 6 elements. The length of the straight unloaded bar is $5000 \pi = 15707.9633$.

The optimum case is when prestressing starts decreasing the maximum moment in absolute value sense. The optimum value for α is shown in Table 8 which is obtained using Table 7.

As can be seen at $\alpha < 14.1$, the max, prestressed moment is smaller in absolute value than the max, non-prestressed moment for the load = 500.



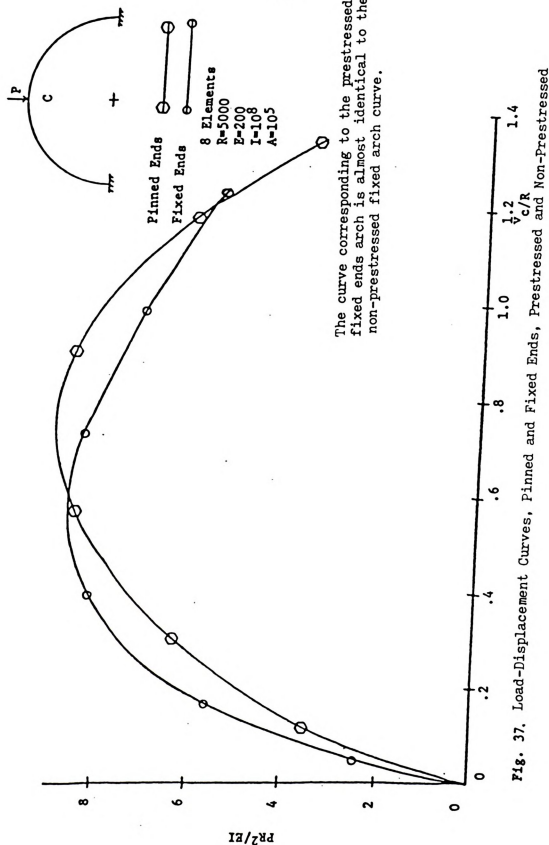
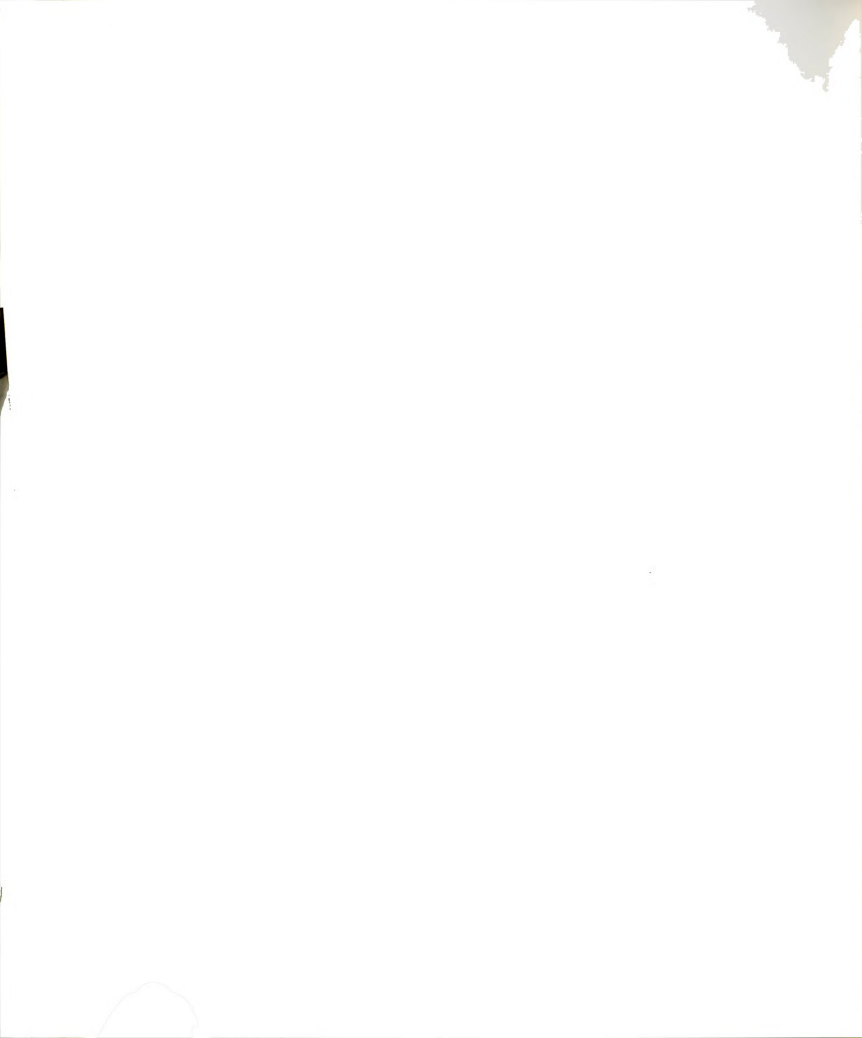


Fig. 37. Load-Displacement Curves, Pinned and Fixed Ends, Prestressed and Non-Prestressed



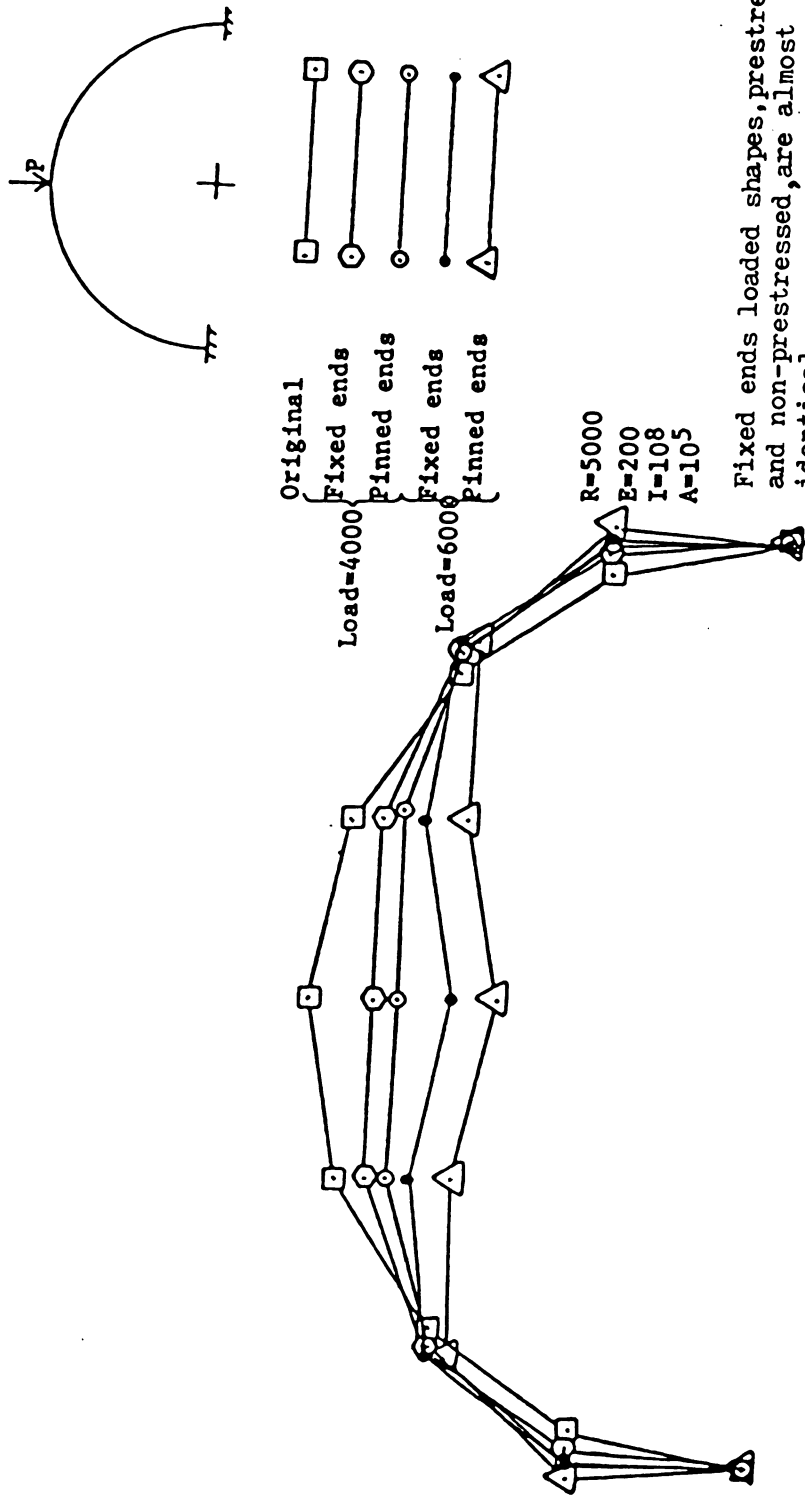
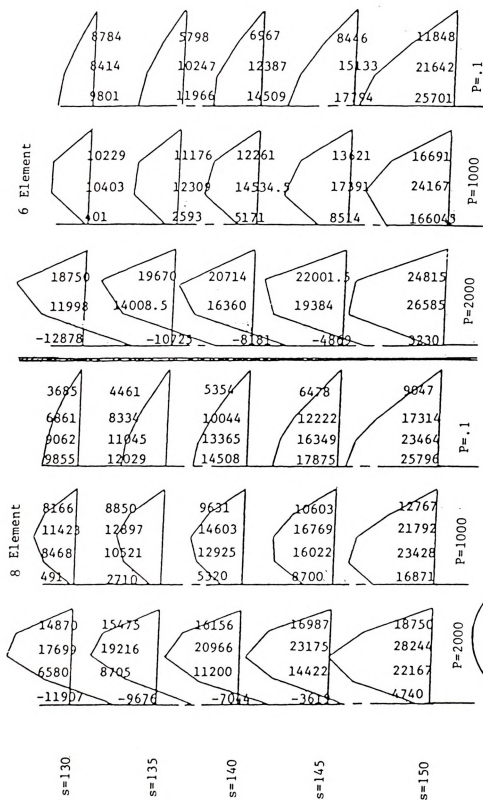


Fig 38. Deflected Prestressed Arch





Circular arcs with fixed length, 150.6 varying chord lengths, s ,
 prestressed into arches with span=100, pinned & loaded

Fig. 39. Moment diagrams for Prestressed Arch, $E=10^4$, $I=100$, $A=10$

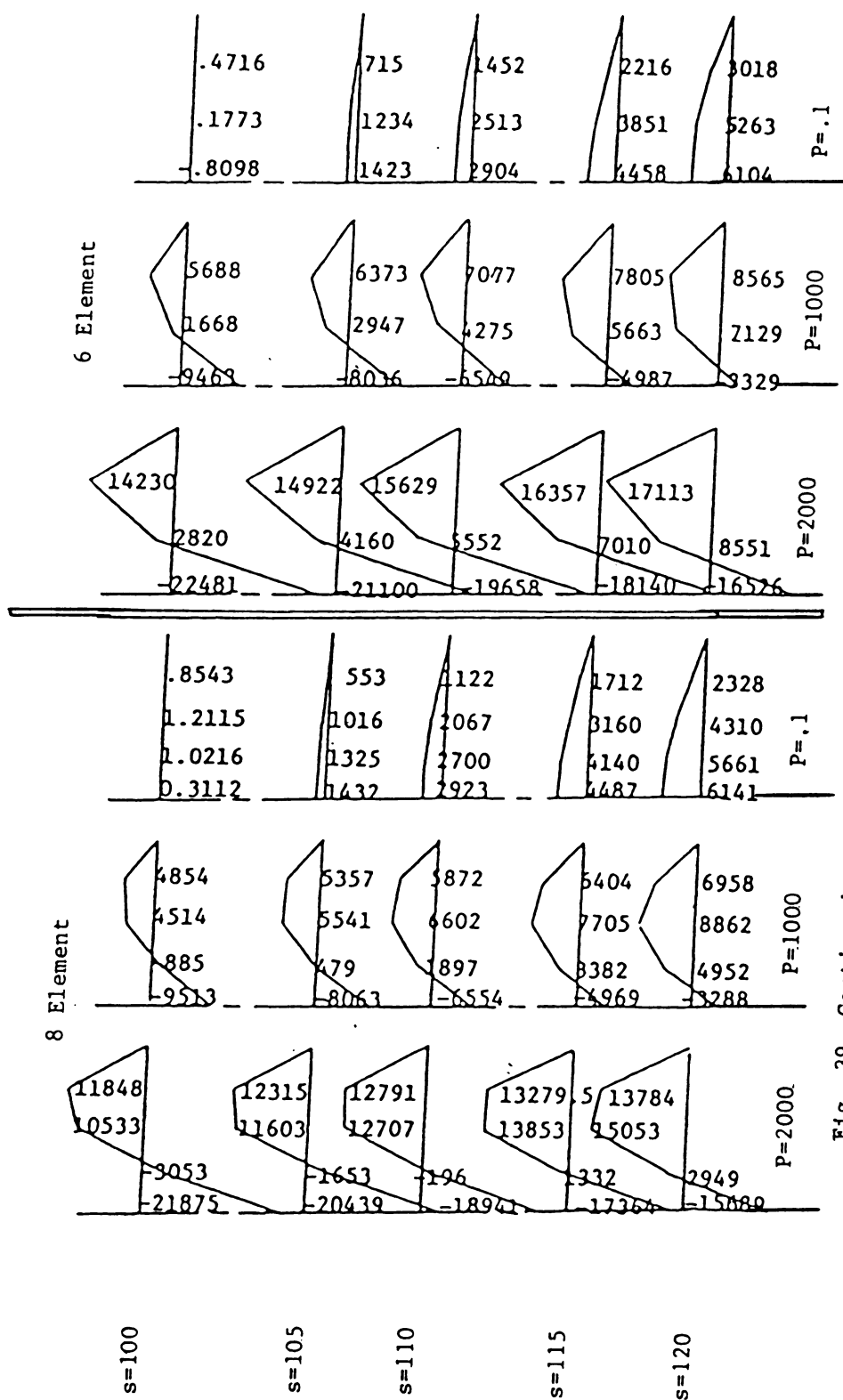


Fig. 39. Continued



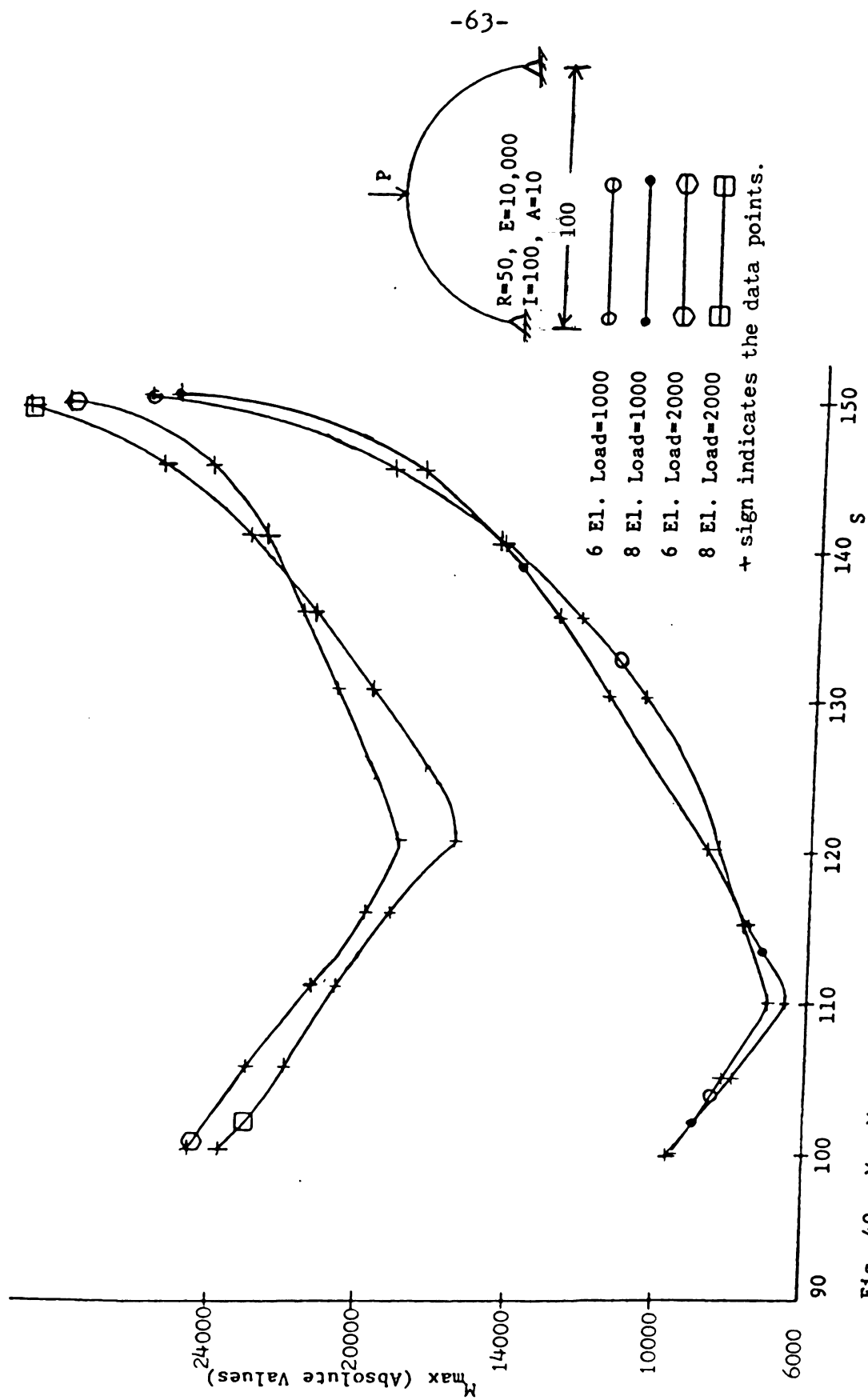


Fig. 40. Max. Moment vs. Span Curves for a Half Circle Prestressed Arch



Table 7- Max. Moment for Straight Bar Bent Into Arch With $E=200,1 \times 10^8$
 $A=10^3$, Load=500

α deg.	Max. Non-Prestressing Moment			Max. Prestressing Moment		
	4 el. at node 3	6 el. at node 4	4,6	4 el. at nodes 2,4	6 el. at nodes 2,4	4,6
180	-361367	-381801	-398148.2	4.35682E6	4.22677E4	4.12273E6
126	-369780	-385876	-398752.8	2.9448E6	7.86022E6	2.792556E6
90	-382609	-393219	-401707	2.26413E6	2.1885E6	2.127996E6
30	-583679	-492641	-419810.6	1.00837E6	901374	815777.2
25	-723215	-540395	-394139	952391	816562	707898.8
23	-857666	-	-	955124	-	-
22.17	-972435	-	-	972404	-	-
22.15	-	-976455	-	-	973131	-
20	-	-651833	-	-	769356	-
17.78	-	-817271	-	-	817869	-
17.7	-	-817271	-	-	818620	-
17.5	-	-857532	-	-	827265	-

Table 8 - Optimum α for the Prestressed Arch of Table 7.

No. of Elements	Optimum in Degrees	Max. Non- Prestressed Moment	Max. Pre- Prestressed Moment
4	22.17	-972435	972404
6	17.7	-818899	818620
4,6	14.124	-696070.2	695592.8

Finally, circular arcs of fixed length of 150 and varying chord lengths, s , was prestressed into arches with a span of 100. Then the ends were pinned and the arch was loaded at the crown with a vertical load. The program used is the same as the one used for problem I, except in the data processing the coordinates of the nodes of the arches with different spans were inputted and the span was set equal to 100 for all arches in the calculations.

Fig. 39 shows the max moments for 6 and 8 element arches. Fig. 40

is obtained using Fig. 39 to plot the absolute values of the max. moments vs. the original span. From this, Table 9 was obtained. This shows that the values of s for which the maximum moment is the lowest, are 111.14 and 122.79 for the loads of 1000 and 2000, respectively. The corresponding values of moment are 5975 and -13854, respectively.

Table 9 - Optimum Span and Max. Moment for the Prestressed Arch of Fig. 40

No. of Elements	Optimum Span		Optimum Max. Moment	
	Load=1000	Load=2000	Load=1000	Load=2000
6	110	120.5	7077	-17100
8	110.5	121.5	6595	-15680
6,8	111.4	122.79	5975	-13854

4.3 Prestressing by Axial Force

In section 4.2 an arch prestressed by moments applied at the ends was studied. In this section, a study is made of a straight bar compressed axially to form an arch. Then the arch is fixed at the ends and loaded (Fig. 41). For the comparative unprestressed case, a parabolic arch is approximated by a set of elements whose ends are located on the parabola with the same span as the prestressed arch. Ratios of H/L = 0.125, 0.375, and 0.5 were used. The locations of the nodes were found using a trial and error method to solve a set of equations resulting from setting the lengths of the elements equal. For the prestressed case, an initially straight bar was used with a length equal to the number of elements times the length of each element as found in the parabolic unprestressed case. Then the program was run for the



straight bar ($\theta=90$ for all elements) with a unit load at the crown. If this small load is not applied, the vertical reaction would be equal to zero and in the iteration procedure a division by zero would result. After convergence, the new shape is loaded and the program run to give the final prestressed loaded shape, axial forces, and moments.

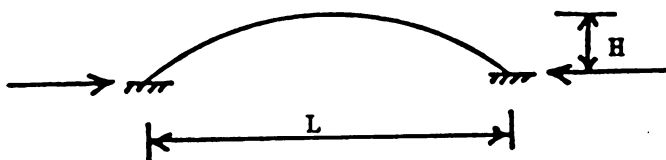
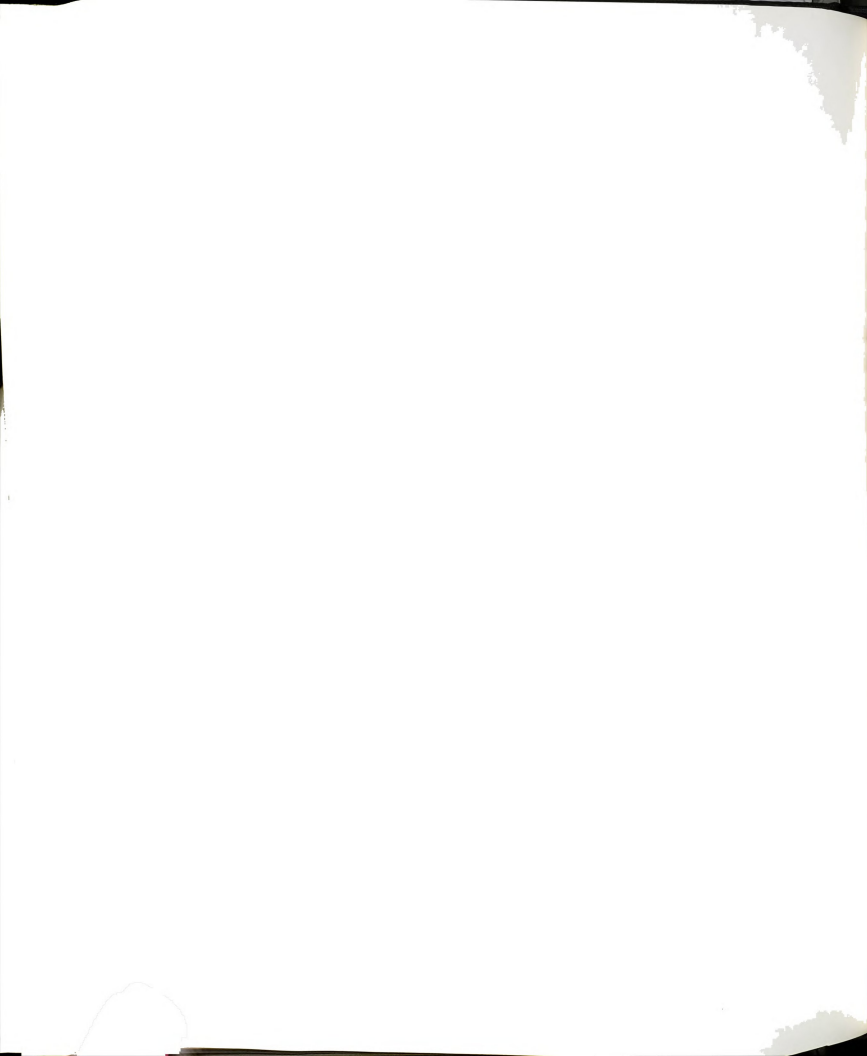


Fig. 41 - Prestressed Arch, By Axial Force

The load vs. vertical crown displacement curves are shown in Figs. 42-50 for 3 different loadings: vertical concentrated load at the crown, uniform load over the entire span, and uniform load over half of the span. Three ratios of H/L were studied: 0.125, 0.375, and 0.5. Figs. 54 and 55 show the deflected shapes. These figures also show the curves and shapes corresponding to the parabolic arch with the same span, non-prestressed and fixed at the ends. As can be seen from these figures, prestressing the arch causes greater displacements and smaller buckling loads (Table 10). Table 10 and Fig. 52 also show that the maximum axial forces corresponding to the loading conditions stated in Fig. 51 get larger with prestressing. This would be expected since the prestressing process produces an initial force.

The moment diagrams for certain loads smaller than the buckling load are shown in Fig. 51. Again, prestressing increases the maximum moments. For these loads the moments for 8 and 10 elements are within less than 7% difference. These are shown in Table 11.

It can be seen that the non-prestressed arch is more desirable. Thus, although there may be constructional advantages in forming



lightweight curved frames by using an initially straight bar, the moments and axial forces are greater than for an initially curved bar with the same loadings and the same span.

Note that the loads in Table 10 for concentrated loads correspond to the peak values of the symmetrical load-displacement curve, since the bifurcation to an unsymmetrical mode could not be found. This agrees with Masur's results (33) that the symmetric case always governs. Therefore, the peak values of the symmetrical part of the curves are entered in the table. However, as shown in Fig. 42, unsymmetric equilibrium modes were found. These do not correspond to bifurcation loads found in the pinned end arch and will not lead to finding the buckling loads.

It should also be noted that the peak values and the bifurcation loads were found using the polynomial process described in section 3.1.

Fig. 53 compares the unloaded shapes of the non-prestressed arch and the prestressed parabolic one.

Table 10- Buckling Loads

H/L	Loading Condition	Buckling Load	
		$\frac{PL^2}{EI}$ Concent.	$\frac{qL^3}{EI}$ Uniform
		Non-Prest.	Prest.
.5	(a)	51.57	37.51
	(b)	193.15	78.65
	(c)	128.15	100.00
.375	(a)	48.95	38.92
	(b)	222.10	93.50
	(c)	132.05	107.92
.125	(a)	22.97	22.50
	(b)	64.50	60.55
	(c)	75.30	70.50

(a) Crown Concentrated (b) Uniform Over Entire Span
(c) Uniform Over Half of The Span

Table 11 - Max. Moments and Axial Forces

H L	Type of Loading	Intensity of Load $\frac{PL_2}{EI}$ Coeff. $\frac{PL_3}{EI}$ Uniform	Max. Abs. Values of the Moments $\frac{W}{PL_2}$ Concomit. $\frac{W}{QL^2}$ Unif.						% diff. $\frac{8.10}{8.10}$		Max. Axial Force $\frac{S}{QL}$ Unif.	
			Non-Prestressed			Prestressed			Non-Prest.	Prest.	Non-Prest.	Prest.
			8	10	8, 10	8	10	8, 10				
0.5	Concentrated at crown	12.00	.05441	.05478	.05545	.20324	.19967	.19334	1.91	4.87	.6731	1.0524
	Uniform entire span	48.00	.00001	.00001	.00001	.04603	.04633	.04687	0.0	1.83	.5198	.5695
	Uniform half span	48.00	.01822	.01800	.01762	.06327	.06259	.06137	3.32	3.00	.3673	.4373
	Concentrated at crown	16.00	.05603	.05567	.05503	.14420	.14781	.15423	1.79	6.96	.7851	1.1633
.375	Uniform entire span	80.00	.00001	.00001	.00001	.02618	.02647	.02699	0.0	3.10	.5616	.6140
	Uniform half span	24.00	.01511	.01527	.01555	.10384	.10543	.10825	2.94	4.25	.3818	.5532
	Concentrated at crown	8.00	.05459	.05379	.05236	.14081	.14020	.13891	4.09	1.35	1.932	3.0233
	Uniform entire span	48.00	.00011	.00011	.00011	.02943	.02884	.02780	0.0	5.55	1.0935	1.2075
.125	Uniform half span	32.00	.01893	.01896	.01903	.04753	.04673	.04529	.53	4.72	.5881	.8344



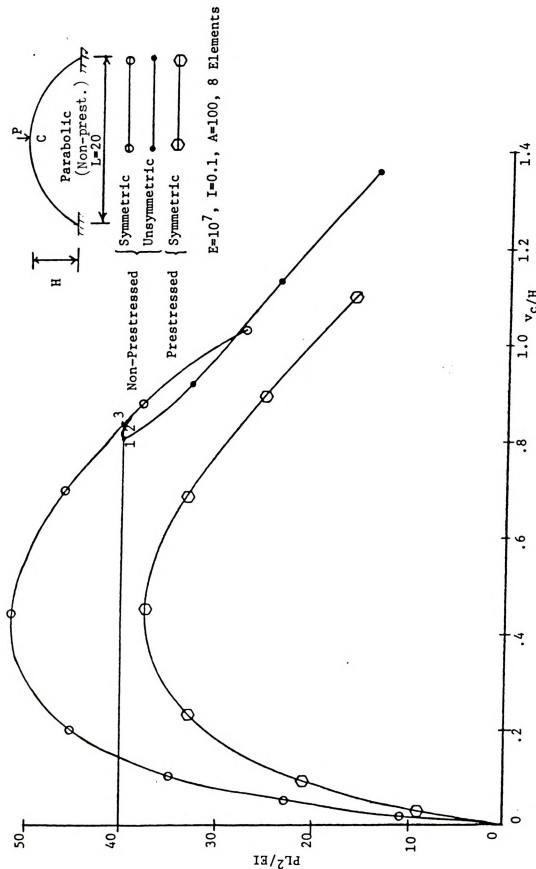
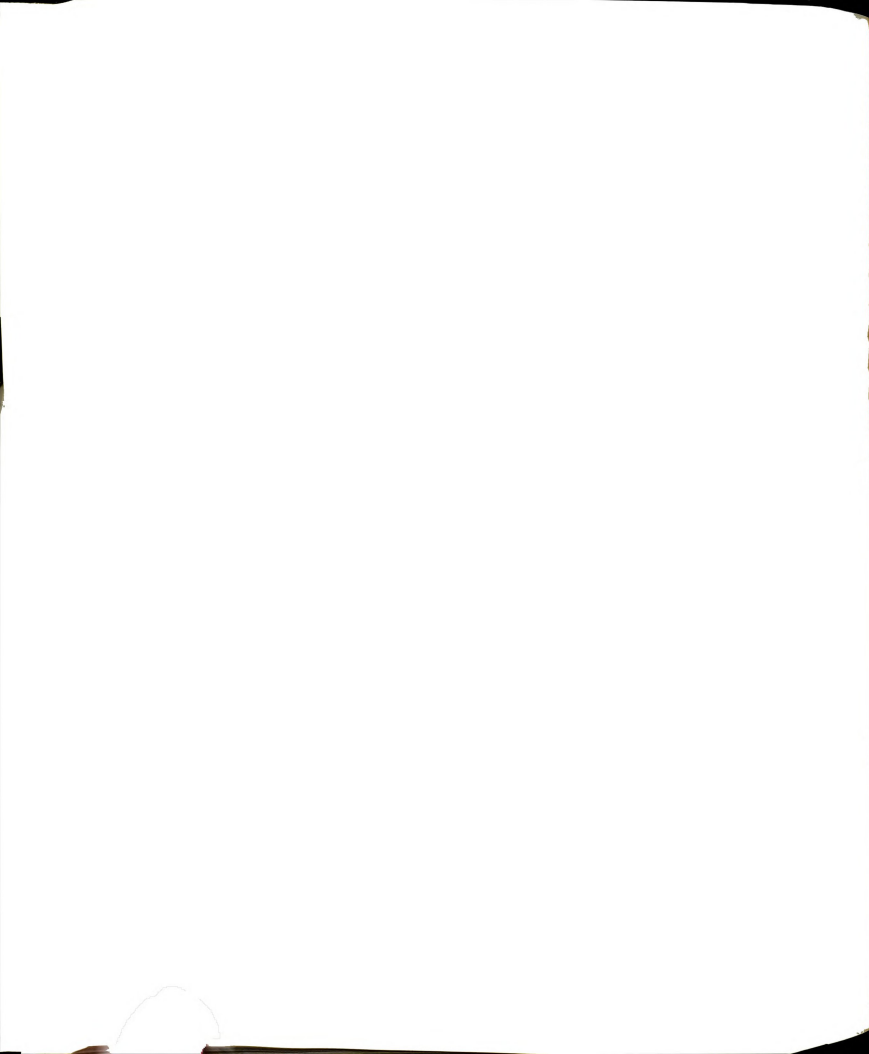


Fig. 42. Load - Displacement Curves for Concentrated Load, $\frac{H}{L} = 0.5$
Prestressing by Axial Force



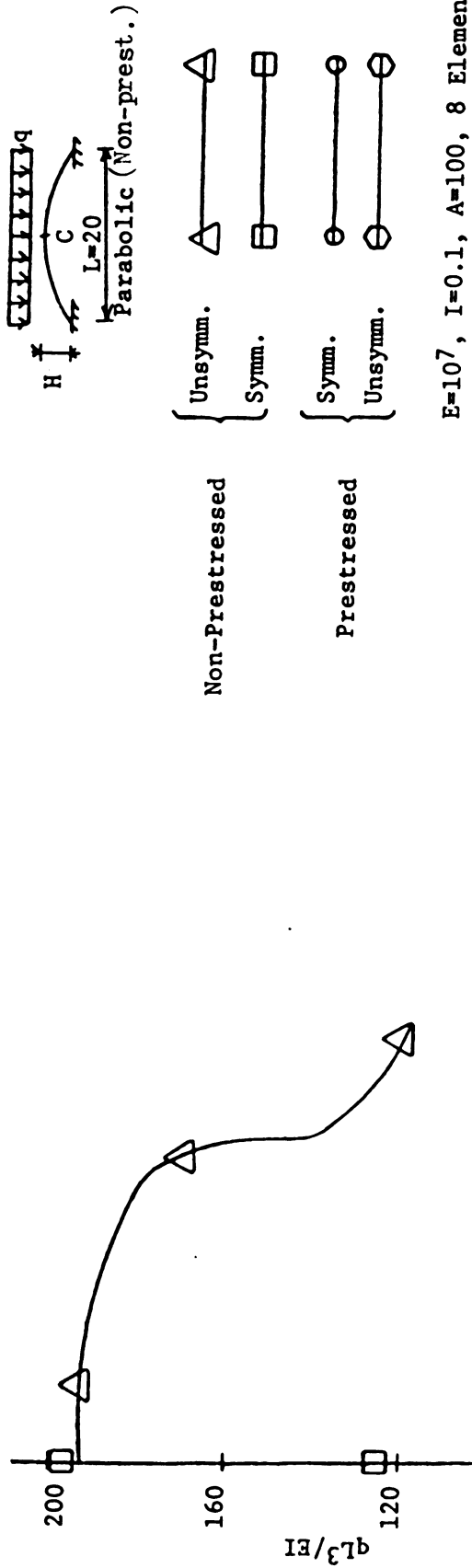
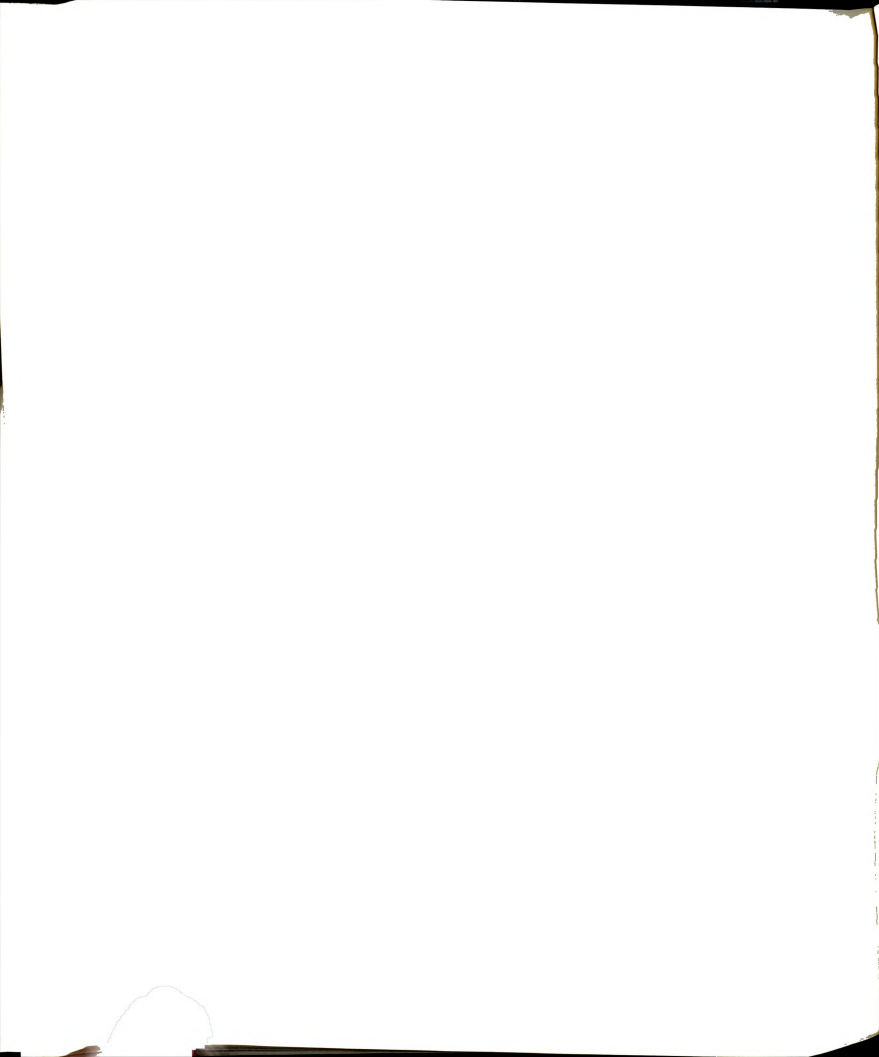
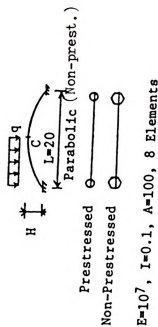


Fig. 43. Load - Displacement Curves for Uniform Load Over Entire Span, $H/L=0.5$
Prestressing by Axial Force





$E=10^7$, $I=0.1$, $A=100$, 8 Elements

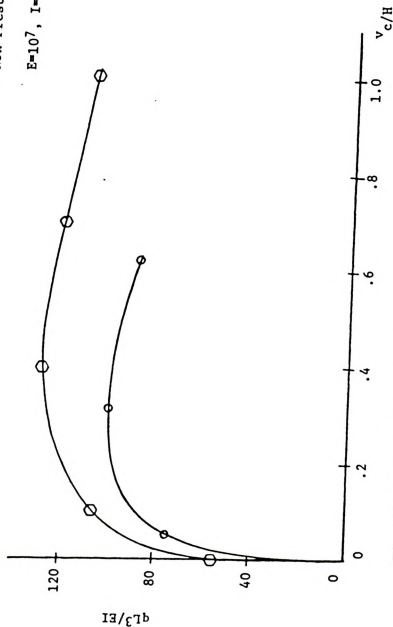


Fig. 44. Load - Displacement Curves for Uniform Load Over Half of the Span, $H/L=0.5$, Prestressing by Axial Force

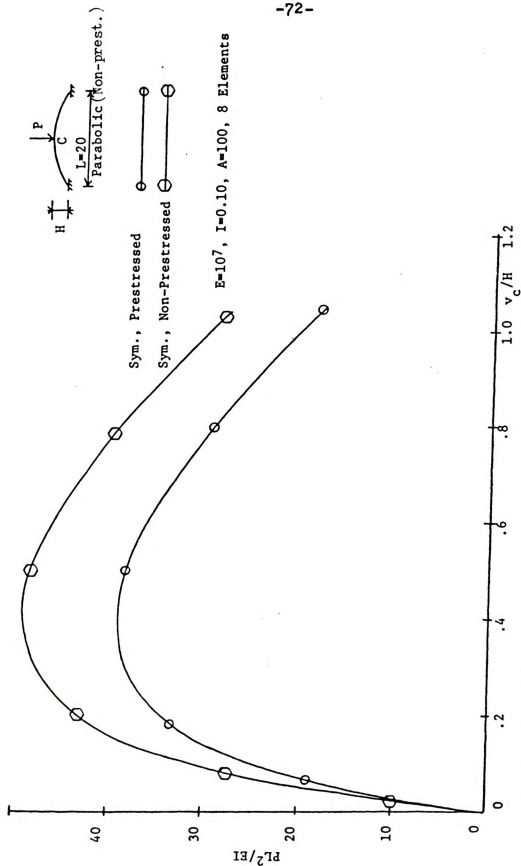
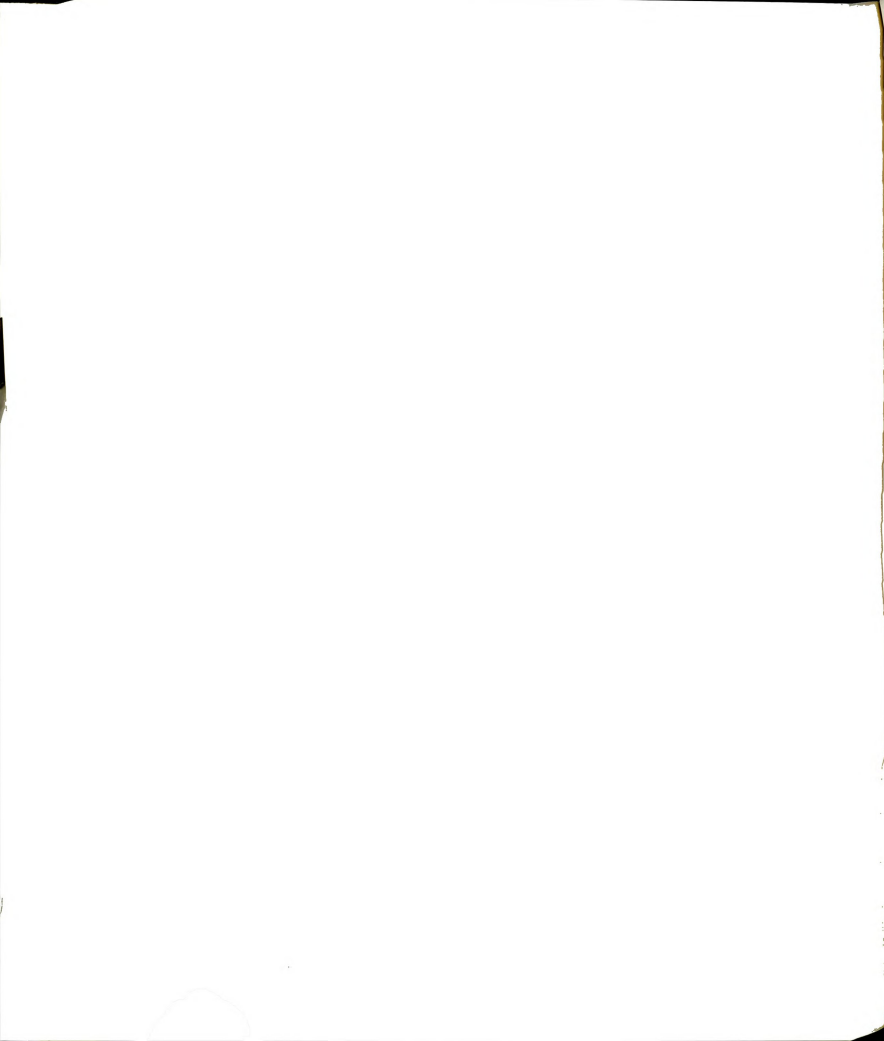


Fig. 45. Load - Displacement Curves for Concentrated Load, $H/L=0.375$, Prestressing by Axial Force



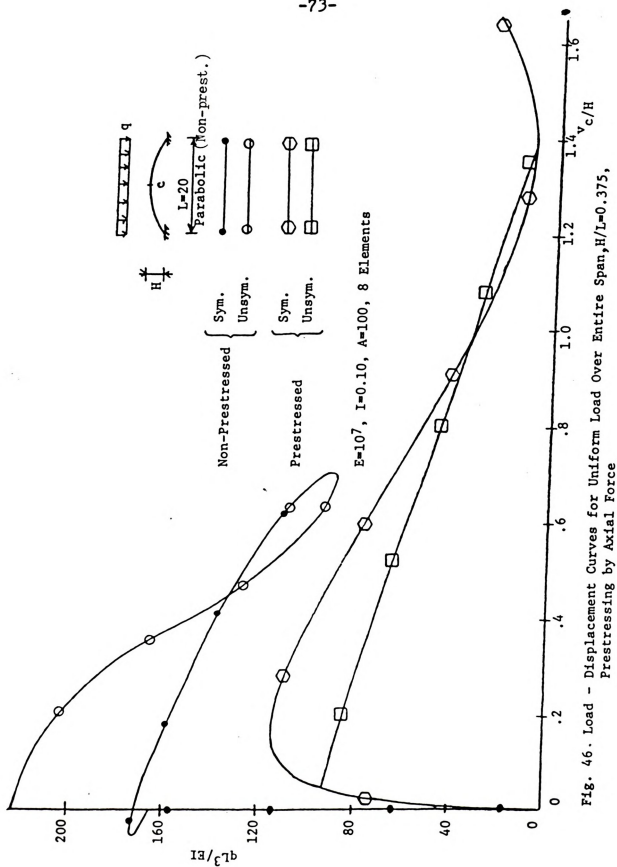


Fig. 46. Load - Displacement Curves for Uniform Load Over Entire Span, $H/L=0.375$, Prestressing by Axial Force

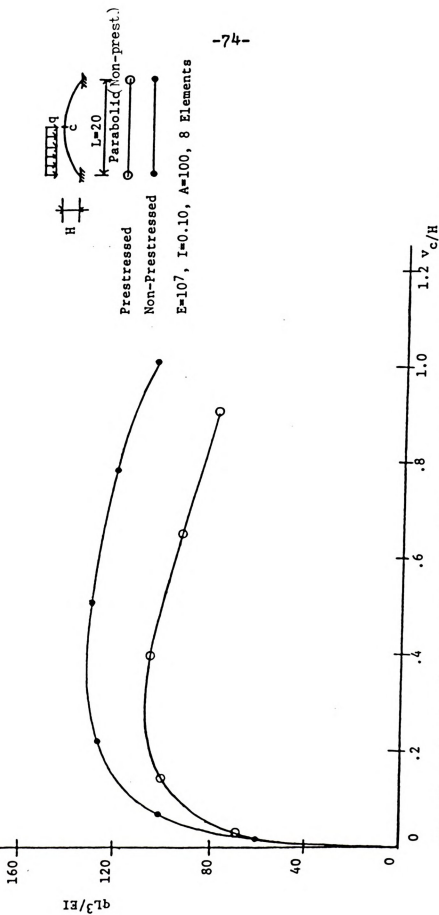


Fig. 47. Load - Displacement Curves for Uniform Load Over Half of the Span, $H/L=0.375$, Prestressing by Axial Force

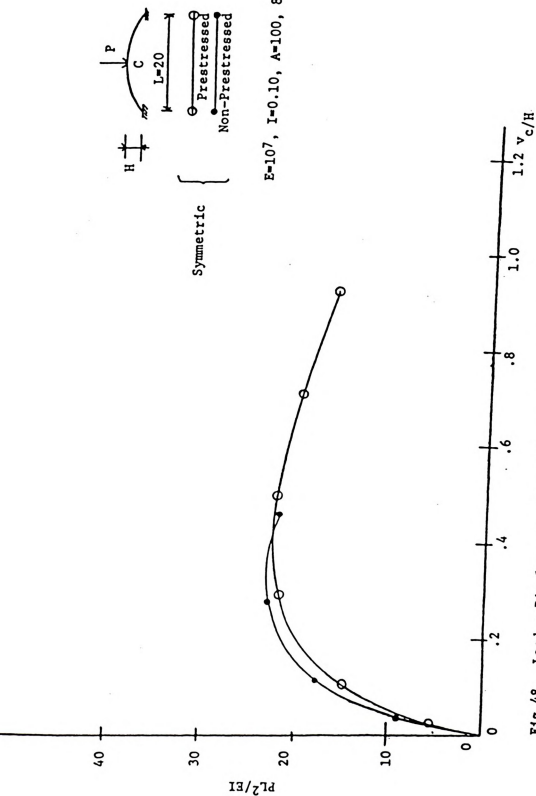
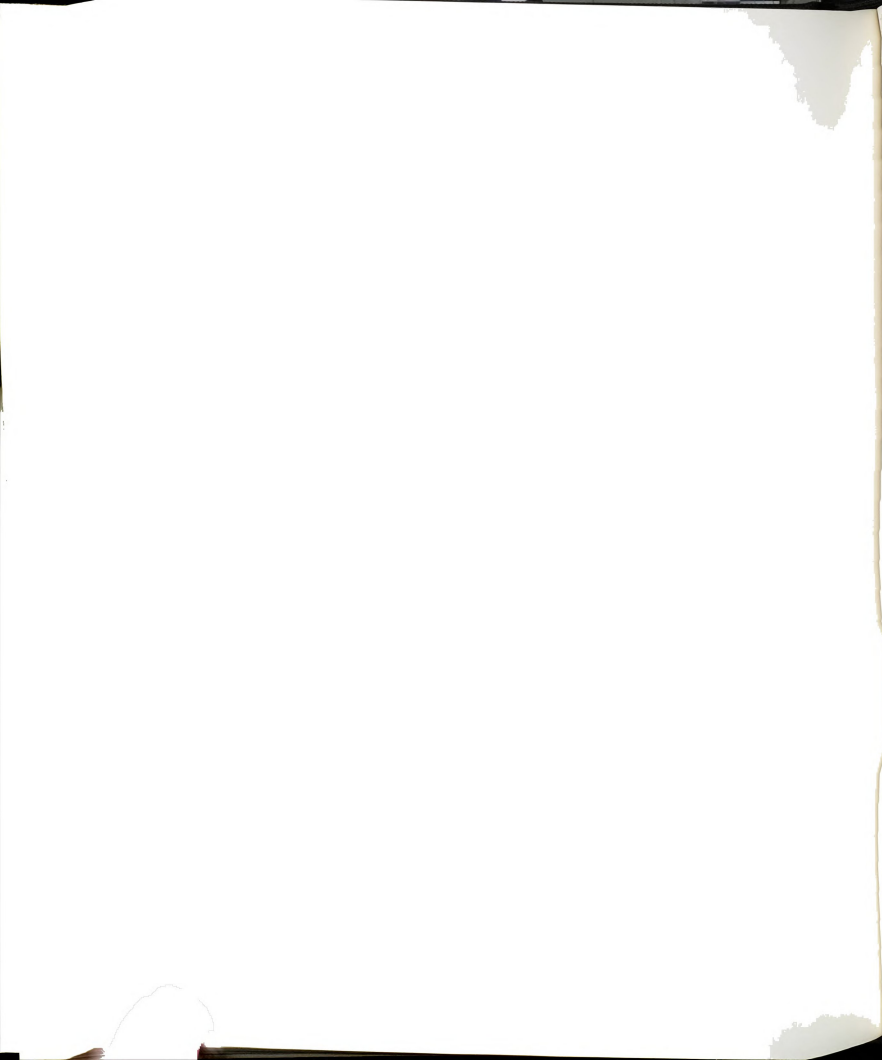


Fig.48. Load - Displacement Curves for Concentrated Load, $H/L=0.125$, Prestressing by Axial Force



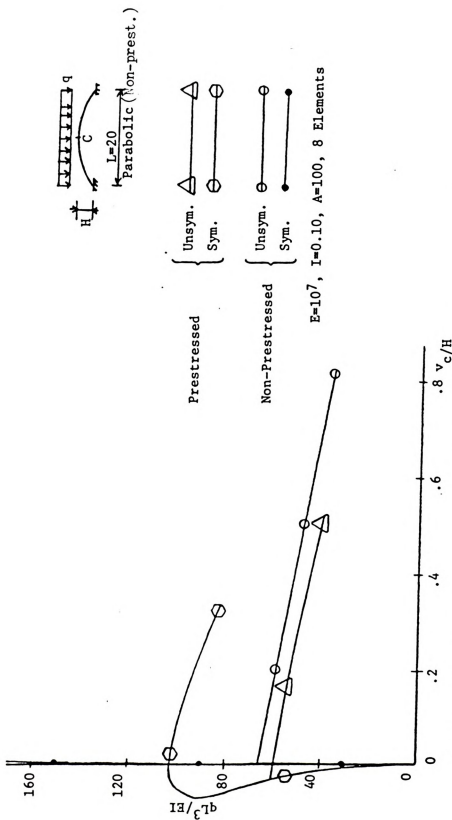


Fig.49. Load - Displacement Curves for Uniform Load Over Entire Span, $H/L=0.125$, Prestressing by Axial Force

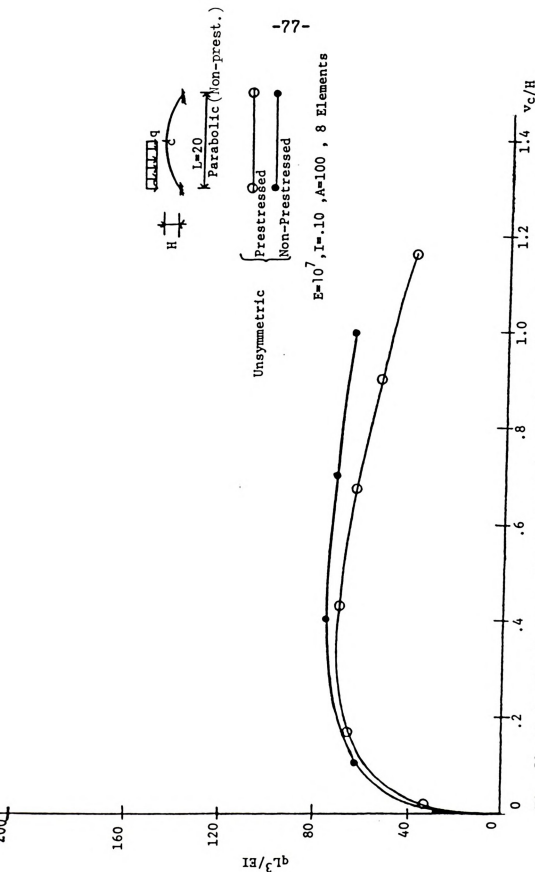
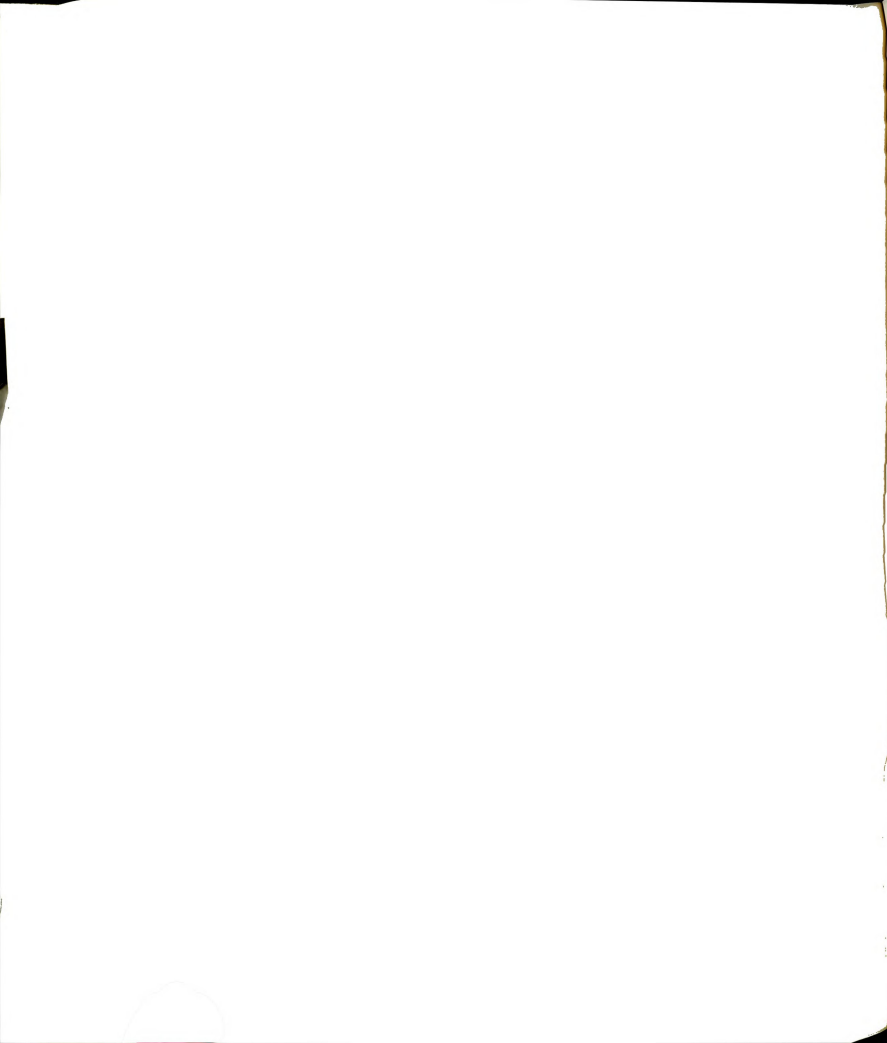
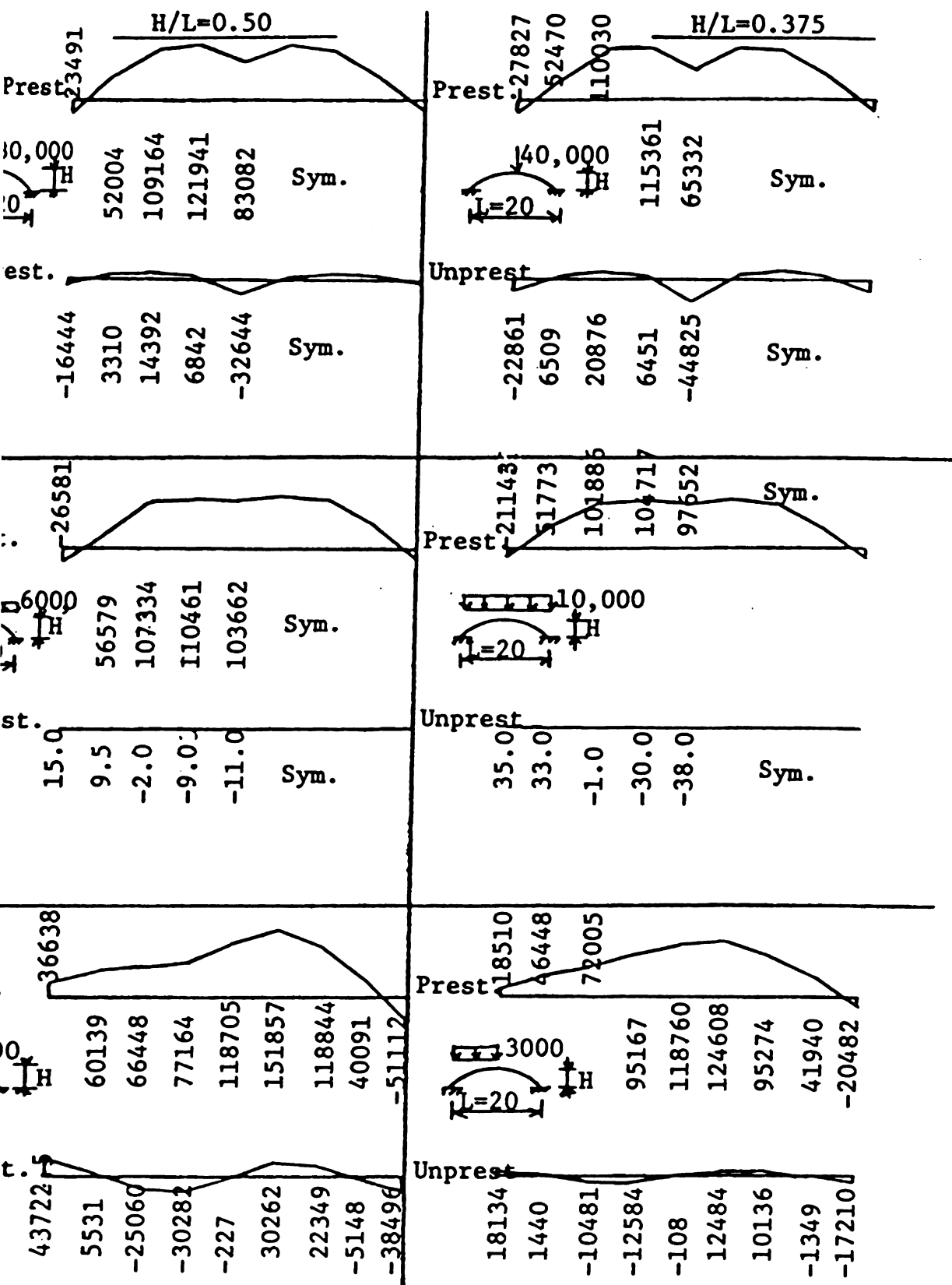


Fig. 50. Load - Displacement Curves for Uniform Load Over Half of the Span, $H/L=0.125$, Prestressing by Axial Force





$E=10^7$, $I=.10$, $A=100$, 8 Elements, Parabolic Arch (For Non-prest.)

51. Moment Diagrams, Prestressing by Axial Force

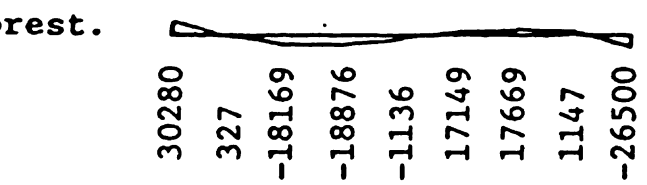
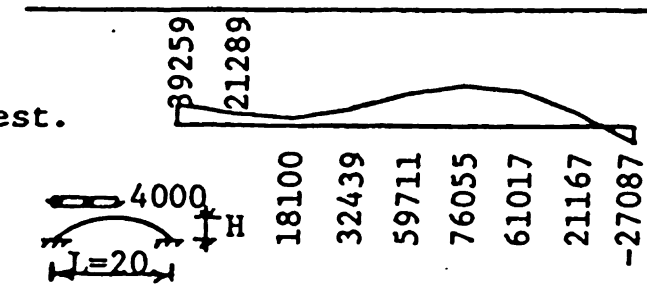
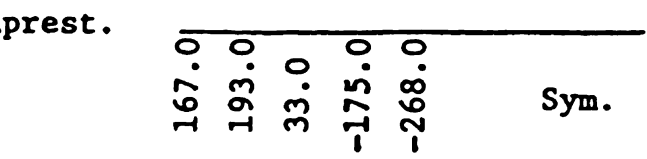
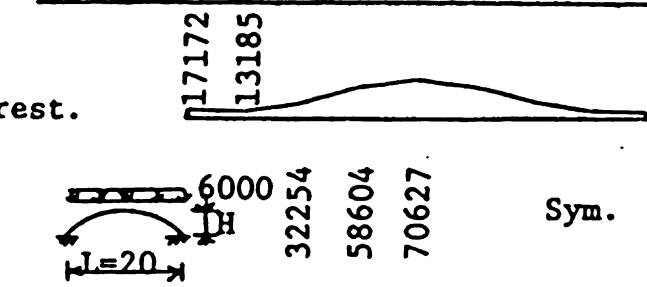
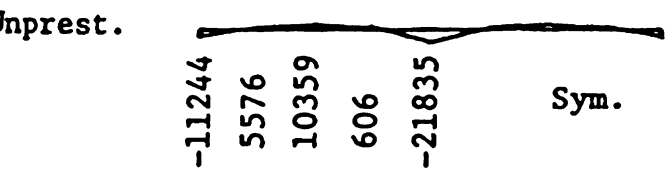
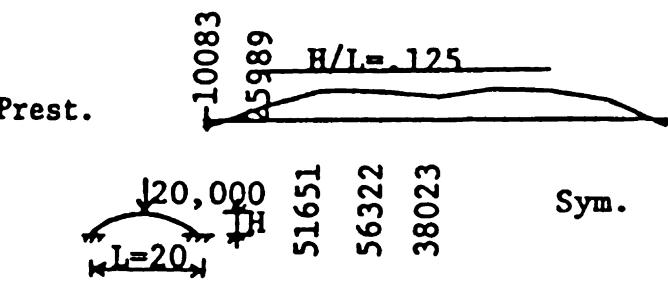
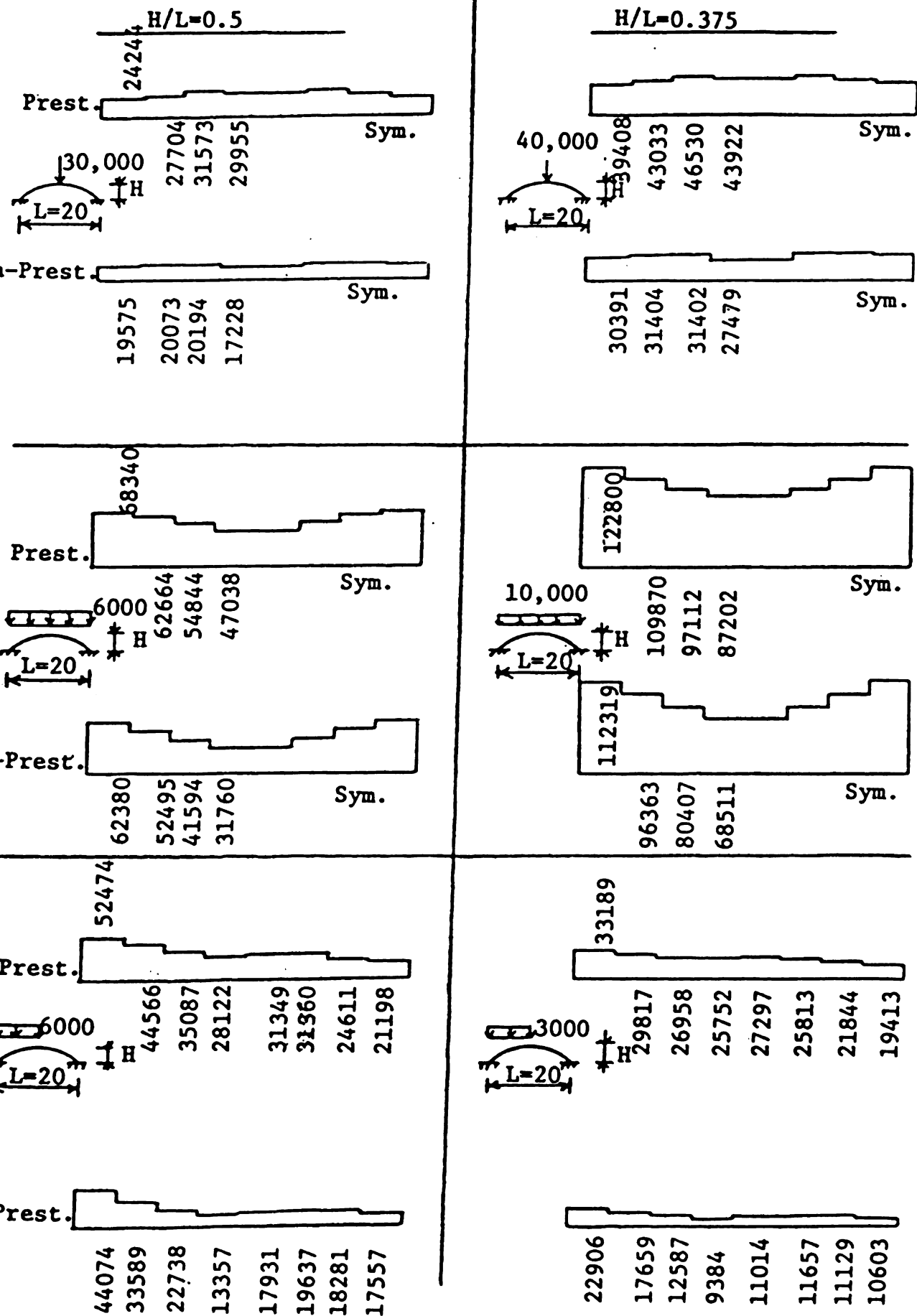


Fig. 51. Continued



, I=0.10, A=100, 8 Elements, Parabolic Arch (For Non-prest. case)

52. Axial Force Diagrams, Prestressing by Axial Force

58879

H/L=0.125

Prest.



59682
60466
60082

Sym.

-Prest.

38138
38639
38501
37707

Sym.

Prest.

144903
140060
136558
135105

Sym.



-Prest.

131216
126055
122319
120347

Sym.

Prest.

66750
63590
61172
59919
60865
60915
59237
58304



-Prest.

47050
42975
40386
39004
39583
40203
39698
38771



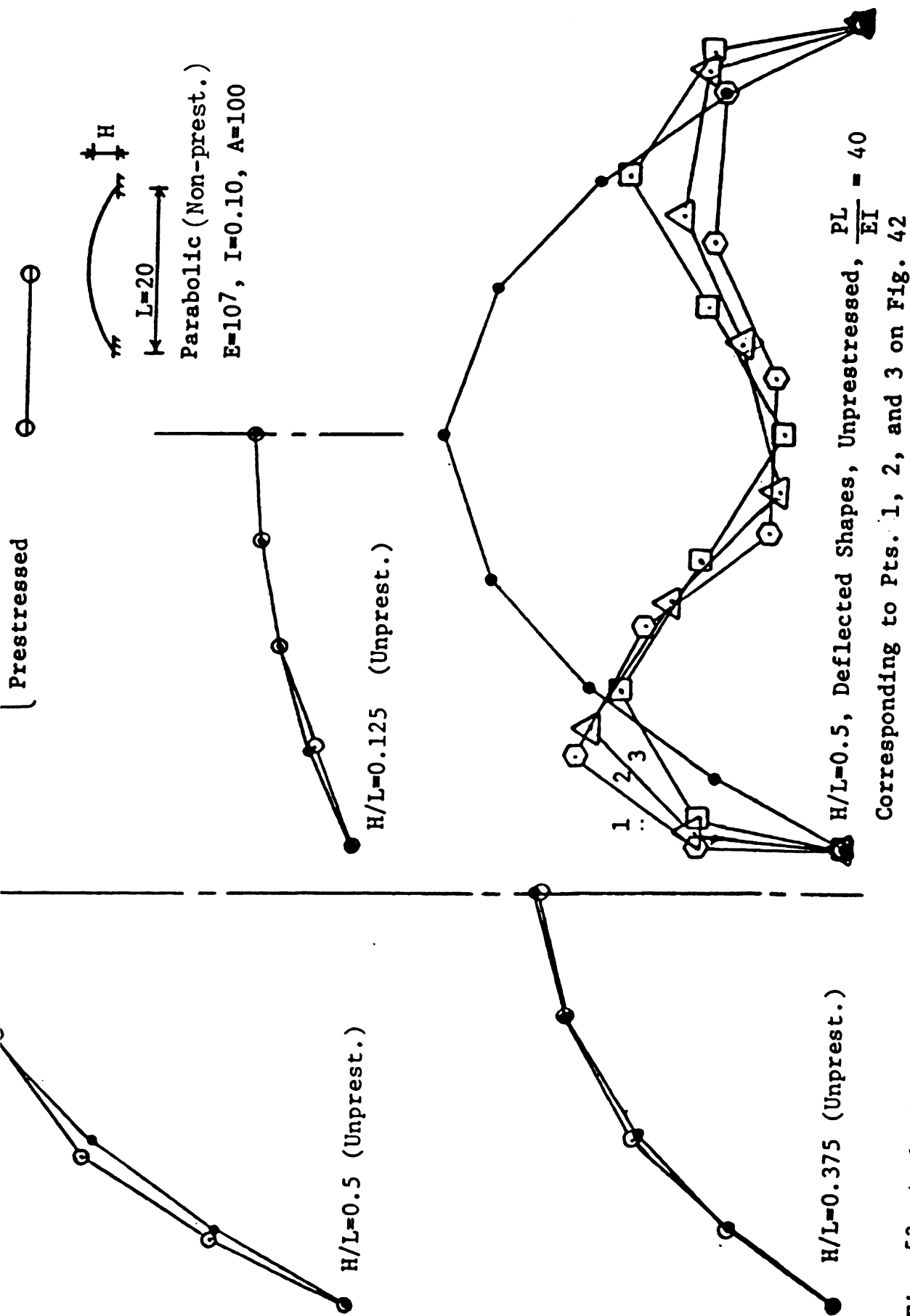


Fig. 53. Arch Shapes, Prestressing By Axial Force
Corresponding to Pts. 1, 2, and 3 on Fig. 42



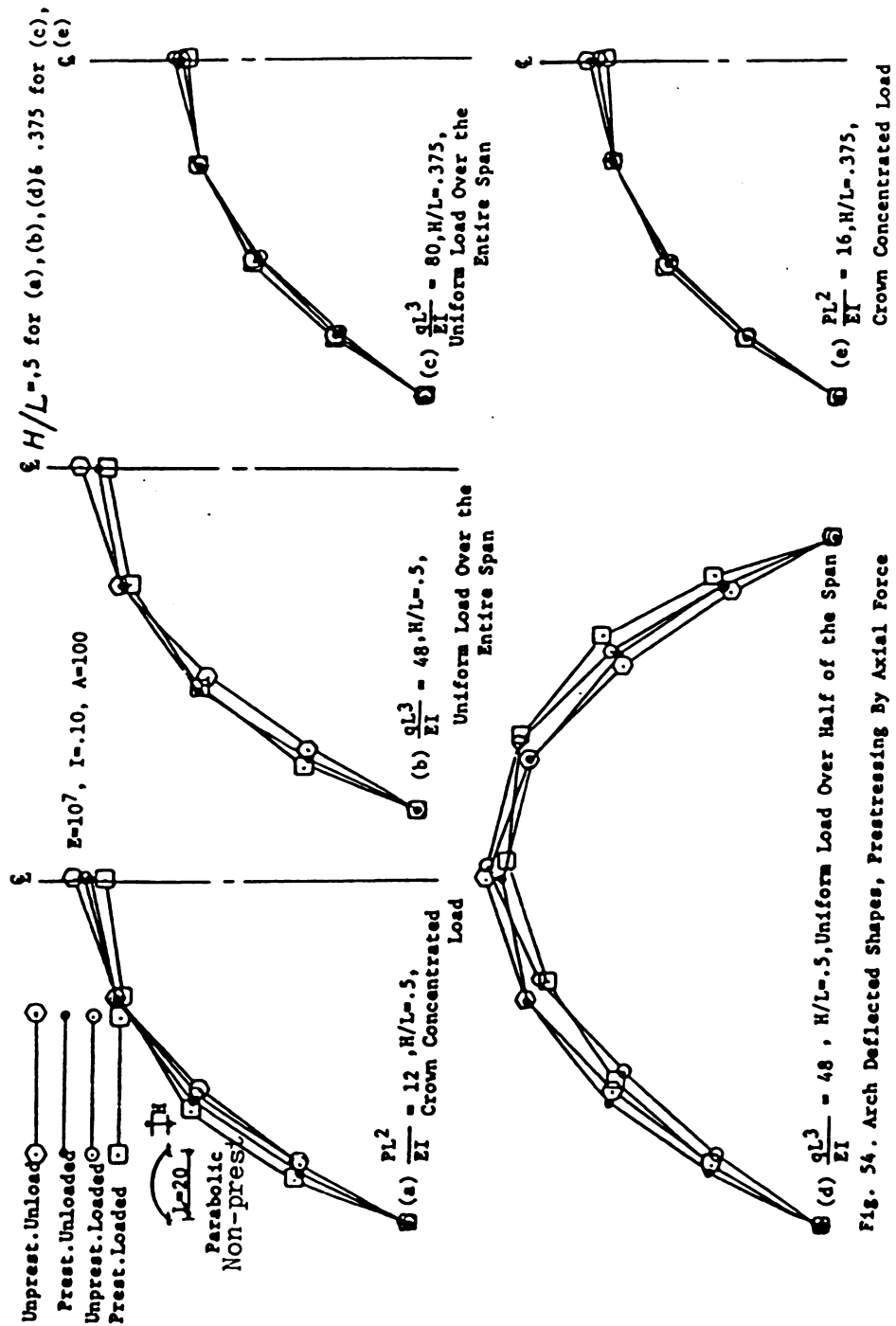


Fig. 54. Arch Deflected Shapes, Prestressing By Axial Force



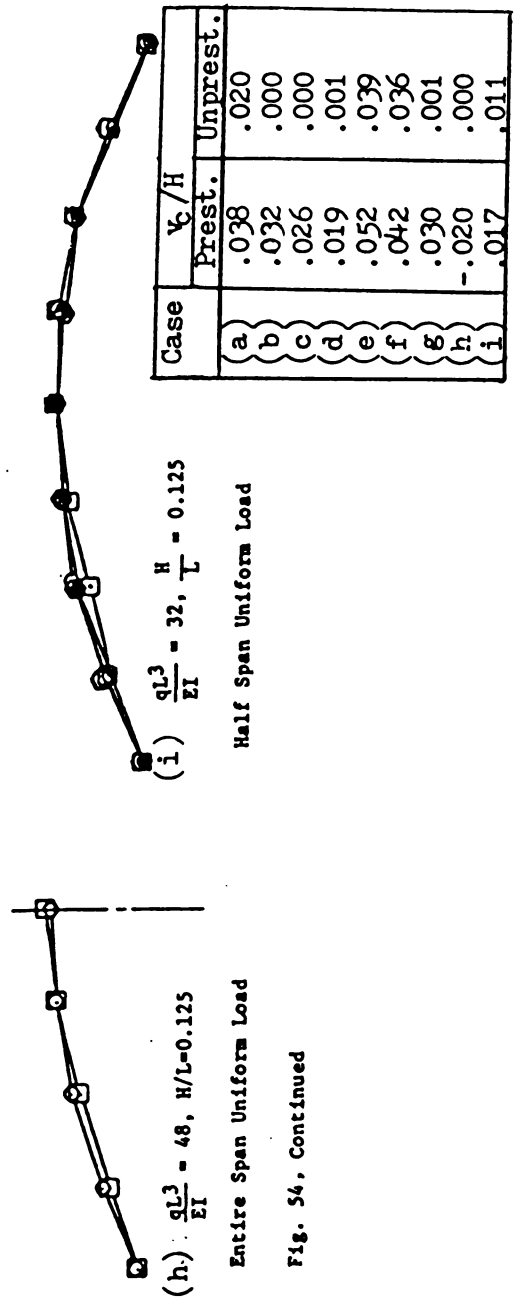
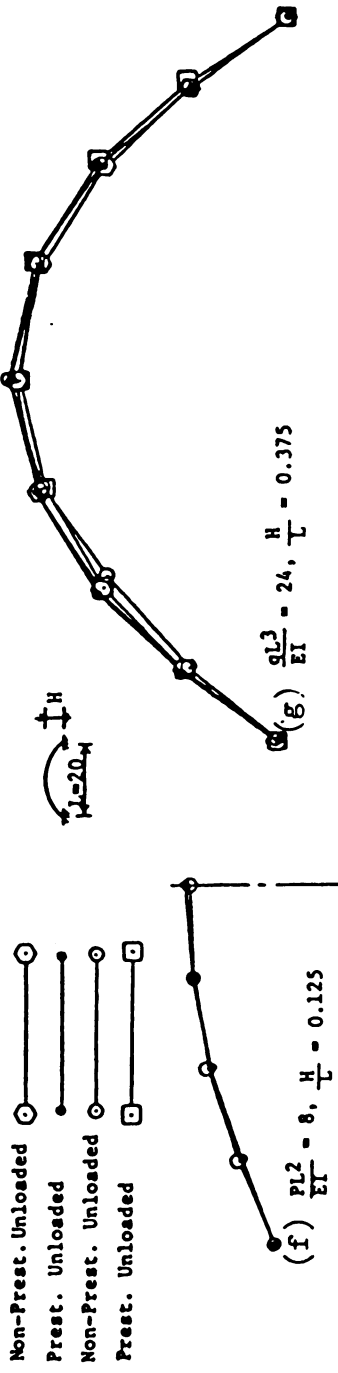


Fig. 54, Continued



CHAPTER V

CONCLUSIONS AND FUTURE STUDY

5.1 The Problem Summary and Conclusions

The elastic non-linear behavior of arches has been investigated using a rigid bar-spring node physical model. The influence of bending and axial deformation has been included. The load displacement curves and the deflected shapes for a variety of loads and for fixed and pinned supports have been obtained. The effect of cables at different positions has also been studied. Prestressing a straight bar into circular arches with different spans, and also circular arches with different spans into a half circle arch has been investigated. The results obtained are in good agreement with the known solutions, when such solutions are available.

For a pinned end arch with a concentrated load at the crown and a pinned support beam with a distributed load over half of the span, the results are in errors by less than 5% and in most cases about 1% compared with the ones obtained by others. The error for a quarter circle arch loaded radially or vertically is about 1%. The results for a non-prismatic parabolic arch with uniform load over the entire span are with less than 4.5% error with the previously obtained solutions.

Prestressing a straight bar by axial force to form an arch fixed at the ends results, in general, in lower buckling loads and greater forces in the arch and therefore does not achieve a better design.



This was studied for a concentrated load at the crown and a uniform load over the entire or half of the span. Attaching the cables to the arch loaded vertically does not help the arch at loads near the critical load. However, cables are effective and useful for the horizontal loads. As summarized in Tables 7-9 (Section 4.2), a study was made of circular arcs of a fixed length but initially with different radii and chord lengths and then prestressed into arches of the same span. It was found that this technique can reduce the maximum moment in the final loaded arch. The optimum initial length was found to vary depending on the load, being greater for larger loads.

Based upon these results it may be concluded that the model and procedure used are accurate and that it is not necessary to take more than 10 elements, eleven nodes, when two or three point extrapolation is employed to produce good results. Sometimes this extrapolation gives more accurate results than when 100 elements are used. The method is also economical. All the work to solve the two dimensional problems was done using a TRS-80 micro-computer.

It should also be noted that using this model, variable geometry and elastic properties can be accounted for. A case in which the moment of inertia was not constant was studied in this thesis.

5.2 Future Studies

Several additional problems are suggested by the work done here. These include the determination of shear effects. If $\delta(i)$ is the shear deformation in element i perpendicular to the element axis, lumped at node i , then $\Delta\theta_s(i-1) = \frac{\delta(i)}{L(i)}$ where $\Delta\theta_s(i-1)$ = the rotation of node $i-1$ due to the shear deformation and $L(i)$ = the length of element i . Then $\Delta\theta_s(i-1)$ would be added to the bending rotation at node $i-1$ to obtain the total



rotation at node i-1. The effect of variation in geometry and elastic properties can also be studied. A slight change in the program will make it possible to be used to investigate the behavior of arches with a combination of different support and loading conditions.

The space arch under in-plane and out-of-plane loading may be studied using the same model extended to 3 dimensions. Torsion could be taken by torsional springs at the nodes. Several approaches have been tried as explained in Appendix E, but none of them has led to satisfactory results.

The non-elastic behavior of arches can also be studied by modifying the program used for this thesis.



APPENDICES

A. Newton's Algorithm

The Newton's algorithm can be used to improve the initial values in an iterative manner.

For three simultaneous non-linear equations

$$f(a,b,c)=0 \quad (a)$$

$$g(a,b,c)=0 \quad (b) \quad (A.1)$$

$$h(a,b,c)=0 \quad (c)$$

if a_0, b_0 , and c_0 are approximate solutions, then better solutions may

be a_1, b_1 , and c_1 , where

$$\begin{Bmatrix} a_1 \\ b_1 \\ c_1 \end{Bmatrix} = \begin{Bmatrix} a_0 \\ b_0 \\ c_0 \end{Bmatrix} - \begin{bmatrix} \frac{\partial f_0}{\partial a_0} & \frac{\partial f_0}{\partial b_0} & \frac{\partial f_0}{\partial c_0} \\ \frac{\partial g_0}{\partial a_0} & \frac{\partial g_0}{\partial b_0} & \frac{\partial g_0}{\partial c_0} \\ \frac{\partial h_0}{\partial a_0} & \frac{\partial h_0}{\partial b_0} & \frac{\partial h_0}{\partial c_0} \end{bmatrix}^{-1} \begin{Bmatrix} f_0 \\ g_0 \\ h_0 \end{Bmatrix} \quad (A.2)$$

where

$$f_0 = f(a_0, b_0, c_0)$$

$$g_0 = g(a_0, b_0, c_0)$$

$$h_0 = h(a_0, b_0, c_0)$$

The equivalent terms may be evaluated numerically by three successive repetitions of the chain analysis. That is, the functions f_0, g_0 , and h_0 corresponding to the three initial values a, b , and c can be calculated. f, g , and h represent the three error terms corresponding to a, b , and c , respectively. It should be noted that f, g , and h would include other parameters such as the ones corresponding to



Geometry and elastic properties.

In the next chain of analysis, a small increment Δa is given to the value of a , and f_1, g_1 , and h_1 , the corresponding values of f , g , and h are found. Similarly, (f_2, g_2, h_2) and (f_3, g_3, h_3) corresponding to the increments Δb and Δc can be computed. Then using the approximation of formula (2) in section (2.2) of the thesis regarding the derivatives of the functions, we find the improved values of a, b , and c , i.e., a_1, b_1 , and c_1 , respectively.

$$\begin{Bmatrix} a_1 \\ b_1 \\ c_1 \end{Bmatrix} = \begin{Bmatrix} a_0 \\ b_0 \\ c_0 \end{Bmatrix} - \begin{bmatrix} \frac{f_1 - f_0}{\Delta a} & \frac{f_2 - f_0}{\Delta b} & \frac{f_3 - f_0}{\Delta c} \\ g_1 - g_0 & g_2 - g_0 & g_3 - g_0 \\ \frac{\Delta a}{h_1 - h_0} & \frac{\Delta b}{h_2 - h_0} & \frac{\Delta c}{h_3 - h_0} \end{bmatrix}^{-1} \begin{Bmatrix} f_0 \\ g_0 \\ h_0 \end{Bmatrix} \quad (\text{A.3})$$

The procedure may be used to improve a set of more than three initial values using a larger matrix.

Computer Program Listing to Find the Peak Value of Load-
Displacement Curve

The following symbols have been used:

Displacement of the 4 points determined from the load-
displacement curve (data), $I=1, 2, 3, 4$.

Displacement value of the peak point with positive determinant in
the solution of the quadratic equation resulting from setting
 $dy/dx=0$

Displacement value of the peak point with negative determinant in
the solution of the above equation;

Determinant of the equation $dy/dx=0$;

Peak load value corresponding to DM;

Peak load value corresponding to DN;

Coefficients of the polynomial, $I=1, 2, 3, 4$.



```

1  LPRINT"INTERPOLATION TO FIND MAX. LOAD OF LOAD-DISPL. CURVE USING 3RD DEGREE POLYNOMIAL"
2  LPRINT"*****"
3  LPRINT CHR$(27)"Q"
1200 R=4
1205 DIM A(R,R),B(R,R),D(R),P(R),S(R)
1210 PRINT"INPUT D(I); I=1 TO 4"
1220 INPUT D(1),D(2),D(3),D(4)
1230 PRINT"INPUT LOADS P(I); I=1 TO 4"
1240 INPUT P(1),P(2),P(3),P(4)
1250 FOR I=1 TO R
1260 A(I,1)=1
1270 A(I,2)=D(1)
1280 A(I,3)=D(1)*2
1290 A(I,4)=D(1)*3
1295 LPRINT"A(";I;",";J)=";A(I,1);A(I,2);A(I,3);A(I,4)
1300 NEXT I
1310 LPRINT"D(I), (I=1 TO 4) =" ;D(1);D(2);D(3);D(4)
1320 LPRINT"P(I), (I=1 TO 4) =" ;P(1);P(2);P(3);P(4)
1330 FOR I=1 TO R
1340 B(I,1)=1
1350 NEXT I
1530 FOR J=1 TO R
1532 FOR I=J TO R
1534 IF A(I,J)<0 THEN 1542
1536 NEXT I
1538 LPRINT"SINGULAR MATRIX"
1540 GOTO 1830
1542 FOR K=1 TO R
1544 T=A(J,K)
1546 A(J,K)=A(I,K)
1548 A(I,K)=T
1550 T=B(J,K)
1552 B(J,K)=B(I,K)
1554 B(I,K)=T
1556 NEXT K
1558 E=1/A(J,J)
1560 FOR K=1 TO R
1562 A(J,K)=E*A(J,K)
1564 B(J,K)=E*B(J,K)
1566 NEXT K
1568 FOR L=1 TO R
1570 IF L=J THEN 1582
1572 E=-A(L,J)
1574 FOR K=1 TO R
1576 A(L,K)=A(L,K)+E*A(J,K)
1578 B(L,K)=B(L,K)+E*B(J,K)
1580 NEXT K
1582 NEXT L
1584 NEXT J
1586 LPRINT"MATRIX INVERSE"
1588 FOR I=1 TO R
1590 LPRINT"I=";I;": ";B(I,1);B(I,2);B(I,3);B(I,4)

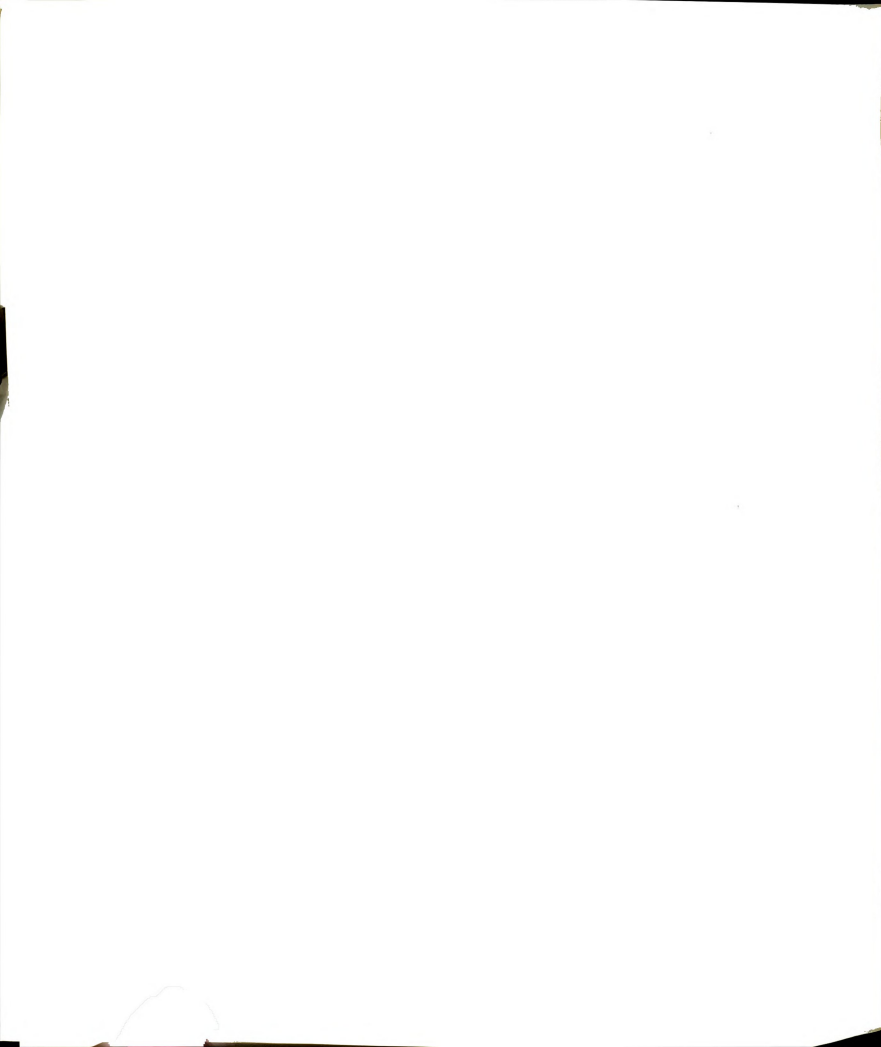
```



```

1592 NEXT I
1594 FOR J=1 TO R
1595 S(I)=0
1596 FOR K=1 TO R
1598 S(I)=S(I)+B(I,K)*P(K)
1600 NEXT K
1602 NEXT I
1604 LPRINT"COEF. MATRIX"
1606 LPRINT
1608 FOR J=1 TO R
1610 LPRINT"J=";J;" , S(I)=";S(I)
1614 NEXT I
1650 PRINT"IF DISPL. OF ANOTHER LOAD, PRINT 1":INPUT DL
1660 IF DL<>1 THEN 1710
1670 PRINT"WHAT DISPL.?"
1680 INPUT DP
1690 PP=S(1)+S(2)*DP+S(3)*(DP(2)+S(4)*(DP(3)
1695 LPRINT
1700 LPRINT"DP=";DP;"PP=";PP
1710 PRINT"IF ANOTHER DISPL., PRINT 2":INPUT AN
1720 IF AN=2 THEN 1670
1730 DT=S(2)*(2-3*S(1)+S(3)
1732 IF DT<0 THEN 1755
1734 DM=(-S(2)+SOR(DT))/(3*S(1))
1736 DN=(-S(2)-SOR(DT))/(3*S(1))
1740 PM=S(4)+S(3)*DM+S(2)*(DM(2)+S(1)*(DM(3)
1742 PN=S(4)+S(3)*DN+S(2)*(DN(2)+S(1)*(DN(3)
1750 LPRINT"W/ POSITIVE SOR(DT): DM=";DM;" PM=";PM
1752 LPRINT"W/ NEGATIVE SOR(DT): DN=";DN;" PN=";PN
1754 GOTO 1760
1755 LPRINT"DETERMINANT TO CALCULATE DMAX IS NEGATIVE"
1760 LPRINT"*****"
1830 END

```



C. Listing of the Main Computer Program

A simple modification will make it possible to use this program for a fixed end arch prestressed by axial force.

The following symbols have been used (other symbols have been defined in Section 1.3):

BD = The Horizontal Distance Between the Cable Base and the Plane of the Arch;
CE = Cable Modulus of Elasticity;
CM = Cable Cross Sectional Area;
EA = Element Cross Sectional Area;
EI = Element Moment of Inertia;
EH = Error in Horizontal Displacement of the Right Support;
EL = Element Length;
EM = Error in Moment or Rotation of the Right Support;
EP = Error Limit Allowed;
EV = Error In Vertical Displacement of the Right Support;
GH = Guessed Value of the Horizontal Reaction of the Left Support;
GV = Guessed Value of the Vertical Reaction of the Right Support;
GR = Guessed Value of the Rotation of the Right Support;
HN = Final Horizontal Load at a Node Including the Effect of Cables;
IC = Allowed Number of Iterations;
ID = 1 If Cable Base to the Left of the Node, and Any Other Number Otherwise;
IE = 1 If No Cable For the Node, and Any Other Number Otherwise;
LN = Final Element Length After Axial Deformation;
NE = Number of Elements;
NN = Number of Nodes;
R = Radius of the Half Circle Arch;
RI = Rise of the Right Support With Respect to the Left Support;
SC = Slope Change of Each Element
SM = Final Slope Change of Each Element
TC = The Change In Slope Between Elements (I-1) and I;
TH = Original Angle Between the Element and the Vertical;
TN = Final Angle Between the Element and the Vertical (After Rotation);
VD = Horizontal Distance Between the Cable Base and the Node Where the Cable is Attached to;
VN = Final Vertical Load at a Node Including the Effect of Cables;
VV = Horizontal Distance Between the Left Support and the Node Where the Cables are Attached to;
XL = Arch Span;
XM = Moment at each Node;
XN = Final X-Coordinate of the Node;
YN = Final Y-Coordinate of the Node;



```
1 PRINT"PROG.(MTTHESIS);ARCH W/ CHOICE OF PINNED OR FIXED
  ENDS;CABLES; & PRESTRESSING"
5 PRINT"NON-LINEAR BEHAVIOR: ARCH-FRAME: RIGID BAR MODEL-
  VERSION'V'-SP"
6 PRINT"IF FIXED ENDS, TYPE 1":INPUT F
7 PRINT"IF PRESTRESSED, TYPE 1":INPUT P
10 INPUT"NUMBER OF ELEMENTS";NE
12 NN=NE+1
15 DIM EL(NE),TH(NE),E(NE),EI(NE),A(NE),VL(NN),HL(NN),
  XN(NN),YN(NN),TN(NE),AF(NE),SF(NE),AD(NE),LN(NE),
  XM(NN),TC(NN),HE(NN+1),VE(NN+1),ME(NN+1)
16 DIM BD(NN),VD(NN),CL(NN),CD(NN),CE(NN),CM(NN),CF(NN),
  IE(NN),ID(NN),VN(NN),HN(NN)
17 DIM EA(NE)
20 INPUT"ERROR LIMIT-EPS";EP
21 PRINT"IF SEMI-CIRCULAR ARCH,TYPE 1":INPUT AC
22 IF AC=1 GOTO 41
25 PRINT"INPUT ELEMENT LENGTH,ANGLE(THETA),MODULUS,I,A"
30 FOR I=1 TO NE
35 PRINT I: INPUT EL(I),TH(I),E(I),EI(I),EA(I)
40 NEXT I: GOTO 45
41 INPUT"RADIUS";R:PRINT"FOR EACH ELEMENT,INPUT E, I & A"
42 FOR I=1 TO NE
43 PRINT I: INPUT E(I),EI(I),EA(I):TI=3.1415927/NE:
  EL(I)=2*R*SIN(TI/2)
44 TH(I)=TI*(I-.5):NEXT I
45 PRINT"INPUT NODE LOADS- VERTICAL, HORIZONTAL"
50 FOR I=1 TO NN
55 PRINT I:INPUT VL(I),HL(I)
60 NEXT I
65 FOR U=1 TO 3
70 PRINT"INPUT SPAN,RISE,NO.OF ITERATIONS,GUESS VERT.R,
  HOR.R,ROTATION
75 INPUT XL,RI,IC,GV,GH,GR
77 HB=GH: VB=GV: RB=GR
78 FOR I=1 TO NN:VN(I)=VL(I):HN(I)=HL(I)
79 NEXT I
80 II=1:XN(1)=0:YN(1)=0:TC(1)=0:N=0:IX=0
81 IF F=1 GOTO 82 ELSE 86
82 IF P=1 GOTO 83 ELSE 84
83 MO=(E(1)*EI(1)*(TH(2)-TH(1)))/EL(1):GOTO 85
84 MO=0
85 XM(1)=MO+GR*(E(1)*EI(1)*2/EL(1)):GOTO 90
86 XM(1)=0
90 TN(1)=TH(1)+GR
95 SN=SIN(TN(1)):CS=COS(TN(1))
100 AF(1)=((GV-VN(1))*CS)+((GH+HN(1))*SN)
105 SF(1)=((VN(1)-GV)*SN)+((GH+HN(1))*CS)
110 AD(1)=((AF(1)*EL(1)))/(E(1)*EA(1))
115 LN(1)=EL(1)-AD(1)
150 XN(2)=LN(1)*SN:YN(2)=LN(1)*CS
```



```

151 IF IX<>0 GOTO 155
152 PRINT*PRINT 1 IF NO CABLES FOR NODE 1":INPUT IE(1)
153 IF IE(1)=1 GOTO 162
154 PRINT*INPUT BD(1),VDB(1),CL(1),CA(1),CME(1)":INPUT
    BD(1),VD(1),CL(1),CM(1),CE(1)
155 IF IE(1)=1 GOTO 162
156 UU=VD(1)-XN(1):BK=ATN(ABS(YN(1))/UU):CC=SQR((UU)*
    (UU)+(YN(1))*(YN(1))):CN=SQR((CC)*(CC)+(BD(1))*(
    BD(1)))
157 CD(1)=CL(1)-CN:CF(1)=((CD(1))*(CE(1))*(CM(1)))/(CN):
    BC=(BD(1))/(CN):CP=ATN(BC/SQR(-BC*BC+1)):CB=2*(CF(1))
    *(COS(CP)):IF CD(1)>0 GOTO 162
158 CH=-(CB)*(COS(BK)):CV=-(CB)*(SIN(BK)):VN(1)=VL(1)+CV:
    HN(1)=HL(1)+CH
159 AF(1)=((GV-VN(1))*CS)+((GH+HN(1))*SN):SF(1)=((VN(1)-
    GV)*SN)+((GH+HN(1))*CS)
160 AD(1)=((AF(1)*EL(1))/(E(1)*EA(1)):LN(1)=EL(1)-AD(1)
161 XN(2)=LN(1)*SN:YN(2)=LN(1)*CS
162 FOR I=2 TO NE:J=1-I:K=1+I
163 PRINT"I=";I;"SF(J)=";SF(J);"LN(J)=";LN(J);"XM(J)=";
    XM(J)
165 TC(I)=TH(I)-TH(J)
170 SC=((SF(J)*LN(J)/2.0 +XM(J))*LN(J))/(E(J)*EI(J))
171 IF F=1 GOTO 172 ELSE 173
172 IF P=1 GOTO 175
173 TN(I)=TN(J)+TC(I)+SC:GOTO 180
175 TN(I)=TN(J)+SC
180 CA=COS(TN(I)):SA=SIN(TN(I))
181 IF F=1 GOTO 182 ELSE 185
182 IF P<>1 GOTO 185
183 CS=COS(SC):SN=SIN(SC)
184 GOTO 190
185 CS=COS(TC(I)+SC):SN=SIN(TC(I)+SC)
190 AF(I)=AF(J)*CS+SF(J)*SN+HN(I)*SA-VN(I)*CA
195 SF(I)=-AF(J)*SN+SF(J)*CS+HN(I)*CA+VN(I)*SA
200 XM(I)=XM(J)+SF(J)*LN(J)
205 AD(I)=(AF(I)*EL(I))/(E(I)*EA(I))
210 LN(I)=EL(I)-AD(I)
215 ST=((SF(I)*LN(I)/2.0+XM(I))*LN(I))/(E(I)*EI(I))
220 SM=XM(I)*(LN(I)+LN(J))/(E(J)*EI(J)+E(I)*EI(I))
221 IF F=1 GOTO 222 ELSE 224
222 IF P=1 GOTO 225
224 TN(I)=TN(J)+TC(I)+SM:GOTO 230
225 TN(I)=TN(J)+SM
230 CA=COS(TN(I)):SA=SIN(TN(I))
231 IF F=1 GOTO 232 ELSE 235
232 IF P<>1 GOTO 235
233 CS=COS(SM):SN=SIN(SM):GOTO 240
235 CS=COS(SM+TC(I)):SN=SIN(SM+TC(I))
240 AF(I)=AF(J)*CS+SF(J)*SN+HN(I)*SA-VN(I)*CA

```

```

245 SF(I)=-AF(J)*SN+SF(J)*CS+HN(I)*CA+UN(I)*SA
250 XM(I)=XM(J)+SF(J)*LN(J)
255 AD(I)=(AF(I)*EL(I))/(E(I)*EA(I))
260 LN(I)=EL(I)-AD(I)
261 PRINT"LN(";I;")=";LN(I)
262 XN(K)=XN(I)+LN(I)*SA
263 YN(K)=YN(I)+LN(I)*CA
264 IF IX<>0 GOTO 270
265 PRINT*PRINT 1 IF NO CABLES FOR NODE ";I
266 INPUT IE(I)
267 IF IE(I)=1 GOTO 288
268 PRINT*PRINT BD(I),VDB(I),CL(I),CA(I),CME(I):INPUT
BD(I),VD(I),CL(I),CM(I),CE(I)
269 PRINT*PRINT 1 IF CABLE BASE TO THE LEFT OF THIS NODE":
INPUT ID(I)
270 IF IE(I)=1 GOTO 288
271 IF ID(I)=1 GOTO 273
272 W=VD(I)-XN(I):GOTO 274
273 W=XN(I)-VD(I)
274 BK=ATN(ABS(YN(I))/W):CC=SQR((W)*(W)+(YN(I))*
(YN(I))):CN=SQR((CC)*(CC)+(BD(I))*(BD(I)))
275 CD(I)=CL(I)-CN:CF(I)=((CD(I))*(CE(I))*(CM(I)))/(CN)
:BC=(BD(I))/(CN):CP=ATN(BC/SQR(-BC*BC+1)):CB=2*
(CF(I))*(COS(CP)):IF CD(I)>0 GOTO 288
276 IF ID(I)=1 GOTO 278
277 CH=-(CB)*(COS(BK)):GOTO 279
278 CH=(CB)*(COS(BK))
279 CV=-(CB)*(SIN(BK)):UN(I)=VL(I)+CV:HN(I)=HL(I)+CH
280 AF(I)=AF(J)*CS+SF(J)*SN+HN(I)*SA-UN(I)*CA:SF(I)=-
AF(J)*SN+SF(J)*CS+HN(I)*CA+UN(I)*SA
281 XM(I)=XM(J)+SF(J)*LN(J):AD(I)=(AF(I)*EL(I))/(E(I)*
EA(I)):LN(I)=EL(I)-AD(I)
282 SM=XM(I)*(LN(I)+LN(J))/(E(J)*EI(J)+E(I)*EI(I)):
TN(I)=TN(J)+SM+TC(I)
283 CA=COS(TN(I)):SA=SIN(TN(I)):CS=COS(SM+TC(I)):SN=
SIN(SM+TC(I))
284 AF(I)=AF(J)*CS+SF(J)*SN+HN(I)*SA-UN(I)*CA:SF(I)=-
AF(J)*SN+SF(J)*CS+HN(I)*CA+UN(I)*SA
285 XM(I)=XM(J)+SF(J)*LN(J)
286 AD(I)=(AF(I)*EL(I))/(E(I)*EA(I)):LN(I)=EL(I)-AD(I)
287 PRINT"LN(";I;")=";LN(I):XN(K)=XN(I)+LN(I)*SA:YN(K)=
YN(I)+LN(I)*CA
288 NEXT I
289 NW=NN-1:XM(NN)=XM(NW)+SF(NW)*LN(NW)
290 EH=XL-XN(NN):EV=RI-YN(NN):EM=XM(NN)
291 IF F<1 GOTO 293
292 EM=XM(NN)-(MO-(TN(NE)-TH(NE)))*(E(NE)*EI(NE)*2/EL(NE)))
293 IX=1
295 IF(ABS(EH)-EP)>0 GOTO 310 ELSE 300
300 IF(ABS(EV)-EP)>0 GOTO 310 ELSE 305

```



```

305 IF(ABS(EM)-EP)>0 GOTO 310 ELSE 490
310 IF (N)=0 GOTO 315 ELSE 340
315 IF(II-IC)<0 GOTO 322 ELSE 316
316 PRINT"CYCLE NO.";II;"ERROR H=";EH;"ERROR V=";EV;
    "ERROR M=";EM
317 PRINT"GH=";GH;" GV=";GV;" GR=";GR
318 PRINT"DOES NOT CONVERGE AT CYCLE";II
319 PRINT"* * * * *"
320 GOTO 490
322 PRINT"CYCLE NO.";II;" ERRORH=";EH;" ERRORV=";EV;
    " ERRORM=";EM
325 PRINT"GH=";GH;" GV=";GV;" GR=";GR
330 PRINT"DOES NOT CONVERGE AT CYCLE";II
335 PRINT"+ + + + + + + + + + "
340 N=N+1
345 HE(N)=EH;VE(N)=EV;ME(N)=EM
350 IF(N-1)>0 GOTO 365 ELSE 355
355 GH=1.01*GH
360 GOTO 81
365 IF(N-2)>0 GOTO 385 ELSE 370
370 GV=1.01*GV
375 GH=GH/1.01
380 GOTO 81
385 IF(N-3)>0 GOTO 405 ELSE 390
390 GR=1.01*GR
395 GV=GV/1.01
400 GOTO 81
405 GR=GR/1.01
410 REM-JACOBIAN CORRECTION
415 A1=(HE(2)-HE(1))/(.01*GH); A2=(VE(2)-VE(1))/(.01*GH)
420 A3=(ME(2)-ME(1))/(.01*GH); B1=(HE(3)-HE(1))/(.01*GV)
425 B2=(VE(3)-VE(1))/(.01*GV); B3=(ME(3)-ME(1))/(.01*GV)
430 C1=(HE(4)-HE(1))/(.01*GR); C2=(VE(4)-VE(1))/(.01*GR)
435 C3=(ME(4)-ME(1))/(.01*GR)
440 P1=B2*C3-C2*B3; P2=B1*C3-C1*B3
445 P3=B1*C2-B2*C1; Q1=A2*C3-C2*A3
450 Q2=A1*C3-C1*A3; Q3=A1*C2-C1*A2
455 R1=A2*B3-B2*A3; R2=A1*B3-B1*A3
460 R3=A1*B2-A2*B1
462 PRINT"A1=";A1;"P1=";P1;"B1=";B1;"Q1=";Q1;"C1=";C1;
    "R1=";R1
465 DT=A1*P1-B1*Q1+C1*R1
470 GH=GH-((P1*HE(1)-P2*VE(1)+P3*ME(1))/DT)
475 GV=GV-((-Q1*HE(1)+Q2*VE(1)-Q3*ME(1))/DT)
480 GR=GR-((R1*HE(1)-R2*VE(1)+R3*ME(1))/DT)
485 N=0; II=II+1; GOTO 81
490 PRINT"CYCLE NO.";II;"ERROR H=";EH;"ERRORV=";EV;
    "ERRORM=";EM
495 PRINT"GH=";GH;"GV=";GV;"GR=";GR
498 STOP
500 PRINT" * * * * *"

```




```

505 PRINT"EL.N0";TAB(10)"AXIAL F";TAB(20)"SHEAR F";
    TAB(30)"END M";TAB(40)"AXIAL DEF.";TAB(52)
    "THETA FINAL"
510 FOR I=1 TO NE
515 PRINT I;TAB(10) AF(I);TAB(20)SF(I);TAB(30)XM(I);
    TAB(40)AD(I);TAB(52)TN(I)
520 NEXT I
522 FOR I=1 TO NE
523 IF IE(I)=1 GOTO 525
524 PRINT"I=";I;TAB(10)"CABLE AX. DEFORM.=";CD(I);TAB(10)
    "CABLE AX.FORCE=";CF(I);GOTO 526
525 PRINT"I=";I;TAB(15)"NO CABLES FOR THIS NODE"
526 NEXT I
527 PRINT"NODE NO.";TAB(12)"X-COORD";TAB(24)"Y-COORD";
    TAB(36)"END M"
530 FOR I=1 TO NN
535 PRINT I;TAB(12)XN(I);TAB(24)YN(I);TAB(36)XM(I)
540 NEXT I
541 PRINT"TO OUTPUT RESULTS TO PRINTER, TYPE 1"
542 INPUT Z
543 IF Z=1 GOTO 550 ELSE 545
545 PRINT"IF DIFFERENT LOAD OR ERROR LIMIT,TYPE 2":
    INPUT DL
546 IF DL<>2 GOTO 548
547 INPUT"NEW ERROR LIMIT=";EP; GOTO 45
548 NEXT U
549 END
550 LPRINT"ELEMENT LENGTH THETA E I A"
555 FOR I=1 TO NE
560 LPRINT I;TAB(10)EL(I);TAB(20)TH(I);TAB(30)E(I);
    TAB(40)EI(I);TAB(50)EA(I)
565 NEXT I
570 LPRINT"INITIAL GUESSES- GH=";HB;"GV=";VB;"GR=";RB
575 LPRINT" * * *"
600 LPRINT "EL.N0";TAB(10)"AXIAL F";TAB(20)"SHEAR F";
    TAB(30)"END M";TAB(40)"AXIAL DEF.";TAB(52)"THETA FINAL"
605 FOR I=1 TO NE
610 LPRINT I;TAB(10) AF(I);TAB(20)SF(I);TAB(30)XM(I);
    TAB(40)AD(I);TAB(52)TN(I)
615 NEXT I
616 FOR I=1 TO NE
617 IF IE(I)=1 GOTO 619
618 LPRINT"I=";I;TAB(10)"CABLE AX.DEFORM.=";CD(I);TAB(10)
    "CABLE AX.FORCE=";CF(I);GOTO 620
619 LPRINT"I=";I;TAB(15)"NO CABLES FOR THIS NODE"
620 NEXT I
621 LPRINT"NODE NO.";TAB(10)"X-COORD";TAB(20)"Y-COORD";
    TAB(30)"END M";TAB(40)"VL";TAB(50)"HL"
625 FOR I=1 TO NN
630 LPRINT I;TAB(10)XN(I);TAB(20)YN(I);TAB(30)XM(I);
    TAB(40)VL(I);TAB(50)HL(I)

```


-99-

```
635 NEXT I
637 LPRINT"EPS=";EP;"GHF=";GH;"GVF=";GV;"GRF=";GR;"CYCLES="
    ;II
638 LPRINT"SINGLE PRECISION-VERSION'V'";IF F<>1 GOTO 641
639 IF P<>1 GOTO 641
640 LPRINT"PRE-STRESSED ARCH-MOMENT=";MO
641 GOTO 545
```



D. Alternative Method For 2-D Problems

An alternative method for a 2 dimensional arch and rigid bar-spring node model was also developed (31).

In this method the displacements u, v in x and y directions, respectively, are originally assumed. Then if Φ =angle between the displaced element and horizontal axis x , Ψ =rotation of the element; the moment M , shear force s , and axial force N would be

$$M(i) = -\frac{E(i)I(i)}{L(i)} \left[\Psi(i) - \Psi(i) \right] \quad (D.1)$$

$$N(i) = \frac{E(i)A(i)}{L(i)} \Delta D(i) \quad (D.2)$$

where

$$\Delta D(i) = -L(i) + \sqrt{\left[L(i) \cos[\Phi(i)] + u(i) - u(i-1) \right]^2 + \left[L(i) \sin[\Phi(i)] + v(i) - v(i-1) \right]^2} \quad (D.3)$$

and

$$\Psi(i) = \text{Arctan} \left\{ \frac{\left[v(i) - v(i-1) \right] \cos[\Phi(i)] - \left[u(i) - u(i-1) \right] \sin[\Phi(i)]}{\left[L(i) + u(i) - u(i-1) \right] \cos[\Phi(i)] + \left[v(i) - v(i-1) \right] \sin[\Phi(i)]} \right\} \quad (D.4)$$

Assuming u and v and having the above formulas, the forces, moments, rotations, and axial deformations can be found. Then we see if $\sum F_x = 0$ and $\sum F_y = 0$ (the equilibrium equations at each node) within an acceptable range of error

$$\sum F_x = -N(i) \cos[\Phi(i) + \Psi(i)] + N(i+1) \cos[\Phi(i+1) + \Psi(i+1)] - S(i) \sin[\Phi(i) + \Psi(i)] + S(i+1) \sin[\Phi(i+1) + \Psi(i+1)] + P(i) \sin[\epsilon(i)] \quad (D.5)$$

$$\sum F_y = -N(i) \sin[\Phi(i) + \Psi(i)] + N(i+1) \sin[\Phi(i+1) + \Psi(i+1)] + S(i) \cos[\Phi(i) + \Psi(i)] - S(i+1) \cos[\Phi(i+1) + \Psi(i+1)] - P(i) \cos[\epsilon(i)] \quad (D.6)$$

where

P =load applied at the node and.

ϵ =the angle between P and the vertical axis.

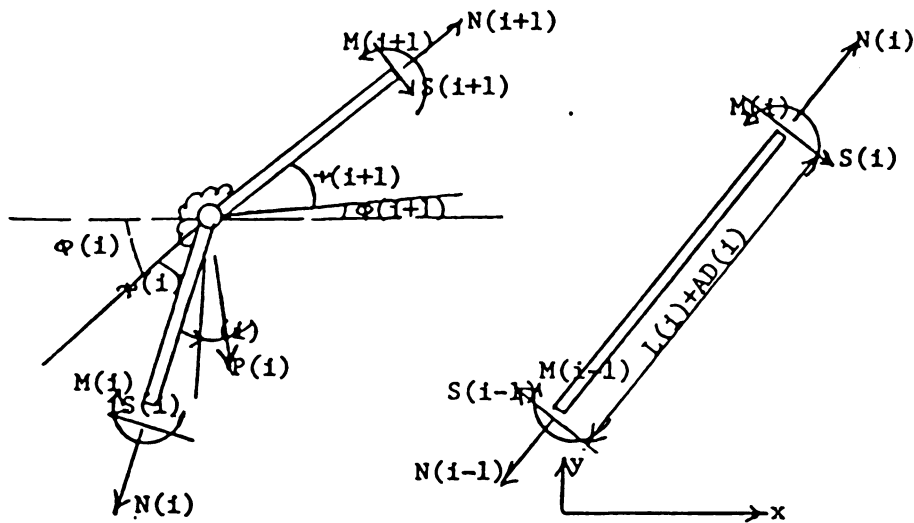


Fig. 55. Typical Mass Point, Forces, and Moments

If convergence is not satisfied, the initial guesses for u and v are improved using Newton's algorithm, and the process is repeated until convergence is achieved; that is, the equilibrium equations are satisfied.

This method has not led to a satisfactory result for the model used.

E. Space Arch

In space arches the same rigid bar-spring node model was used. A basic difficulty exists now because of the fact that the rotational displacements about the three dimensional axes are not commutative.

The final configuration of a body depends on the sequence of rotations.

That is, when rotated about say, x , then y and finally z , the body will not be in the same place necessarily as when rotated about say, y , then x and finally z axes. The addition of twist makes space arches

more complicated than the plane arches. However, if rotations are small, they are commutative and can be added as vectors. Therefore, the arch can be studied under a small load causing small displacements. The

coordinate system will be updated and the new configuration will be the reference one for the next load increment. The procedure continues until the last load increment is applied and the corresponding configuration is then the one corresponding to the final cumulative applied load which may not be small. This method of updated coordinates is used for 3-D arches.

To study this problem, other than the assumptions made in the 2-D case, it is also assumed that no shear deformations are allowed and that the first and last elements are in one plane and stay in that plane. The latter becomes more of a reality if we make the two elements small enough.

The iteration procedure is as follows (7 and 39);

(a) Guess the initial values for the reactions in x , y , and z directions, R_x , R_y and R_z , moment vectors in local s and t directions, M_s and M_t , and finally Dy , the change in α_y which is the angle between the first element and y axis. S is the longitudinal axis (Fig. 56)

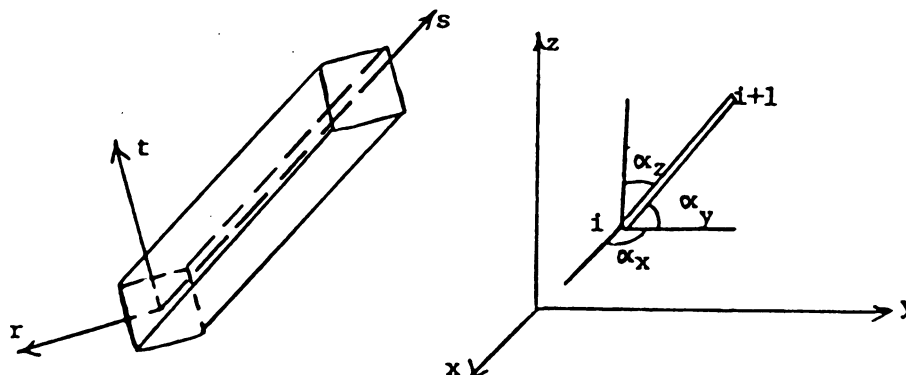


Fig. 56. Local and Global axes (Space Arch)

(b) If T = direction cosines of the local axes r, s , and t with respect to x, y , and z , and P and Q are applied forces in (x, y, z) and (r, s, t) coordinate systems, respectively and R is the reaction vector, then

$$\{Q(1)\} = [T]\{P+R\} \quad (E.1)$$

$$AD(1) = Q_s(1)L(1)/E(1)A(1)$$

For a pinned ends arch $M_r(1)=0$ so;

$$\begin{Bmatrix} M_x \\ M_y \\ M_z \end{Bmatrix} = [T]^{-1} \begin{Bmatrix} 0 \\ M_s \\ M_t \end{Bmatrix} \quad (E.2)$$

(c) Having the displacements that we find from the forces and moments in step b, final coordinates of node 2 can be found. From then on with an iterative manner we find the rotations about the three local axes having the moments and forces in the previous element (or node). Then the new transformation matrix is found. To do so if we let E be the cosines of the angles between element 1 before and after rotations about the three local axes, then

$$[T]_{\text{new}} = [E][T]_{\text{old}} \quad (E.3)$$

We can also find F, the transformation matrix from the local axes of element i-1 to the local axes of element i

$$[F] = [T(i)] [T^{-1}(i-1)] \quad (E.4)$$

(d) Find the new moments and forces due to the applied loads and the forces and moments in element or node i-1.

$$\{Q\} = [F] \{Q(i-1)\} + [T(i)] \{P(i)\} \quad (E.5)$$

$$\{M\} = [F] \begin{Bmatrix} M_r(i-1) - Q_t(i-1)L(i-1) \\ M_s(i-1) \\ M_t(i-1) + Q_r(i-1)L9i-1 \end{Bmatrix} \quad (E.6)$$

(e) Find the axial deformation AD and also $\beta(i)$, $\alpha(i)$ and $\gamma(i)$, the twist and rotations about the two local axes t and r, respectively.

$$\beta(i) = M_s(i)L(i)/2G_j(i) + M_s(i-1)L(i-1)/2G_j(i-1)$$

where G_j = torsional property of the element

$$\alpha(i) = M_t(i)[L(i) + L(i-1)] / [E(i-1)I_t(i-1) + E(i)I_t(i)] \quad (E.7)$$

$$\gamma(i) = M_r(i)[L(i) + L(i-1)] / [E(i-1)I_r(i-1) + E(i)I_r(i)] \quad (E.8)$$

where I_r and I_t are the moments of inertia with respect to the local r and t axes, respectively.

The new transformation matrices, moments, and forces can be found doing one more iteration.

(f) Having the final deformation, the final coordinates of node i+1 can be calculated.

(g) Proceed to the next element. At the end, the 6 errors at the right support are the three displacements in x, y, and z directions, change in the angle with x axis, α , moment about x (coincident with the local r axis) and $\beta(n-1) - M_s(n+1)L(n)/2G_j(n)$ where n=number of elements. $\beta(n+1)$ is the total twist. To find $\beta(n+1)$ we find the components of $\beta(i)$ on the s axis of the last node and add them. Here, due to the small size of the displacements, β was treated as a vector perpendicular to the plane of the node.

(h) Having the errors and the guessed initial values, we improve the latter using Newton's algorithm with a 6x6 matrix. The iteration continues until convergence is satisfied. Then the displaced arch is set as the reference configuration and after updating the coordinate system, the procedure will be repeated for the next increment of load

until the last load increment has been taken care of.

It should be noted that the small rotations have been taken by others (43) as less than 15° .

The method was tried for 2 dimensional loads and arch but the values obtained were not satisfactory.

Other methods have also been used to solve the 3-D problem including a method using the principle of minimum potential energy. The principle states (7) that among all displacement configurations that satisfy internal compatibility and kinematic boundary conditions, those that satisfy the equations of equilibrium make the potential energy a stationary value. If the stationary value is a minimum, the equilibrium is stable.

To apply the principle to the arch problem, after having the coordinates of all nodes, we assume the displacements of each node. From the original and final coordinates of the nodes, we find the bending and torsional rotations, $\alpha(i)$, $\delta(i)$, and $\beta(i)$ and also the axial deformation of each element, $AD(i)$. Then if

$$\begin{aligned} K_{\alpha} &= EI_{\alpha} / L & (a) \\ K_{\delta} &= EI_{\delta} / L & (b) \\ K_{\beta} &= GJ / L & (c) \\ K_{\Delta} &= EA / L & (d) \end{aligned} \quad (E.9)$$

the total potential energy is equal to

$$U = 1/2 \left\{ \sum_{i=1}^{n+1} [K_{\alpha}(i)\alpha^2(i) + K_{\beta}(i)\beta^2(i) + K_{\delta}(i)\delta^2(i)] + \sum_{i=1}^n K_{\Delta}(i)AD^2(i) \right\} \quad (E.10)$$

and the element (i, j) of the stiffness matrix would be

$$K(i, j) = \frac{\partial^2 U}{\partial u(i) \partial u(j)}$$

where $u(i)$ and $u(j)$ are the displacements of the i th and j th degrees of freedom. To compute the derivatives of u we can use the method developed in case I of this chapter.

From the above formulation, two procedures can be developed. The steps for the first one are as follows:

- (a) Assume initial values for all displacements of all nodes
- (b) Find rotations and axial deformations
- (c) Find the total potential energy, U
- (d) Test for convergence. That is, see if U is a minimum. If $\frac{\partial U}{\partial u} = 0$ within acceptable error range for all $u(i)$ then convergence is satisfied. We have the final configuration. If not, go to step (e)
- (e) Having the initial values and errors and using the Newton's algorithm, we improve the initial values and go back to step (b).

The second procedure includes the following steps:

(a) Assume initial values for $u(i)$, forming displacement vector D which includes three displacements and three rotations about the three global axes for each node.

(b) Find the rotations and axial deformations.

(c) Find the stiffness matrix, K , which is the second derivative of the total potential energy.

(d) Find the force vector due to the displacements

$$F = -KD \quad (E.11)$$

(e) Find the unbalanced force

$$F_u = F + P \quad (E.13)$$

Where P is the vector of the applied forces.

(f) Find the displacements due to the unbalanced force D

$$D_u = K^{-1} F_u \quad (E.14)$$

(g) Test for convergence. If not satisfied go to step (h).

(h) Find the new displacement vector

$$D_{\text{new}} = D_{\text{old}} + D_u \quad (E.15)$$

and go back to step (b).

To test convergence, one way is first to compute

$$E = t_u / u_m \quad (E.16)$$

Where t_u is the value of the specified type of deformation of each node due to unbalanced forces and u_m is the maximum initial value for that type of deformation. If t_u is, say, the value of the displacement in x direction due to the unbalanced forces, then u_m will be the maximum value of the displacement in x direction of all nodes in the original assumption (step a). We find the 6 maximum values for E corresponding to the 6 types of deformations. If these 6 values are within acceptable range of error then convergence is satisfied.

The above two methods using potential energy have not led to a convergence with a set of satisfactory results.

Projecting the arch onto the three perpendicular planes was also considered to deal with the problem. The space arch was projected onto xoy, xoz, and yoz planes. Each one was treated as an in-plane problem. Moments and forces on the element were found combining the moments and forces of each component. Compatibility was forced to be satisfied by geometrical relationships such as the fact that the sum of the squares of the three direction cosines is equal to one.

This method did not work due to the fact that we cannot take the projection of properties such as moments of inertia, find the effects,

-108-

and then combine them to get the effect caused on the element in space.

BIBLIOGRAPHY

1. Austin, W.J., "In-Plane Bending and Buckling of Arches", Journal of Structural Division, ASCE, Vol. 97, ST 5, May 1971, pp. 1575-1592.
2. Austin, W.J., and Ross, T.J., "Elastic Buckling of Arches Under Symmetrical Loading", Journal of Structural Division, ASCE, Vol. 102, No. ST5, May 1976, pp. 1085-1095.
3. Austin, W.J., Ross, T.J., Tawfik, A.S., and Volz, R.D., "Numerical Bending Analysis of Arches," Journal of Structural Division, ASCE, Vol. 108, No. ST4, April 1982, pp. 849-868.
4. Bathe, K.J. and Bolourchi, S., "Large Displacement Analysis of Three-Dimensional Beam Structures," International Journal for Numerical Methods in Engineering, Vol. 14, April 1979, pp. 961-986.
5. Chajes, A., "Post-Buckling Behavior"; Journal of Structural Division, ASCE, Vol. 109, No. 10, October 1983, pp. 2450-2462.
6. Conway, H.D., and Lo, C.F., "Further Studies on the Elastic Stability of Curved Beams," International Journal of Mechanical Sciences, Vol. 9, No. 10, October 1967, pp. 707-718.
7. Cook, R.D., Concepts and Applications of Finite Element Analysis, John Wiley and Sons, 1974.
8. Dawe, D.J., "Numerical Studies Using Circular Arch Finite Elements," Computers and Structures, Vol. 4, 1974, pp. 729-740.
9. DaDeppo, D.A., and Schmidt, R., "Sidesway Buckling of Deep Circular Arches Under a Concentrated Load," Journal of Applied Mechanics, ASME, Vol. 36, June 1969, pp. 325-327.
10. Dill, E.H., "General Thin Shell Displacement Strain Relations," Proceedings of the 4th United States National Congress of Applied Mechanics, Vol.1, 1962, pp. 529-530.
11. Dym, C.L., "Bifurcation Analysis For Shallow Arches," Journal of Engineering Mechanics Division, ASCE, Vol. 99, EM2, April 1973, pp. 287-301.
12. Encyclopaedia Britannica, Knowledge in Depth, Vol. 1, 1980.

13. Fuji, F., "A Simple Mixed Formulation For Elastica Problems," Computers and Structures, Vol. 17, No. 1, 1983, pp. 79-88.
14. Gallert, M., and Laursen, M.E., "Formulation and Convergence of a Mixed Finite Element Method Applied to Elastic Arches of Arbitrary Geometry and Loading", Computer Methods in Applied Mechanics and Engineering, Vol. 7, No. 3, March 1976, pp. 285-302.
15. Harrison, H.B., "Post-Buckling Behavior of Elastic Circular Arches", Proceedings of the Institute of Civil Engineers, London, England, Vol. 65, June 1978, pp. 283-299.
16. Harrison, H.B., "In-Plane Stability of Parabolic Arches", Journal of Structural Division, ASCE, Vol. 108, ST1, Jan. 1982, pp. 195-205.
17. Huddleston, J.V., "Finite Deflections and Snap-Through of High Circular Arches", Journal of Applied Mechanics, Vol. 35, No. 4, December 1968, pp. 763-769.
18. Hornbeck, R.W., Numerical Methods, Quantum Publishers, Inc., 1975.
19. Janssen, G.J., "A Nonlinear Dynamic Analysis of Line Structural Members", Ph.D. Thesis, 1968, Michigan State University, Michigan.
20. Kerr, A.D and Soifer, M.T., "The Linearization of the Prebuckling State and Its Effect on the Determined Stability Loads," Journal of Applied Mechanics, Vol. 36, No. 4, December 1969, pp. 775-783.
21. Langhaar, H.L., Boresi, A.P., and Carver, D.R., "Energy Methods of Buckling of Circular Elastic Rings and Arches", Proceedings of the Second U.S. National Congress of Applied Mechanics, 1954, pp. 437-443.
22. Lee, L.H.N., and Murphy, L.M., "Inelastic Buckling of Shallow Arches", Journal of the Engineering Mechanics Division, Vol. 94, EM1, Feb. 1968, pp. 225-239.
23. Mattiasson, K., "Numerical Results From Large Deflection Beam and Frame Problems Analysed By Means of Elliptic Integrals", International Journal of Numerical Methods in Engineering, Vol. 17, No. 1, January 1981, pp. 145-153.
24. Nemat-Nassar, S., Variational Methods in the Mechanics of Solids, Pergamon Press, 1980.
25. Noor, A.K and Peters, J.M., "Penalty Finite Element Formulations of Curved Elastica", Journal of the Engineering Mechanics

Division, ASCE, Vol. 110, No. 5, 1984, pp. 694-712.

26. Nordgren, R.P., "On Finite Deflection of an Extensible Circular Ring Segment", International Journal of Solids and Structures, Vol. 2, No. 2, April 1966, pp. 223-233.
27. Ojalvo, M., Demuts, E., and Tokarz F., "Out of Plane Buckling of Curved Elements", Journal of the Structural Division, ASCE, Vol. 95, ST10, October 1969, pp. 2305-2316.
28. Ojalvo, I.U., and Newman, M., "Buckling of Naturally Curved and Twisted Beams", Journal of the Engineering Mechanics Division, ASCE, Vol. 94, EM5, October 1968, 1067-1087.
29. Oran, C., and Bayazid, H., "Another Look at Buckling of Circular Arches", Journal of the Engineering Mechanics Division, ASCE, Vol. 104, EM6, December 1978, pp. 1417-1432.
30. Oran, C., "General Imperfection Analysis in Shallow Arches", Journal of the Engineering Mechanics Division, ASCE, Vol. 106, EM6, December 1980.
31. Rymers, P.C., "Application of a Discrete Element Model to the Study of the Static and Dynamic Stability of Beams, Arches, and Rings", Ph.D. Thesis, 1968, Michigan State University, Michigan.
32. Sabir, A.B., and Lock, A.C., "Large Deflection, Geometrically Nonlinear Finite Element Analysis of Circular Arches", International Journal of Mechanical Sciences, Vol. 15, 1973, pp. 37-47.
33. Schreyer, H.L., and Masur, E.F., "Buckling of Shallow Arches", Journal of the Engineering Mechanics Division, ASCE, Vol. 92, EM4, August 1966, pp. 1-19.
34. Schmidt, R., and DaDeppo, D.A., "A Survey of Literature on Large Deflection of Non Shallow Arches, Bibliography of Finite Deflections of Straight and Curved Beams, Rings, and Shallow Arches", Industrial Mathematics, Vol. 21, Part 2, 1971, pp. 91-114.
35. Sheinman, I., "Large Deflection of Curved Beam With Shear Deformation", Journal of the Engineering Mechanics Division, ASCE, Vol. 108, EM4, August 1982, pp. 636-647.
36. Sokolinikoff, I.S., Mathematical Thoery of Elasticity, Second Edition, McGraw-Hill Book Company, NY, 1956.
37. Timoshenko, S.P., and Gere, J.M., Theory of Elastic Stability, Second Edition, McGraw-Hill Book Company, NY, 1961.

38. Timoshenko, S.P., and Woinowsky-Krieger, S., Theory of Plates and Shells, Second Edition, McGraw-Hill Company, NY, 1959.
39. Wang, Chu-Kia, Matrix Methods of Structural Analysis, Second Edition, American Publishing Company, Madison, WI, 1970.
40. Watwood, V.B., and Hartz, B.J., "An Equilibrium Stress Field Model for Finite Element Solutions of Two Dimensional Elasto Static Problems", International Journal of Solids and Structures, No. 4, (1968), pp. 857-873.
41. Wempner, G.A., and Patrick, G.E., "Finite Deflections, Buckling and Post-Buckling of an Arch", Proceedings of the Eleventh Midwestern Mechanics Conference, Vol. 5, Iowa State University, August 1969, pp. 439-450.
42. Wen, R.K., and Lange, J. "Curved Beam Element For Arch Buckling Analysis", Journal of the Structural Division, ASCE, Vol. 107, ST11, November 1981, pp. 2053-2069.
43. Wen, R.K., and Rahimzadeh, J. "Non-linear Elastic Frame Analysis by Finite Element", Ph.D. Thesis, 1981, Michigan State University, Michigan.
44. Wolde-Tinsae, A.M., and Assaad, M.C., "Non-linear Stability of Prebuckled Tapered Arches", Journal of EM Division ASCE, Vol. 110, No. 1, January 1984, pp. 84-94.
45. Wood, R.D., and Zienkiewicz, O.C., "Geometrically Non-linear Finite Element Analysis of Beams, Frames, Arches, and Axisymmetric Shells", International Journal of Computers and Science, Vol. 7, No. 6, December 1977, pp. 725-735.
46. Wunderlich, W., Stein, E., and Bathe, K.J., "Non-linear Finite Element Analysis in Structural Mechanics", Proceedings of the Europe - U.S. Workshop, Ruhr Universitat Bochum, Germany, July 28-31, 1980.
47. Yamada, Y., and Ezawa, Y., "On Curved Finite Elements for the Analysis of Circular Arches", International Journal for Numerical Methods in Engineering, Vol. 11, 1977 pp. 1635-1651.

MICHIGAN STATE UNIVERSITY LIBRARIES



3 1293 03146 3957